R & M No. 3845

R &M No. 3845

PROCUREMENT EXECUTIVE, MINISTRY OF DEFENCE

Aeronautical Research Council
Reports and Memoranda

JET INTERFERENCE ON SUPERCRITICAL WINGS

PART 1: EXPERIMENTS ON A TWO-DIMENSIONAL WING
PART II: EXPERIMENTS ON A SWEPT WING

by

J.A. Bagley
A.G. Kurn

Aerodynamics Department,
R.A.E., Farnborough, Hants.

London: Her Majesty's Stationery Office

£15 NET

PART I UDC 533.695.17 : 533.697.4 : 533.693.9 : 533.693.2 : 533.6.048.2
PART II UDC 533.695.17 : 533.697.4 : 533.693.9 : 533.693.1 : 533.6.048.2

JET INTERFERENCE ON SUPERCRITICAL WINGS

PART I: EXPERIMENTS ON A TWO-DIMENSIONAL WING

PART II: EXPERIMENTS ON A SWEPT WING

By J. A. Bagley† and A. G. Kurn
Aerodynamics Department, RAE Farnborough

REPORTS AND MEMORANDA No.3845*
January 1977

SUMMARY

Wind tunnel tests have been made to investigate the influence of the jets from several different nozzles on the pressure distribution on adjacent wing panels with supercritical profiles. In Part I, an existing unswept wing panel was used for the tests; in Part II, a 25° swept wing panel was tested, and additional measurements were made with pylons fitted to two of the nozzles.

The nozzle shapes and their location relative to the wing were chosen to represent a modern airbus configuration with fan engines. The results indicate that, in the cruise configuration, the influence of the jet is fairly small, and in most cases it simply reinforces certain features of the pressure distribution measured without jet blowing.

* Replaces RAE Technical Reports 77007 and 77008 - ARC 37279 and 37281

† Now at Science Museum, South Kensington, London

LIST OF CONTENTS

Part I

EXPERIMENTS ON A TWO-DIMENSIONAL WING

by

J. A. Bagley
A. G. Kurn

SUMMARY

Wind tunnel tests have been made to investigate the influence of the jets for three different nozzles on the pressure distribution on an adjacent unswept supercritical wing. The nozzle shapes and locations were chosen to represent a modern airbus configuration with fan engines. The results indicate that jet interference is normally small, but that significant features of the flow can be identified.

1 INTRODUCTION

The work reported here is an extension of earlier wind tunnel tests[1-3] to investigate the influence of the jet flow from an under-wing engine nacelle on the static pressure distribution around the wing. In the present programme, two new features have been investigated, which arise from recent developments in aircraft design.

The first feature is the use of 'supercritical' wings, which are designed to have a large extent of supersonic flow on the upper surface and a considerable amount of rear loading. Such a choice of load distribution allows the designer to use thicker wings than were possible in the past, but if this possibility is exploited the velocity distribution on the lower surface has two characteristics: a peak value near mid-chord which will reach (or slightly exceed) the local speed of sound, and a steep adverse pressure gradient behind this peak back to about 90% chord followed by a favourable gradient (ie an acceleration in the local velocity) towards the trailing edge. The earlier work has already shown that the influence of the jet is largely confined to the lower surface of the wing and it was envisaged that adverse interference effects might arise there on such 'advanced' wing sections: the peak velocity might be increased and the aft adverse pressure gradient made more steep.

The second new feature which has been covered in the present tests is the recent development of shorter afterbodies for engines of high by-pass ratio. The previous tests were made at a time when emphasis was on the use of longer fan cowls to achieve increased silencing; subsequent work by Rolls Royce Ltd[4] has shown that improved performance can be obtained by deleting the fan-stream thrust reverser and using a shorter gas-generator afterbody with a steeper boat-tail and smaller wetted area. There is some evidence that the use of such a nacelle shape gives even better performance when tested close to a wing, leading to a surmise that there are favourable interference features for such a configuration, which remain to be explained in terms of changes in the flow field.

The present experiment was planned as a preliminary stage in an investigation of these features, and was carried out in the RAE 2ft × 1½ft transonic wind tunnel with its associated jet blowing rig. The same two-dimensional unswept wing, spanning the tunnel, was used as in the previous tests[3]. Although this is not strictly a supercritical section, it was designed to incorporate rear-loading, and at a suitable elevated Mach number it exhibits the appropriate characteristics of a sonic peak velocity near mid-chord on the lower surface, followed by a steep adverse pressure gradient. The upper-surface pressure distribution is

not representative, but as already noted, it is the jet interference with the lower surface flow which is of primary concern.

These tests were essentially exploratory, intended to discover whether there were any unexpected features in the flow. It was appreciated that all the features of the flow field appropriate to a swept-winged aircraft could not be represented, but it was judged that the comparison with the earlier work using this same unswept wing would be valuable. A further series of tests using a wing with 25 degrees sweepback was planned to follow the tests described here.

The present tests are fairly limited in scope, comprising pressure measurements at one angle of incidence on the wing alone and in the presence of a jet blowing from each of three different nozzles. The details of these nozzles and of the test programme are given in section 2. The interference effects of the three nozzles are compared in section 3; the zero thrust conditions are discussed in section 3.1, and section 3.2 covers the influence of jet blowing. A brief discussion of the Schlieren observations is given in section 3.3 and conclusions are presented in section 4.

2 EXPERIMENTAL DETAILS

2.1 Details of the models

The experimental rig has been fully described in Ref 3. Briefly, it comprises a two-dimensional wing mounted between solid glass side-walls in the RAE 2ft × 1½ft transonic tunnel with a slotted roof and floor, and a long air supply pipe cantilevered from the tunnel contraction, on the end of which is mounted an axisymmetric nozzle shaped to represent the rear end of an engine nacelle. Part of the boundary layer developed along the pipe is removed by suction through slots near the end of the tube. The wing chord is 152.4 mm and the section RAE 2806 for which the ordinates are given in Table 1.

The shorter of the two nozzles tested in the previous programme[3] is quite similar to the '11 degree afterbody' which has been tested on the Rolls Royce RB 211 engine in both model and full-scale experiments[4]. The RAE afterbody is curved, however, so that the slope at the nozzle exit is about 16 degrees. This nozzle was used again for the present series of tests; it is referred to as the 'RAE nozzle' and its shape is tabulated in Table 2.

The second nozzle tested in this programme is based on the '15 degree short afterbody' developed for the RB 211 [4]; its ordinates are tabulated in Table 3. The two nozzles are illustrated in Fig 1.

This 15 degree afterbody was also tested with a short cylindrical extension to establish whether this had a significant effect on the flow field.

This third nozzle was included because such an extension had been proposed by Rolls Royce Ltd for use in another test programme, with the objective of representing the core jet in a model where only the fan jet was provided by an external air supply. Similar 'hard-body' representations of propulsive jets have been used before but only with partial success. In the early RAE work[1], an essentially similar solid extension of the centre-body was tested and found to have little influence on the wing pressure distribution; but on the present short afterbody the discontinuity in surface slope at the end of the nozzle was greater, and it was thought that this could produce a greater effect on the external flow. The dimensions of the cylindrical extension are also included in Table 3 and Fig 1.

2.2 Test programme

Pressure distributions on the wing were measured at sixty points on a single chord in line with the axis of the nozzle, and corresponding Schlieren observations of the flow were made. The tests were all made at a particular value of wing incidence (α = 2 degrees) which gave an appropriate type of lower-surface pressure distribution at the 'design' Mach number, $M_\infty = 0.78$. The tests were made at constant tunnel pressure, and the Reynolds number (based on wing chord) varied from $R = 1.33 \times 10^6$ at $M_\infty = 0.72$ to $R = 1.44 \times 10^6$ at $M_\infty = 0.84$. The test Mach numbers are tabulated on Fig 2.

Transition was not fixed during these tests; in the earlier tests it was found to occur naturally (on the isolated wing) at 50 to 55% chord on the lower surface, and 70 to 75% chord on the upper surface. At the higher Mach numbers of the present tests there is evidence of laminar shock boundary layer interaction. Comparison of the measured pressure distributions with calculations by the Firmin-Jones TSP method[10] suggests that this interaction has significantly influenced the shape of the upper-surface pressure distribution, but the lower-surface pressures (which are of interest here) are not affected significantly.

The nozzles were tested at two vertical distances below the wing, as indicated on Fig 2; the lower position was chosen to represent a typical current design (the RB 211 installation on the Lockheed L 1011) and the closer position corresponded to the most distant of the three positions used in the earlier test series[3]. Owing to the difficulty of setting up the nozzle in the tunnel in a

precise manner there are small differences in the vertical positions of the two nozzles. The actual positions tested are tabulated on Fig 2 for reference.

The horizontal location of the nozzle was also chosen to represent the current L 1011 installation; it places the fan exit closer to the leading edge of the wing (in the fore- and aft-direction) than any position tested in Ref 3, although one of the earliest tests[1] used a fan exit location just aft of the leading edge.

Tests were made with the jet total pressure equal to that of the freestream, simulating the zero-thrust condition, or the conditions which would obtain behind a free-flow nacelle; and with the jet blown at three higher pressures. The intention was that the selected jet pressure values would bracket the pressure ratio $H_j/p_0 = 2.4$ which corresponds roughly to an RB 211 engine at design cruise condition. Unfortunately, it was discovered in the latter part of the test that the pressure losses in the supply pipe, between the station where jet pressure is monitored and the nozzle, were higher than expected, and the jet pressure ratios at which tests had been made for the RAE nozzle were all too low, around 2.1 rather than 2.4*.

The values of jet pressure ratio which were actually used in the tests are quoted on the relevant figures (eg Fig 20) and are defined as the mean value of pressure ratio at the annular (fan) exit. Pitot traverses across the exits of the nozzles are plotted in Fig 3. The general shape of the exit profiles is similar for the two nozzles, reflecting the pipe flow profile of the supply tube. The lower level of pressure ratio in the fan exit of the 15 degree nozzle is due to the exit area being slightly larger than the internal pipe area; the flow is evidently choked inside the nozzle rather than at the exit in this case.

3 RESULTS

The experimental results have not been subjected to any wind tunnel corrections. A standard theory[5] for tunnel wall constraint interference predicts a correction in speed of $\Delta M = -0.026$ at $M_\infty = 0.72$ increasing to $\Delta M = -0.067$ at $M_0 = 0.84$. However, other experiments have shown that there is reason to doubt the use of such a simple correction for supercritical wings in slotted wall

---

* The same losses occurred in the earlier tests, so that the jet pressure ratios quoted in Ref 3 for this nozzle are all too high. The correct values are 1.70, 2.09, 2.31 and 2.53, in place of the quoted values 1.9, 2.4, 2.65 and 2.9. The pressure ratios quoted for the other nozzle in Ref 3 are correct.

tunnels; in any case it is not known what allowance should be made for the addition of the jet stream. Since the experiment is essentially exploratory in nature, the uncorrected measurements are considered to be adequate.

In the figures, the results are shown in two forms: as distributions of pressure coefficient C_p on the wing chord directly in line with the nozzle centre-line, and as distributions of ΔC_{p_j}, which is defined as the difference between the pressure coefficient measured with the jet blowing at a particular jet pressure ratio and that measured with $H_j = H_\infty$, ie free-flow or zero-thrust conditions. In this form, the results can be compared directly with those from earlier tests[1-3].

To facilitate comparison of the results, the figures for a given configuration and Mach number are grouped together as indicated by the table below.

M_∞	C_p for $H_j = H_\infty$	C_p for $\frac{H_j}{p_\infty} > 1.9$	ΔC_{p_j}
	$z_n/D_e = 0.6$		
0.72	Fig 4	6	7
0.78	5	6	8
0.80	9	10	11
0.82	12	13	14
0.84	15	16	17
	$z_n/D_e = 0.3$		
0.72	18	19	20
0.78	21	22	23

As in the earlier tests, it was found that the pressures on the upper surface of the wing were unaffected by jet blowing, so most of the illustrations refer only to the lower surface.

3.1 Comparison of the effects of the three nozzles at zero thrust

In Fig 4, the effect of the long supply tube and the various nozzles at $z_n/D_e \doteq 0.6$ on the wing pressure distributions is shown at $M_\infty = 0.72$, where the flow is entirely subcritical. The main effect is a reduction of the effective incidence, reducing the velocities on the upper surface and increasing those near the leading edge on the lower surface. Further back on the lower surface the velocities are reduced as the flow expands past the end of the nozzles.

These effects are an entirely straightforward consequence of the displacement flow around the nozzles, and can be predicted by a simple calculation of the inviscid flow, using appropriate distributions of singularities to represent the bodies. A comparison with calculations by Hardy[6] is presented in Fig 24, which shows this for two nozzles at $M_\infty = 0.72$ and $z_n/D_e = 0.64$. There is an indication of some discrepancy between theory and experiment near mid-chord on the lower surface. This is thought to be associated with movement of the free transition point which slightly alters the location of the steep pressure rise just behind mid-chord; when one set of pressure coefficients is subtracted from the other, a discontinuity appears in the resulting ΔC_p curve. The shift in transition point may simply be due to the presence of the jet (and its noise field); or it may be due to a small difference in wing setting in the two tests, although it is difficult to see how this could have occurred.

Apart from this local difference between theory and experiment the good agreement elsewhere indicates that there is no significant effect of the long pipe ahead of the nozzle. In the theoretical calculations, a nacelle of length equal to three diameters was represented, whereas in the experiment the nacelle is effectively of infinite length. This confirms the conclusion reached by other experimenters[7,8] using blown nacelles with fixed entries, that the influence of the front part of a nacelle mounted below and ahead of the wing is not significant, that is as long as flow separations there are avoided.

Fig 24 also shows that the interference field of the shorter 15 degree afterbody has a peak effect slightly further forward on the wing lower surface than that produced by the longer afterbody, as would be expected. This produces a difference in the shape of the lower-surface pressure distributions; as shown in Fig 5, the pressures are significantly higher between about 5% and 30% chord with the shorter nozzle. Although the shape of the interference curve is different, the magnitude of the interference is virtually identical for the two nacelles, the peak pressure increment at about 40% chord on the lower surface being about the same for both nozzles.

Comparing Figs 4, 5, 9, 12 and 15, it can be seen that the same trends are followed consistently as the freestream Mach number is increased. With the nozzles moved closer to the wing, in Figs 18 and 21, the difference between the two nozzles still has the same general character, but is naturally larger. In all cases, the upper-surface pressures are unaffected by the change of nozzle. Throughout this series of figures, the influence of the small cylindrical extension on the 15 degree nozzle in free-flow conditions is seen to be trivial,

except at the highest Mach number (M_∞ = 0.84, Fig 15). Here, the peak suction on the lower surface is slightly reduced, although the shock position is unaltered.

3.2 Comparison of jet effects from the three nozzles

The difference between the lower-surface pressures measured with the various nozzles is broadly similar throughout the range of Mach numbers tested, and for both values of vertical spacing. With jet blowing, the peak suction on the lower surface is consistently higher for the 15 degree nozzle - see Figs 6, 10, 13, 16, 19 and 22 - but even at the closer spacing the difference is not large.

The influence of the cylindrical extension on the 15 degree nozzle is small except at z_n/D_e = 0.3, M = 0.78 (Fig 22); such differences as do arise are more clearly shown in the values of ΔC_{p_j} in Figs 7, 8, 17 and 20. Although the main features of the flow pattern are unlikely to be significantly affected, it does seem clear that to use such a solid extension piece as a device which purports to compensate for incorrect representation of the core jet could lead to misleading results in detail.

Up to M_∞ = 0.82 , the general trend of the results measured in this series of experiments is very similar to that found in the earlier tests. The values of ΔC_{p_j} , plotted in Figs 7, 8, 11, 14, 17, 20 and 23, show that each nacelle-wing combination has a characteristic shape of interference curve which grows in size as jet pressure rises and as Mach number is increased. For the conventional wing-nacelle spacing, z_n/D_e = 0.6 , the values of ΔC_{p_j} do not significantly exceed -0.2; but at z_n/D_e = 0.3 the jet-induced effects are larger and (especially for the shorter 15 degree nozzle) are certainly large enough to cause some disquiet about possible changes in local flow conditions. However there is no indication that either nozzle has significantly increased the tendency of the lower-surface boundary layer to separate, although the pressure rise is slightly greater for the 15 degree nozzle.

At the highest Mach number tested, M_∞ = 0.84 , there is some indication of a change in the shape of the interference pattern for the longer nozzle (Fig 17), but little evidence for any dramatic change in the general nature of jet interference when the peak local velocity on the lower surface exceeds the sonic value.

Generally, the difference between the curves for the two nozzles indicates that a slightly lower sectional lift coefficient would be obtained with the longer nozzle. This is insignificant in itself, but a similar effect on a finite wing would imply that in a comparison made at a given overall lift coefficient,

the slight local loss of lift near the nacelle would be made up elsewhere on the wing. If this compensation happened to occur on a part of the wing which was particularly critical - where a small change in local lift produced a significant movement of a shock wave on the upper surface, for example - then even such an apparently insignificant difference in the local pressures on the wing near the nacelles might be responsible for a significant difference in the overall drag.

3.3 Schlieren pictures

Schlieren observations were made throughout the tests, and a small selection of pictures is reproduced in Figs 25 to 27.

Fig 25 indicates that the shock on the lower surface is weaker at all Mach numbers with all the nozzles at zero thrust than on the isolated wing: this is simply a consequence of the downwash induced by the nacelles (see section 3.1).

Fig 26 shows a direct comparison of the flows from the three nacelles at $z_n/D_e = 0.3$, $M = 0.78$. The only significant feature is the difference in the pattern of shockwaves on the top and bottom surfaces of the inner nozzle. This shows exactly the same feature as was originally observed in Refs 2 and 3: on the side remote from the wing a number of shocks are visible, which are suppressed on the side closer to the wing. This seems to be a characteristic feature of wing/nacelle interference; it has been noted for example by Munniksma and Joarsma[8], and in other unpublished work. A calculation of the nozzle flow with and without an adjacent wing present by Young[9] for one particular case appears to reproduce this particular feature of the flow and provides an adequate representation more generally of the features of the interference between the jet and the external field.

The photographs reproduced in Fig 26 also show quite striking differences in the pattern of shocks in the jet stream, particularly between the 15 degree nozzles with and without cylindrical extension. However it is thought that these differences are perhaps not of very great significance as regards the interference effects on the wing flows. A further selection of photographs shown in Fig 27 demonstrates some of the wide variety of jet shock patterns obtained during these tests over the higher range of Mach number.

4 CONCLUSIONS

For the reasons explained in the Introduction, the experiments described in this Report can only be regarded as preliminary, and any conclusions must be somewhat tentative. Nevertheless, taken in conjunction with earlier tests, the following points appear to be established by the present work:

(1) The main influence of all the nacelles tested is to produce a downwash over the wing, leading to a reduction in lift, lower velocities on both upper and lower surfaces, and a reduction in shock strength on the lower surface.

(2) The additional influence of jet blowing is confined to the lower surface of the wing, where the distribution of ΔC_{p_j} has a characteristic shape for each wing-nozzle configuration; the magnitude of ΔC_{p_j} increases as free stream Mach number increases and as jet pressure-ratio increases. For values of these parameters appropriate to current 'airbus' configurations with engines of bypass ratio $\doteq$ 5 and typical current engine locations, the values of ΔC_{p_j} do not exceed -0.2.

(3) The difference in the wing pressure distributions obtained with the two nozzles tested (representing alternative nozzles for the RB 211 engine) was small over the range of conditions investigated and no significant changes in the local flow pattern were apparent. However, on a complete aircraft even a small change in sectional lift coefficient could have a significant influence on the drag-rise Mach number and on the overall drag.

(4) The addition of a short cylindrical extension to the centre nozzle, which has been suggested by other workers as a representation of the core jet, had only a small effect on the measured flow in most cases, but at $M_\infty = 0.78$, $z_n/D_e = 0.3$, (where the jet-induced effects on wing pressures are greatest), the results obtained in this way could be definitely misleading.

(5) A characteristic feature of wing-nacelle interference appears to be the suppression of shocks in the jet from the fan nozzle over the core afterbody on the side adjacent to the wing.

Table 1

AEROFOIL ORDINATES
Wing RAE 2806

(Dimensions in millimetres.)

x	z Upper surface	z Lower surface	x	z Upper surface	z Lower surface
0	0	0	64.008	9.314	-8.796
1.524	1.887	-2.017	64.056	9.329	-8.580
3.048	2.791	-2.774	70.104	9.345	-8.311
4.572	3.338	-3.414	73.152	9.332	-8.026
6.096	3.749	-3.929	76.200	9.286	-7.706
7.620	4.145	-4.326	79.248	9.230	-7.363
9.144	4.516	-4.729	82.296	9.141	-6.990
10.668	4.867	-5.077	85.344	9.025	-6.571
12.192	5.194	-5.382	88.392	8.880	-6.175
13.716	5.469	-5.692	91.440	8.684	-5.768
15.240	5.723	-5.954	94.488	8.473	-5.324
16.764	5.982	-6.210	97.536	8.242	-4.907
18.288	6.213	-6.444	100.584	7.978	-4.432
19.812	6.434	-6.683	103.632	7.686	-3.975
21.336	6.632	-6.881	106.680	7.381	-3.528
22.860	6.805	-7.097	109.728	7.033	-3.101
24.384	6.995	-7.295	112.776	6.675	-2.692
25.908	7.168	-7.460	115.824	6.302	-2.253
27.432	7.338	-7.630	118.872	5.900	-1.880
28.956	7.493	-7.785	121.920	5.486	-1.506
30.480	7.625	-7.910	124.968	5.050	-1.204
33.528	7.915	-8.192	128.016	4.605	-0.881
36.576	8.161	-8.418	131.064	4.125	-0.599
39.624	8.382	-8.603	134.112	3.655	-0.343
42.672	8.573	-8.760	137.160	3.150	-0.140
45.720	8.733	-8.895	140.208	2.630	0.008
48.768	8.887	-9.004	143.256	2.075	0.130
51.816	9.007	-9.032	146.304	1.496	0.178
54.864	9.098	-9.030	149.352	0.831	0.107
57.912	9.187	-9.009	152.400	-0.046	-0.127
60.960	9.258	-8.913			

Table 2

RAE NOZZLE ORDINATES
see also Fig 1

(Dimensions in millimetres.)

Outer cowl		
x_j	Inside diameter	Outside diameter
-139.70	41.66	63.30
-114.30	43.18	↓
-101.60	44.45	↓
-95.25	45.47	↓
-88.90	46.74	↓
-82.55	48.77	parallel
-76.20	50.80	↓
-69.85	52.83	↓
-62.99	54.10	↓
-57.91	54.36	63.30
-52.83	↓	63.25
-47.75	↓	62.97
-42.67	↓	62.59
-37.59	↓	62.10
-32.51	↓	61.49
-27.43	parallel	60.73
-22.35	↓	59.89
-17.27	↓	58.98
-12.19	↓	58.04
-7.11	↓	57.07
-2.03	↓	55.91
0	54.36	55.09

Inner cowl		
x_j	Inside diameter	Outside diameter
-85.09	24.13	24.13
-82.55	22.86	27.69
-76.20	↓	30.73
-69.85	↓	33.53
-63.50	↓	35.31
-60.33	↓	35.56
	↓	parallel
-25.40	↓	35.56
-15.88	↓	39.12
-6.35	parallel	40.89
	↓	parallel
0	↓	40.89
2.54	↓	40.62
5.08	↓	40.06
7.62	↓	39.24
10.16	↓	38.20
12.70	↓	37.01
15.24	↓	35.81
17.78	22.86	34.59
20.32	↓	33.38
22.86	↓	32.16
25.40	↓	30.94
27.94	↓	29.72
30.48	↓	28.50
33.02	st. taper	27.28
35.56	↓	26.09
38.10	↓	24.87
40.64	↓	23.65
43.18	↓	22.43
45.09	20.98	21.34

Table 3

15 DEGREE AFTERBODY NOZZLE ORDINATES
see also Fig 1

(Dimensions in millimetres.)

Outer cowl		
x_j	Inside diameter	Outside diameter
	parallel	parallel
-118.05	41.66	63.50
	radius	↓
-105.10	43.99	↓
	st. taper	parallel
-79.89	52.88	↓
	radius	↓
-66.93	55.22	↓
-52.73	↓	63.50
-50.19	↓	63.48
-47.65	↓	63.39
-45.11	↓	63.27
-42.57	↓	63.08
-40.03	parallel	62.86
-37.49	↓	62.57
-34.95	↓	62.24
-32.41	↓	61.85
-29.87	↓	61.41
-27.33	↓	60.91
-26.39	55.22	
-24.79	↓	60.37
-22.25	↓	59.78
-19.71	st. taper	59.13
-17.17	↓	58.42
-14.63	↓	57.67
-14.00	53.75	
-13.18	st. taper	57.21
-9.30	54.05	st. taper
-4.72	53.54	
-4.65	radius	54.56
-2.49	52.63	radius
-2.39	st. taper	53.59
		st. taper
0	51.31	52.38

Inner cowl		
x_j	Inside diameter	Outside diameter
-88.90	23.83	23.83
-87.90	21.83	
-87.47	↓	27.93
-86.04	↓	29.56
-83.19	↓	31.71
-80.33	↓	33.21
-77.47	↓	34.34
-74.61	↓	35.20
-71.76	↓	35.87
-68.90	↓	36.36
-66.04	↓	36.70
-63.18	↓	36.90
-60.33	↓	36.96
	parallel	parallel
-26.39	↓	36.96
	↓	st. taper
-16.26	↓	34.39
-14.81	↓	34.24
-12.09	↓	34.85
-8.18	↓	36.47
-5.99	↓	37.08
-5.18	↓	37.22
-4.12	↓	37.03
-1.85	↓	36.17
	↓	st. taper
23.01	21.83	22.83
extension	parallel	parallel
46.05	21.83	22.83

LIST OF SYMBOLS

A_j	nozzle area at the central and annular exits
A_p	area of the jet air supply pipe upstream of the nozzle
C_p	pressure coefficient on the wing surface
C^*_p	pressure coefficient equivalent to a Mach number of one
c	wing chord (see Fig 2)
D_e	outer cowl diameter at nozzle exit (see Fig 2)
H_j	mean pitot pressure at the annular exit of the nozzle
H_{j_L}	local pitot pressure at the nozzle exit
H_p	pitot pressure in the air supply pipe to the nozzle
H_∞	pitot pressure in the free stream
M_∞	Mach number in the free stream
p_∞	static pressure in the free stream
R	outer cowl radius at the nozzle exit
r	radial position of pitot at the nozzle exit
x	distance along wing chord from leading edge
x_j	distance along nozzle centre line downstream from outer cowl exit (Fig 1)
x_n	distance along nozzle centre line from outer cowl exit to wing leading edge (Fig 2)
y_n	distance from nozzle centre line to wing leading edge (Fig 2)
z_n	distance from upper lip of outer cowl to wing leading edge (Fig 2)
ΔC_p	incremental change in wing pressure coefficient due to adding the nozzle with zero thrust ($H_j = H_\infty$) to the wing alone
ΔC_{p_j}	incremental change in wing pressure coefficient due to an increase in jet pressure from $H_j = H_\infty$

REFERENCES

No.	Author	Title, etc.
1	D.J. Raney A.G. Kurn J.A. Bagley	Wind-tunnel investigation of jet interference for underwing installation of high bypass ratio engines. ARC CP No.1044 (1968)
2	J.A. Bagley	Wind tunnel experiments on the interference between a jet and a wing at subsonic speeds. AGARD CP No.35, Paper 22 (RAE Technical Memorandum Aero 1079) (1968)
3	A.G. Kurn	A further wind tunnel investigation of underwing jet interference. ARC CP No.1156 (1969)
4	T.D. Coombes	A model technique for exhaust system performance testing. AGARD CP No.150, Paper 17 (1974)
5	H.C. Garner (editor)	Subsonic wind tunnel wall corrections. Chapter 6: Wall interference in tunnels with ventilated walls. AGARDograph 109 (1966)
6	B.C. Hardy	A computer program to estimate the interference on a wing due to an engine nacelle at subsonic speeds. Part 1 - description of the method. RAE Technical Report 75074, ARC 36450 (1975)
7	G. Pauley	Interim note on tests with a wing-mounted fan nacelle with fan jet simulated by cold air blowing and alternatively by a gas generator shroud. ARC CP No.1111 (1968)
8	B. Munniksma F. Joarsma	Jet interference of a podded engine installation at cruise conditions. AGARD CP No.150, Paper 7 (1974)
9	C. Young	A theoretical investigation of supersonic jets in subsonic flow fields. ARC CP No.1256 (1972)
10	A.F. Jones M.C.P. Firmin	On the calculation of viscous effects on the supercritical flow over an aerofoil. RAE Technical Report 72233, ARC 34335 (1973)

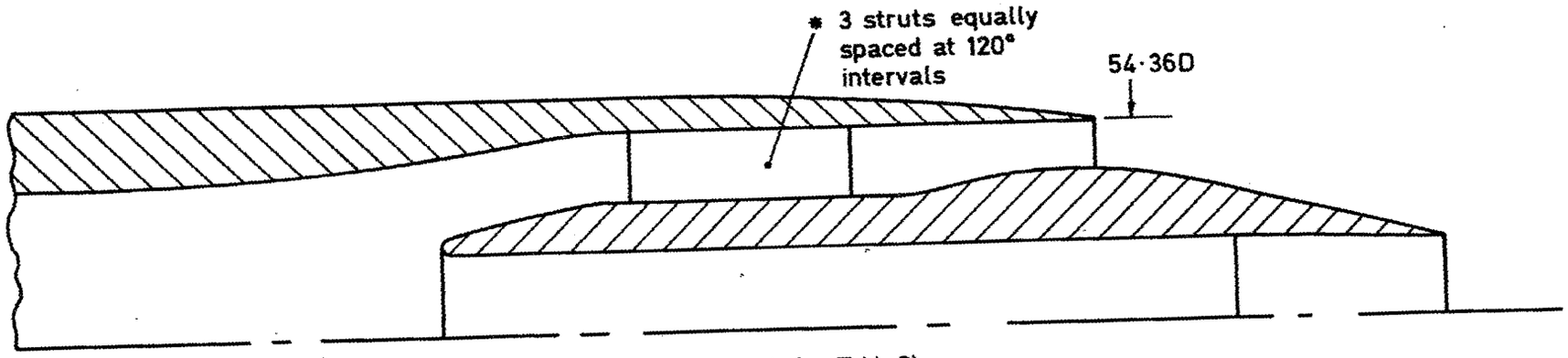

a RAE nozzle (see Table 2)

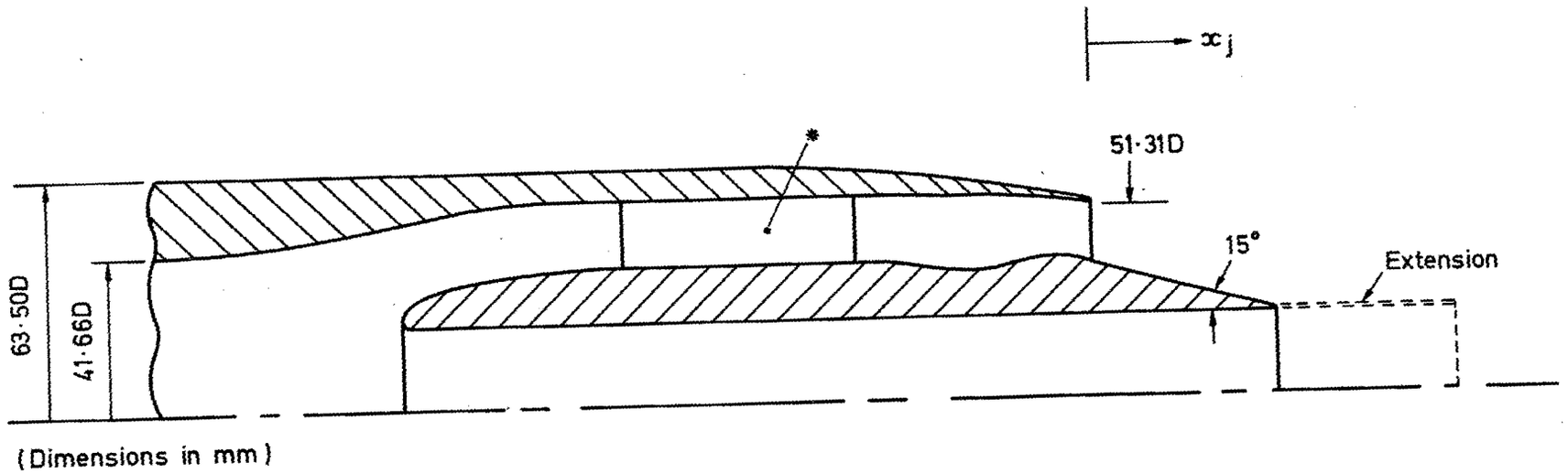

b 15° afterbody nozzle (see Table 3)

Fig 1 Nozzles

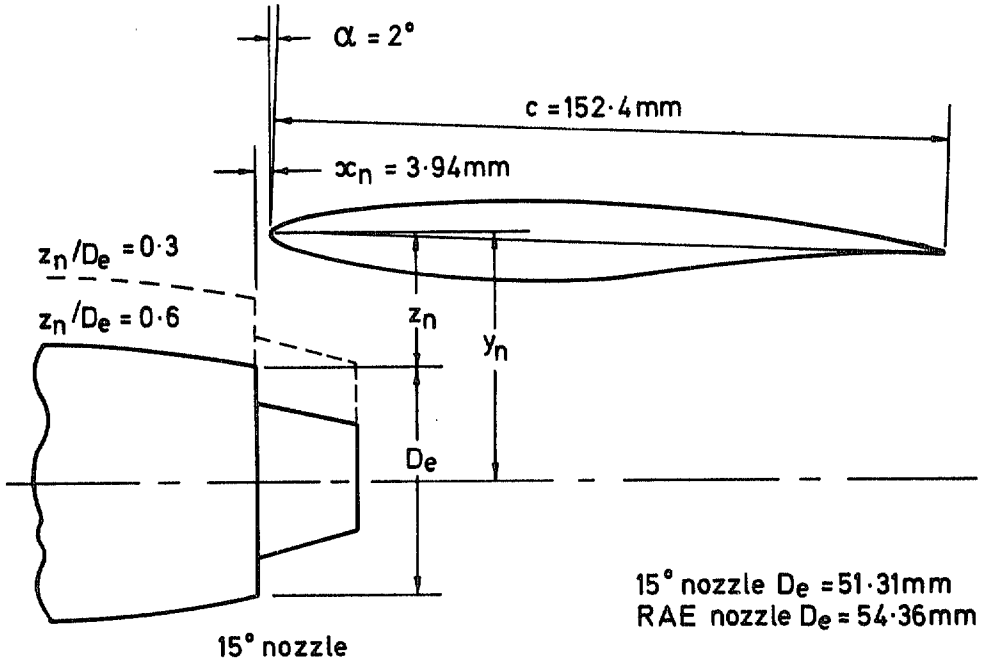

Nozzle	c/D_e	x_n/D_e	y_n/D_e	z_n/D_e	M_∞
RAE	2·80	0·072	0·80	0·30	0·72 0·78
			1·11	0·61	0·72 0·78 0·80 0·82 0·84
15°	2·97	0·077	0·83	0·33	0·72 0·78
			1·14	0·64	0·72 0·78 0·80 0·82 0·84
15° with extension	2·97	0·077	0·83	0·33	0·72 0·78
			1·14	0·64	0·72 0·78 0·84

Fig 2 Test programme

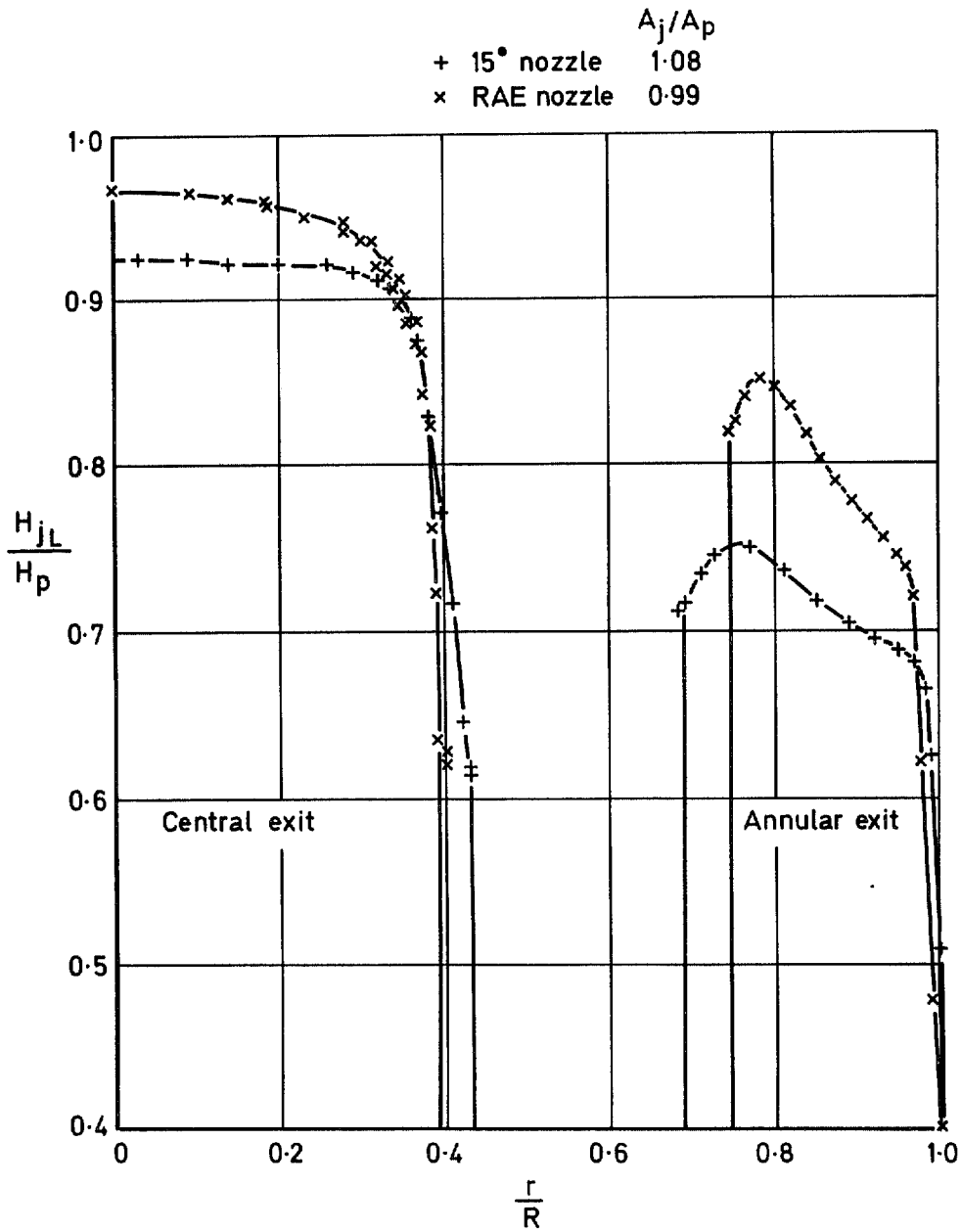

Fig 3 Pitot pressure distributions at the exits of the nozzles with sonic flow

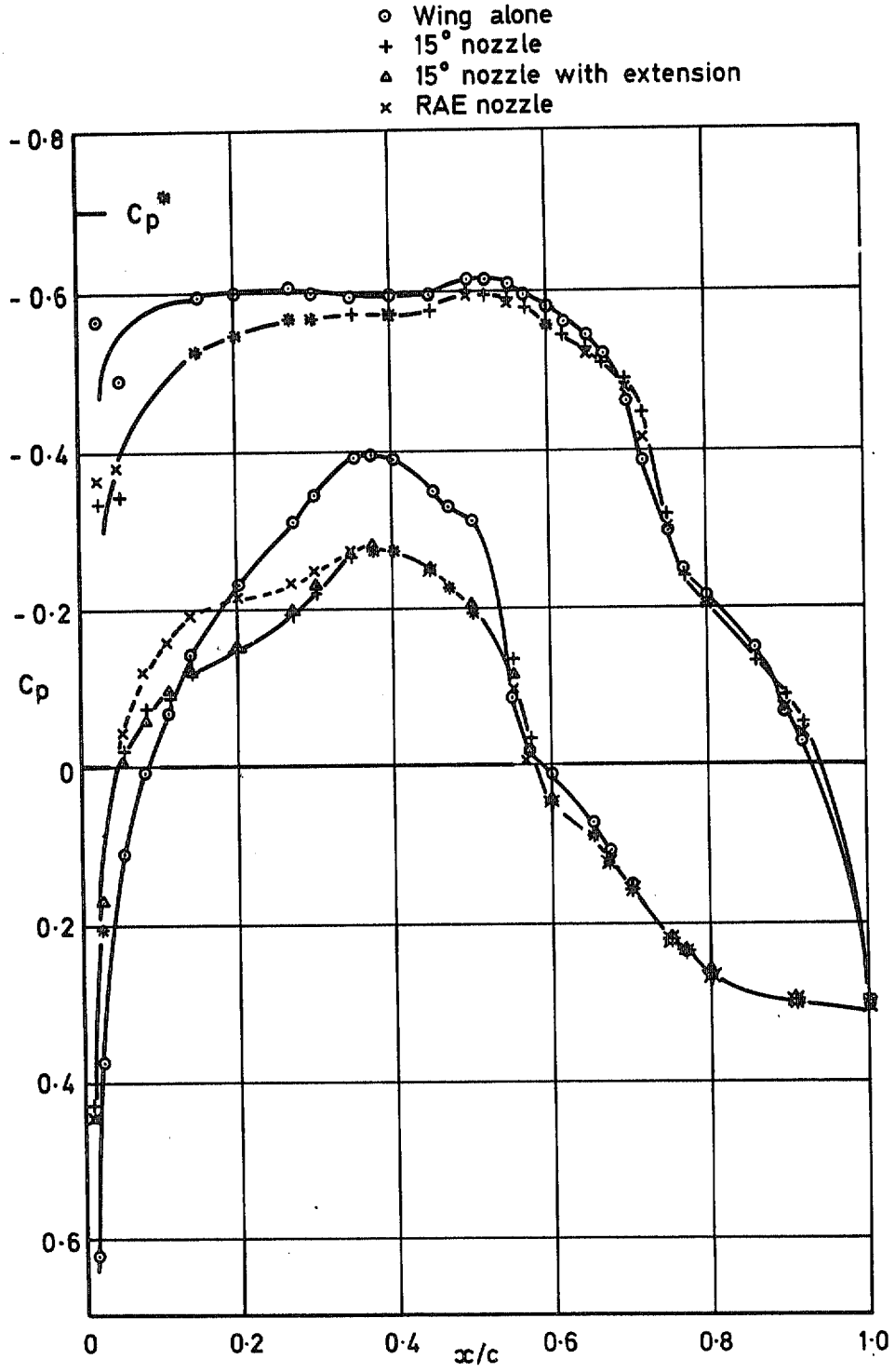

Fig 4 Wing pressure distributions for $z_n/D_e \doteq 0.6$, $M_\infty = 0.72$ and $H_j \doteq H_\infty$

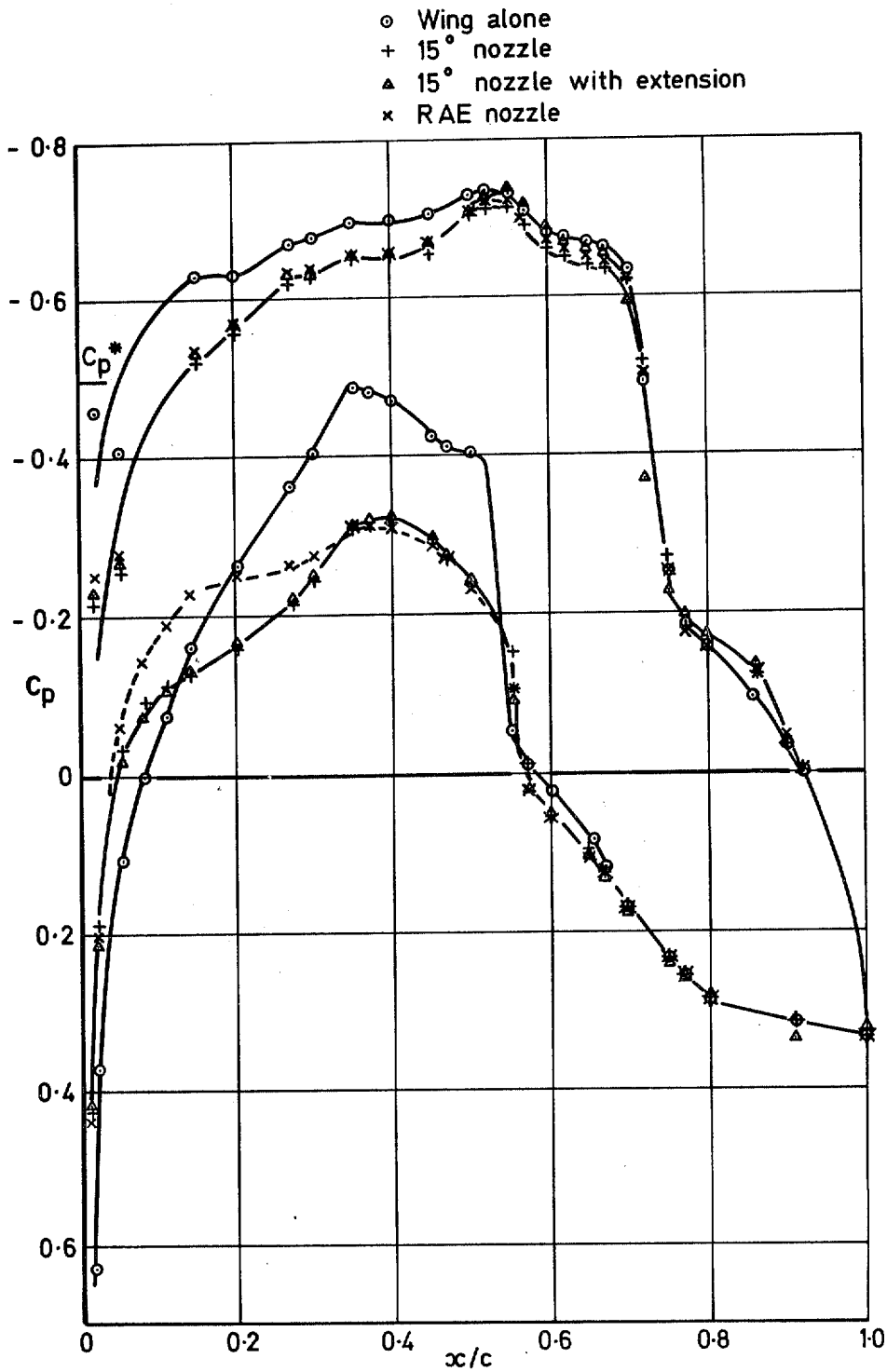

Fig 5 Wing pressure distributions for $z_n/D_e \triangleq 0.6$, $M_\infty = 0.78$ and $H_j \triangleq H_\infty$

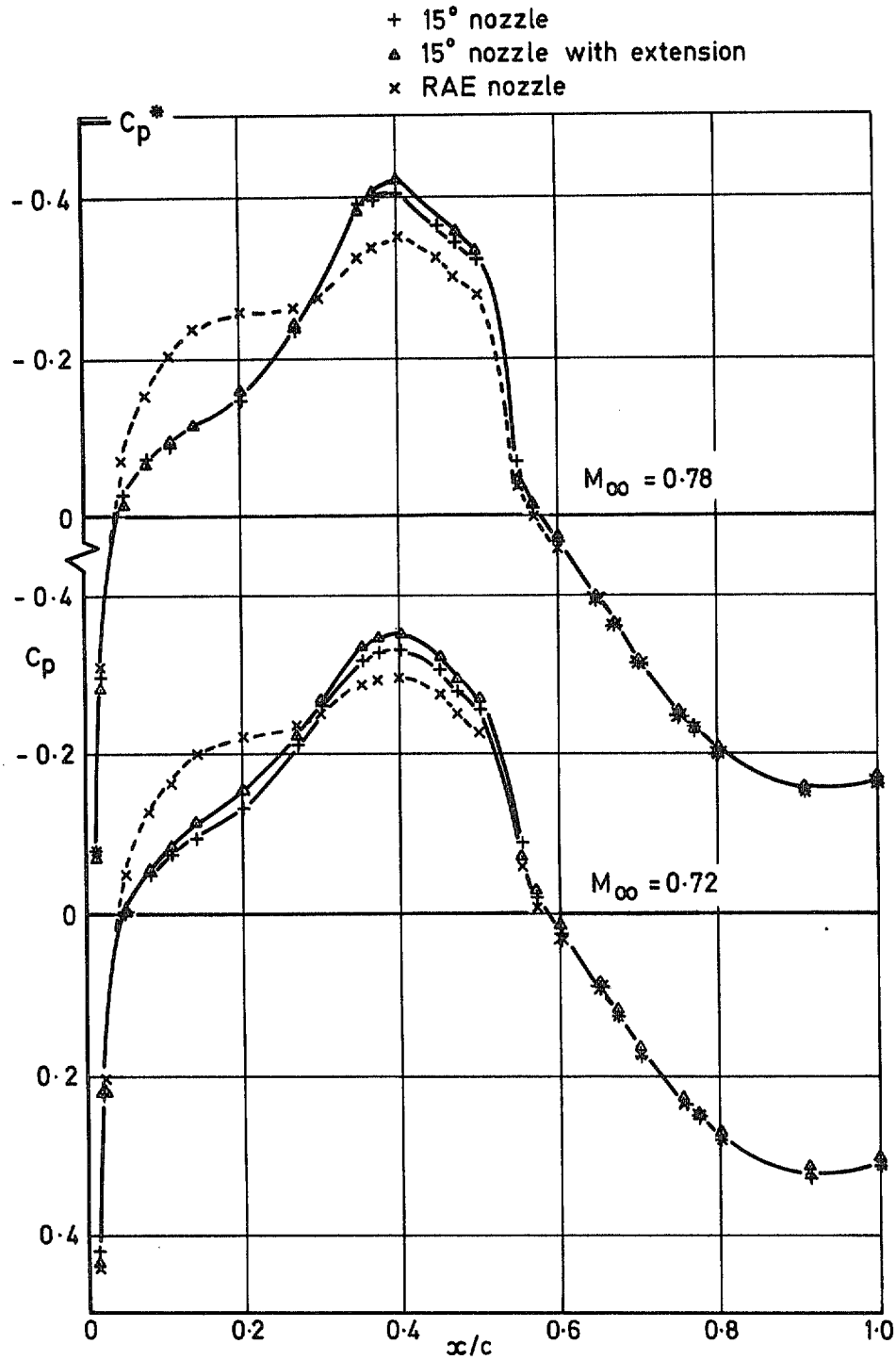

Fig 6 Pressures on wing lower surface for $z_n/D_e \doteq 0.6$ and $H_j/p_\infty \doteq 2.1$

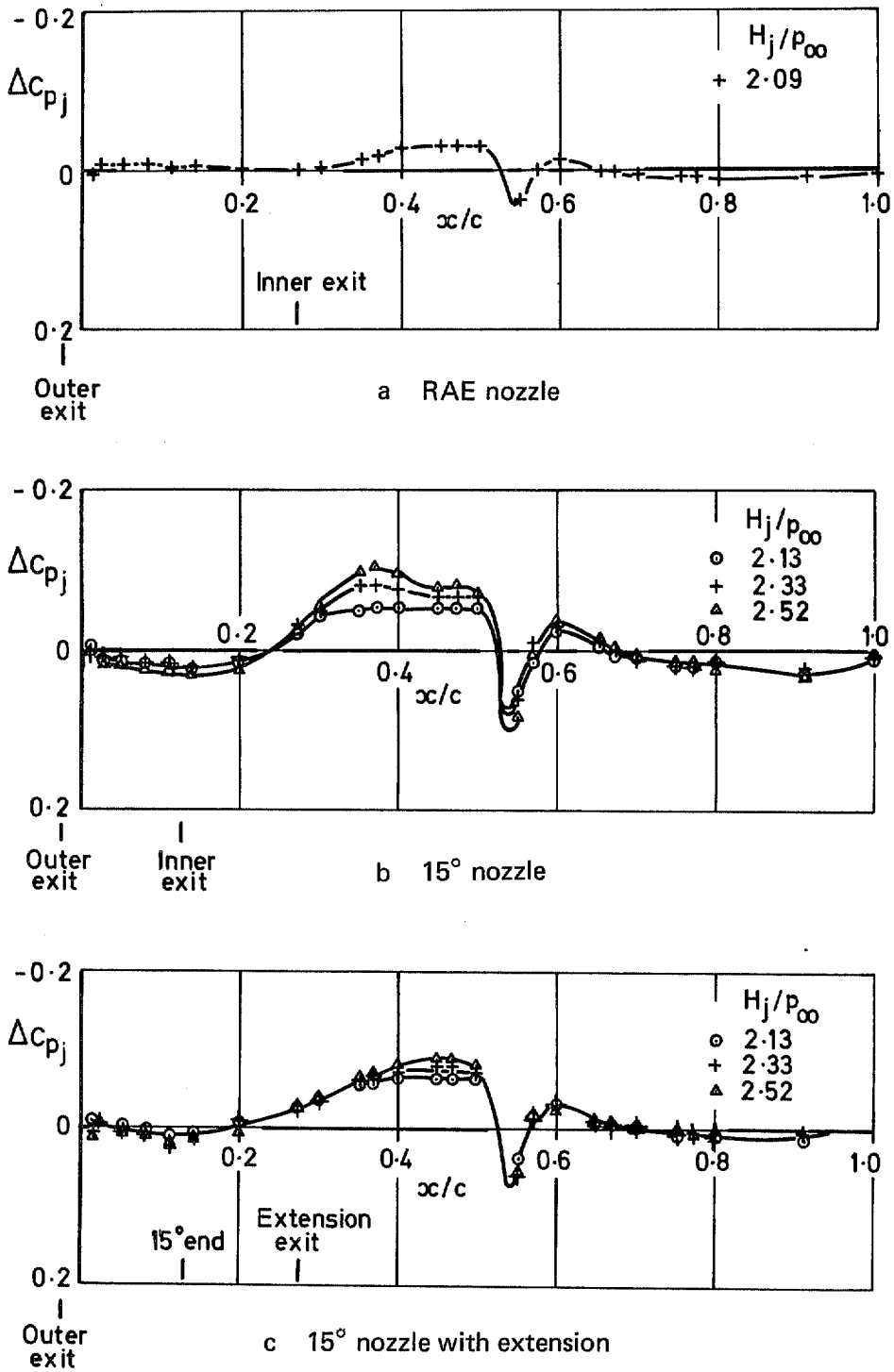

Fig 7 Interference on wing lower surface, $z_n/D_e \doteq 0.6$, $M_\infty = 0.72$

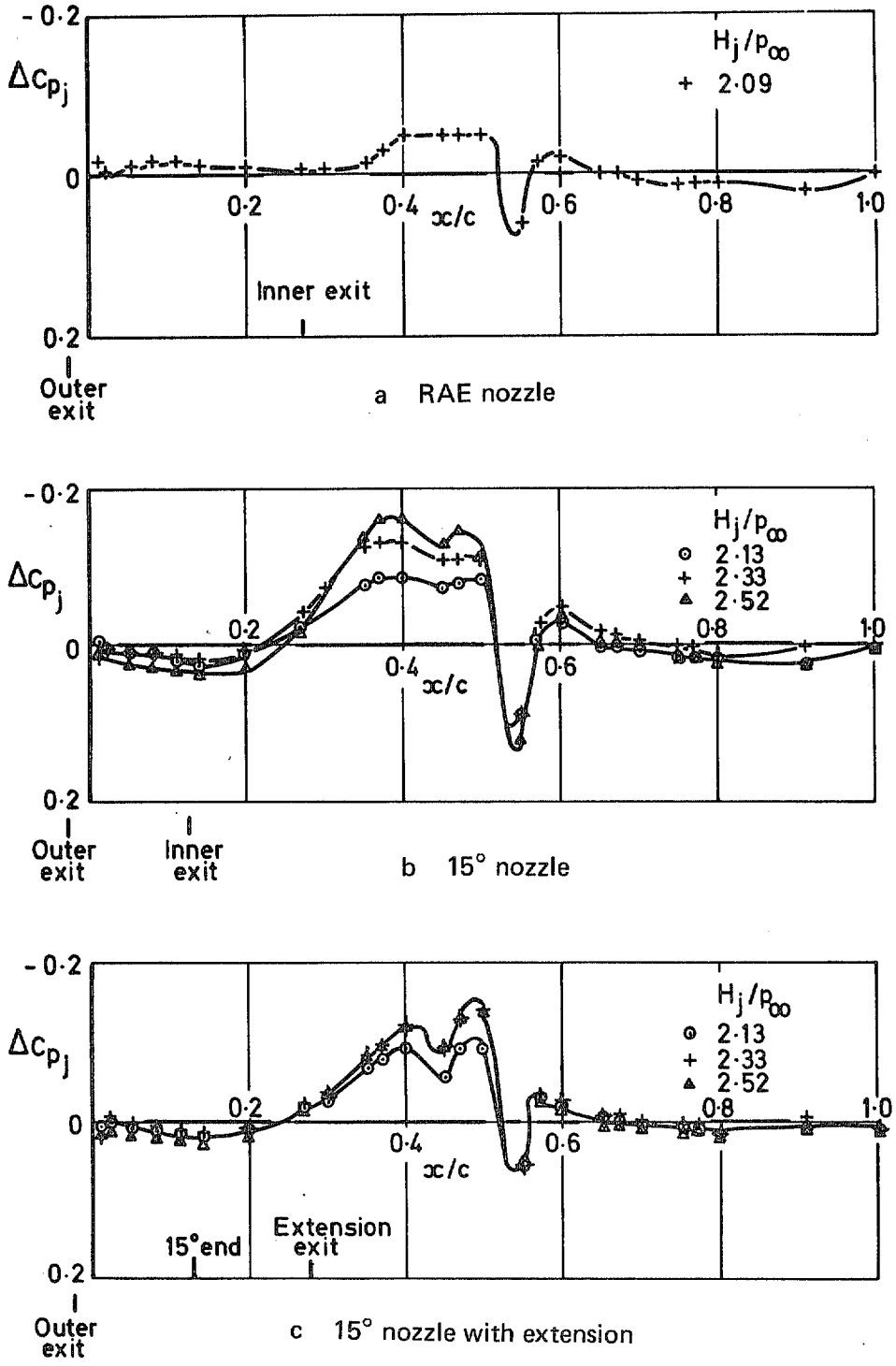

Fig 8 Interference on wing lower surface, $z_n/D_e \simeq 0.6$, $M_\infty = 0.78$

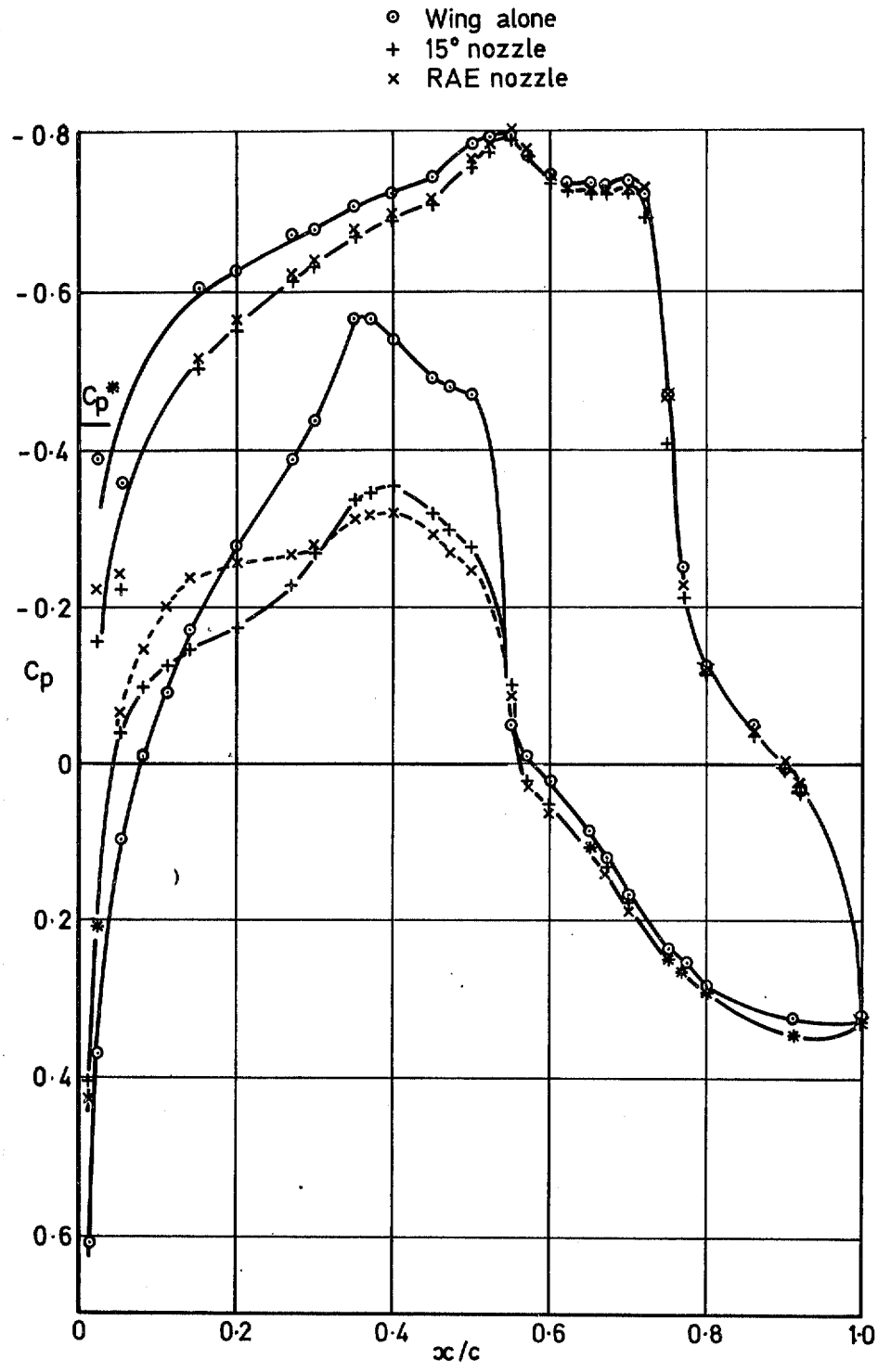

Fig 9 Wing pressure distributions for $z_n/D_e \simeq 0.6$, $M_\infty = 0.80$ and $H_j \simeq H_\infty$

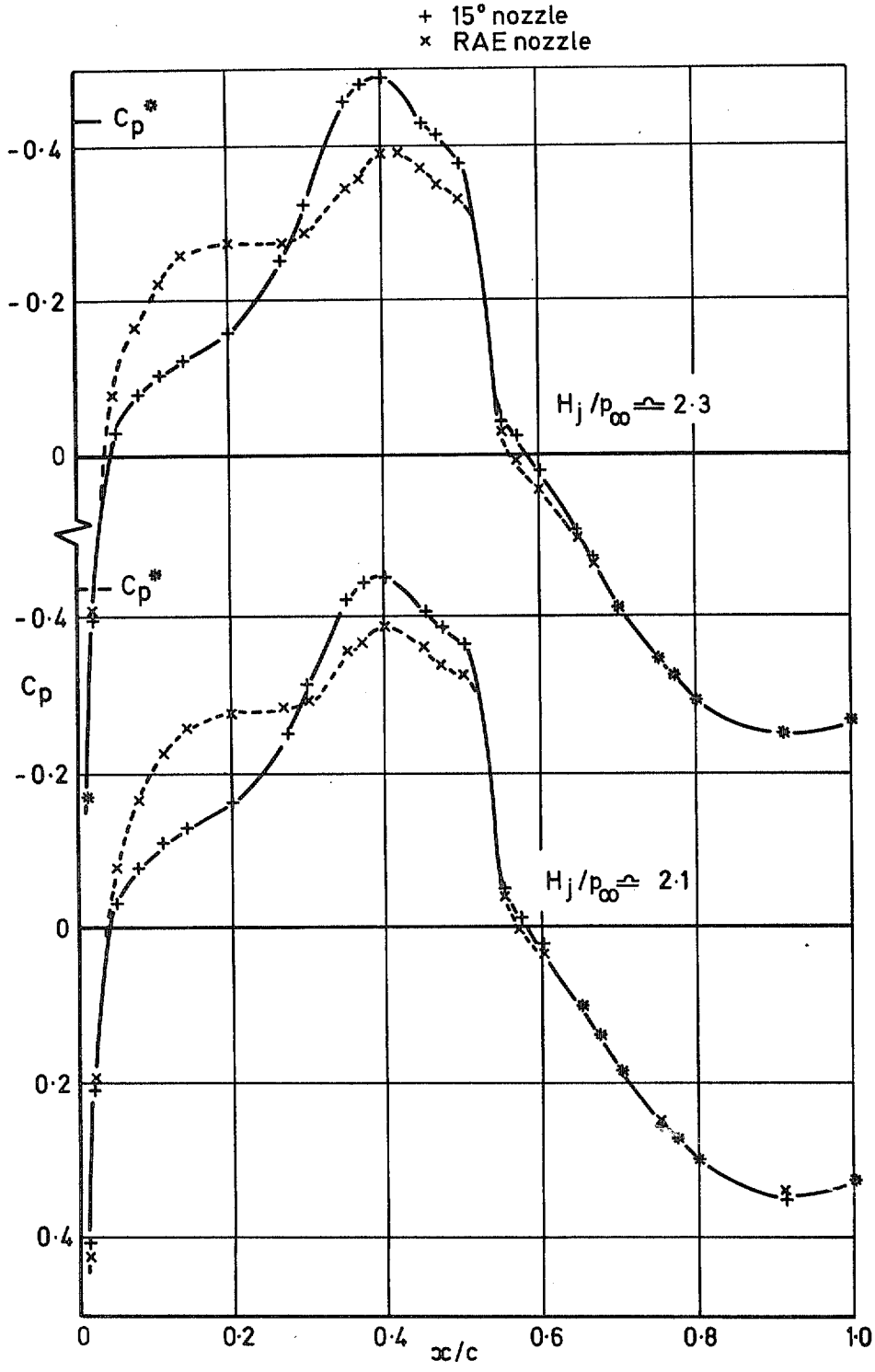

Fig 10 Pressures on wing lower surface for $z_n/D_e \simeq 0.6$ and $M_\infty = 0.80$

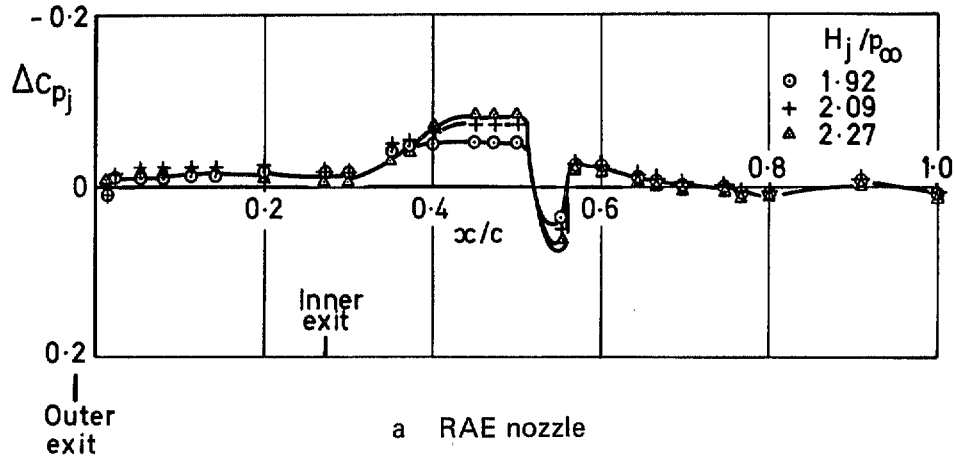

a RAE nozzle

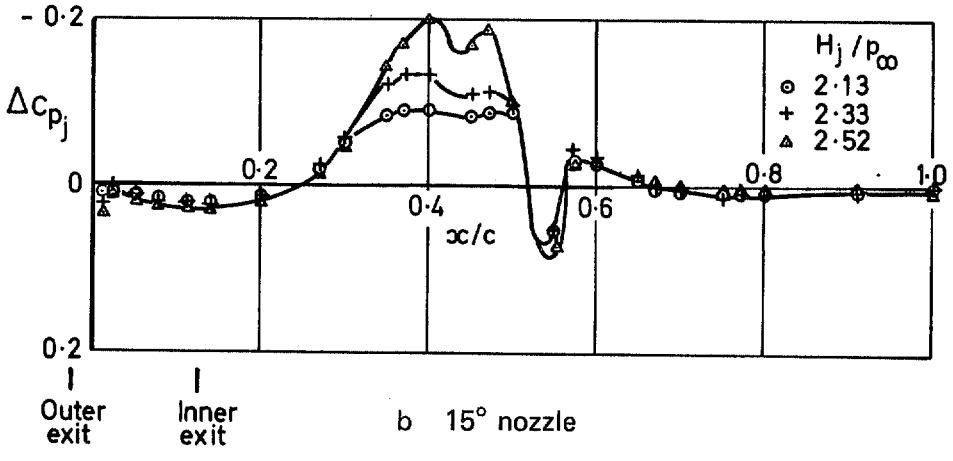

b 15° nozzle

Fig 11 Interference on wing lower surface, $z_n/D_e \triangleq 0.6$ and $M_\infty = 0.80$

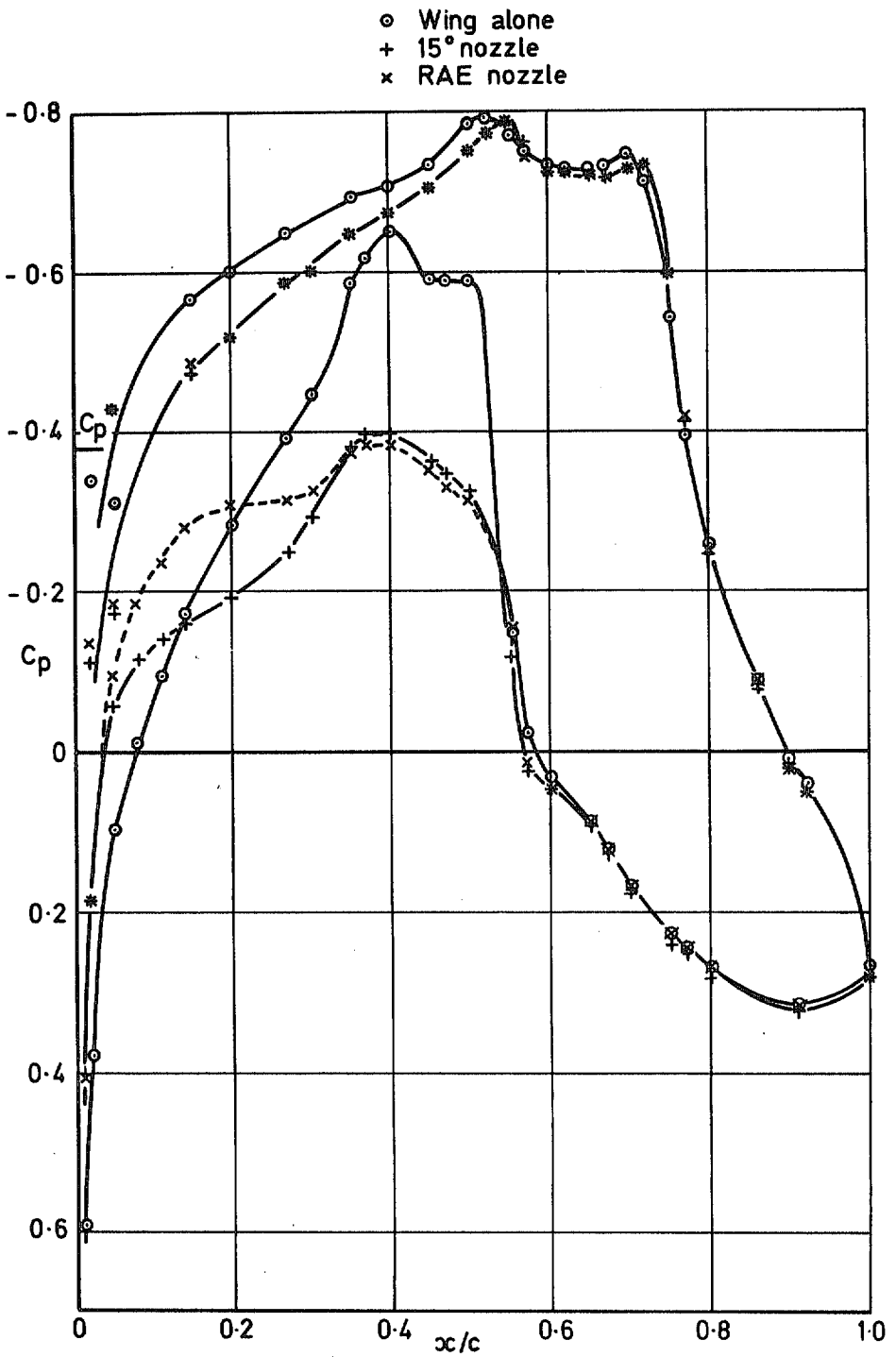

Fig 12 Wing pressure distributions for $z_n/D_e \simeq 0.6$, $M_\infty = 0.82$ and $H_j \simeq H_\infty$

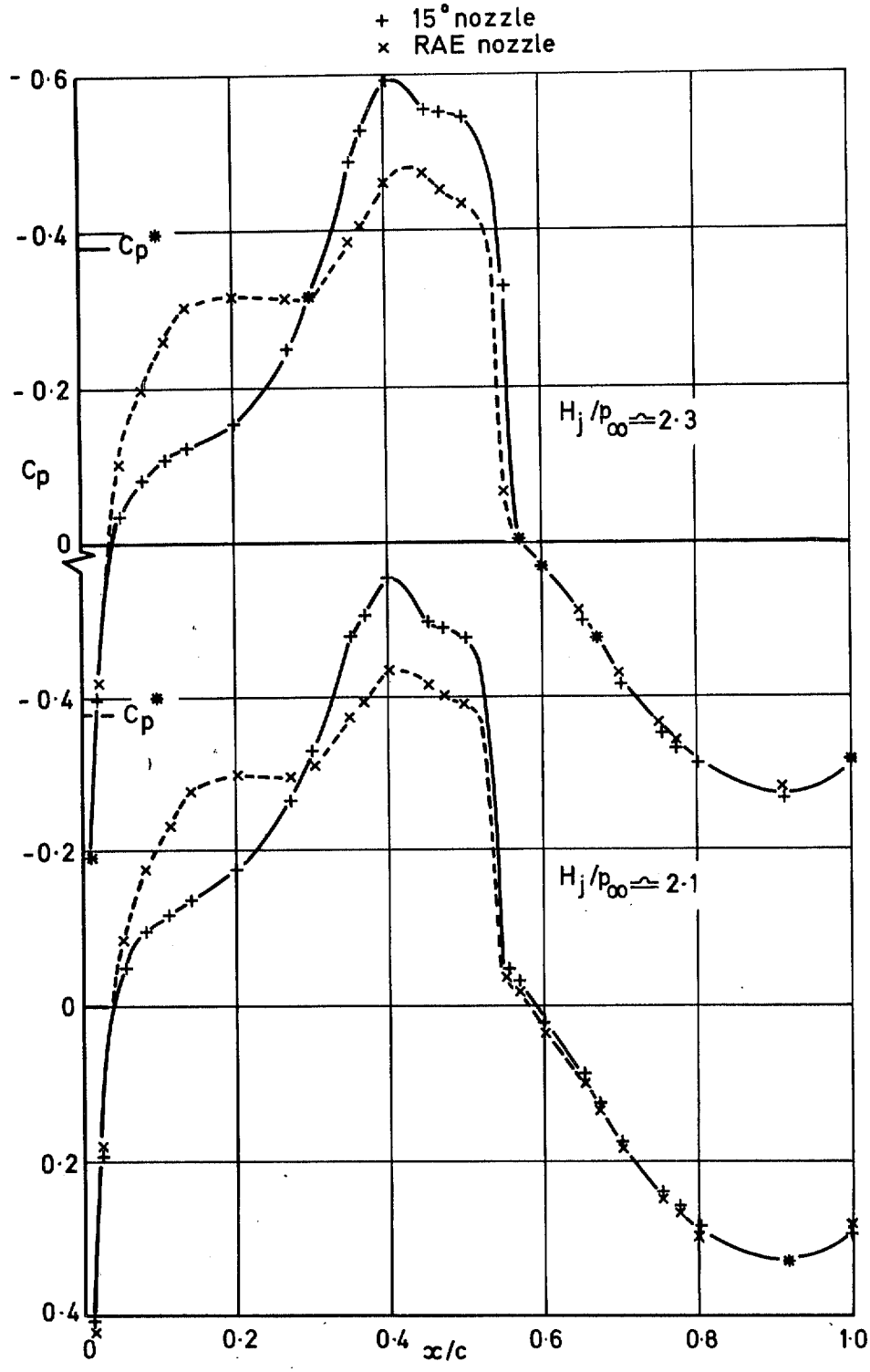

Fig 13 Pressures on wing lower surface for $z_n/D_e \simeq 0.6$ and $M_\infty = 0.82$

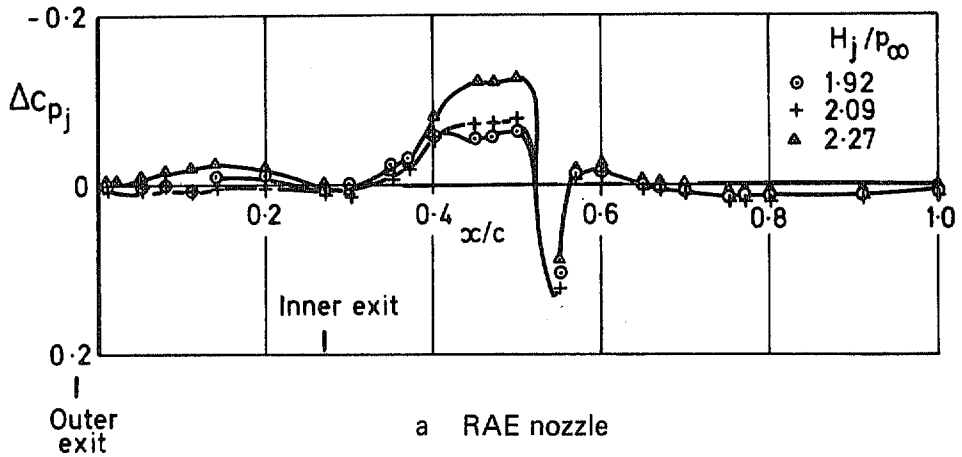

a RAE nozzle

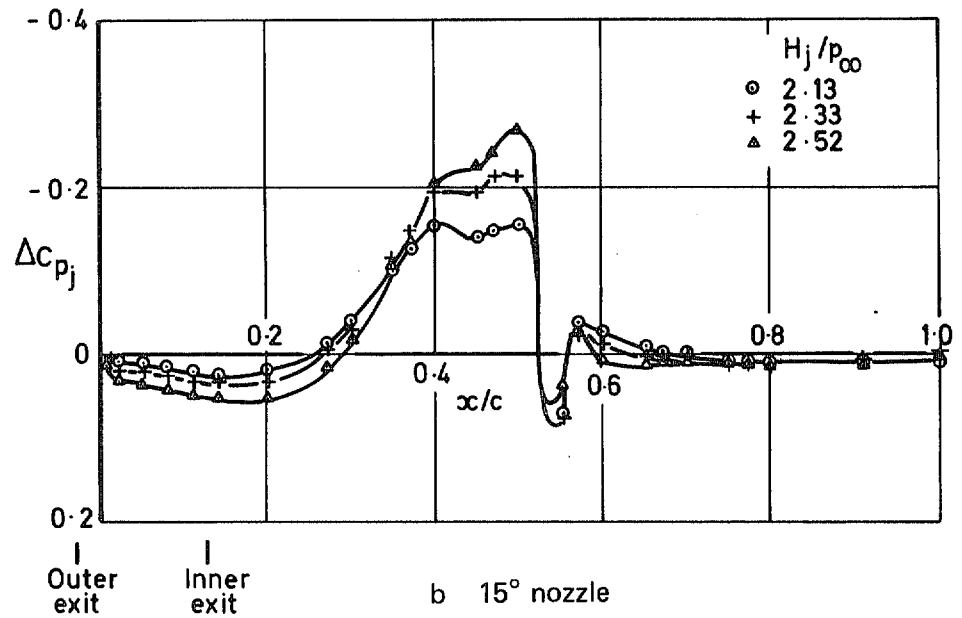

b 15° nozzle

Fig 14 Interference on wing lower surface, $z_n/D_e \doteq 0.6$ and $M_\infty = 0.82$

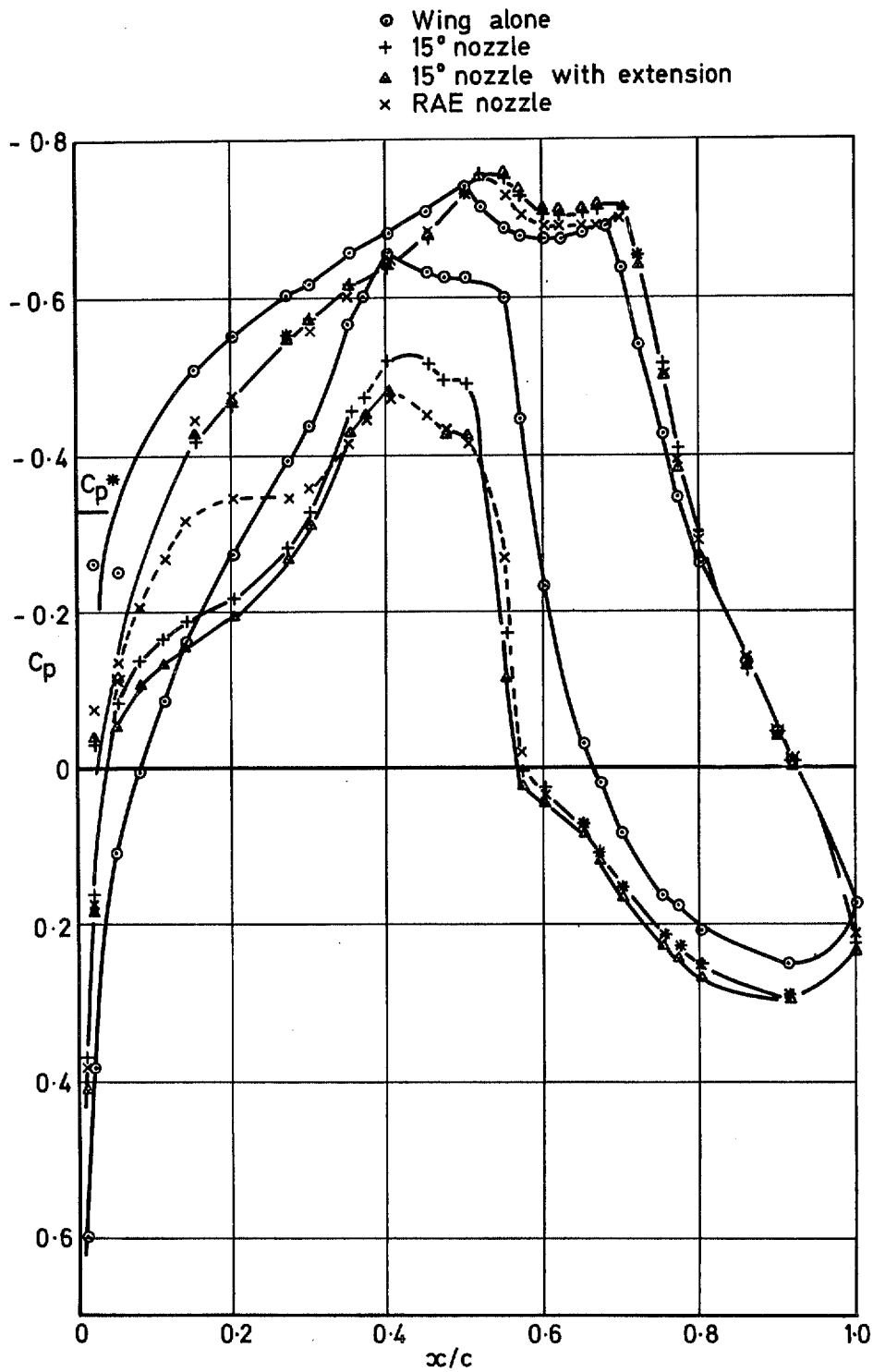

Fig 15 Wing pressure distributions for $z_n/D_e \triangleq 0.6$, $M_\infty = 0.84$ and $H_j \triangleq H_\infty$

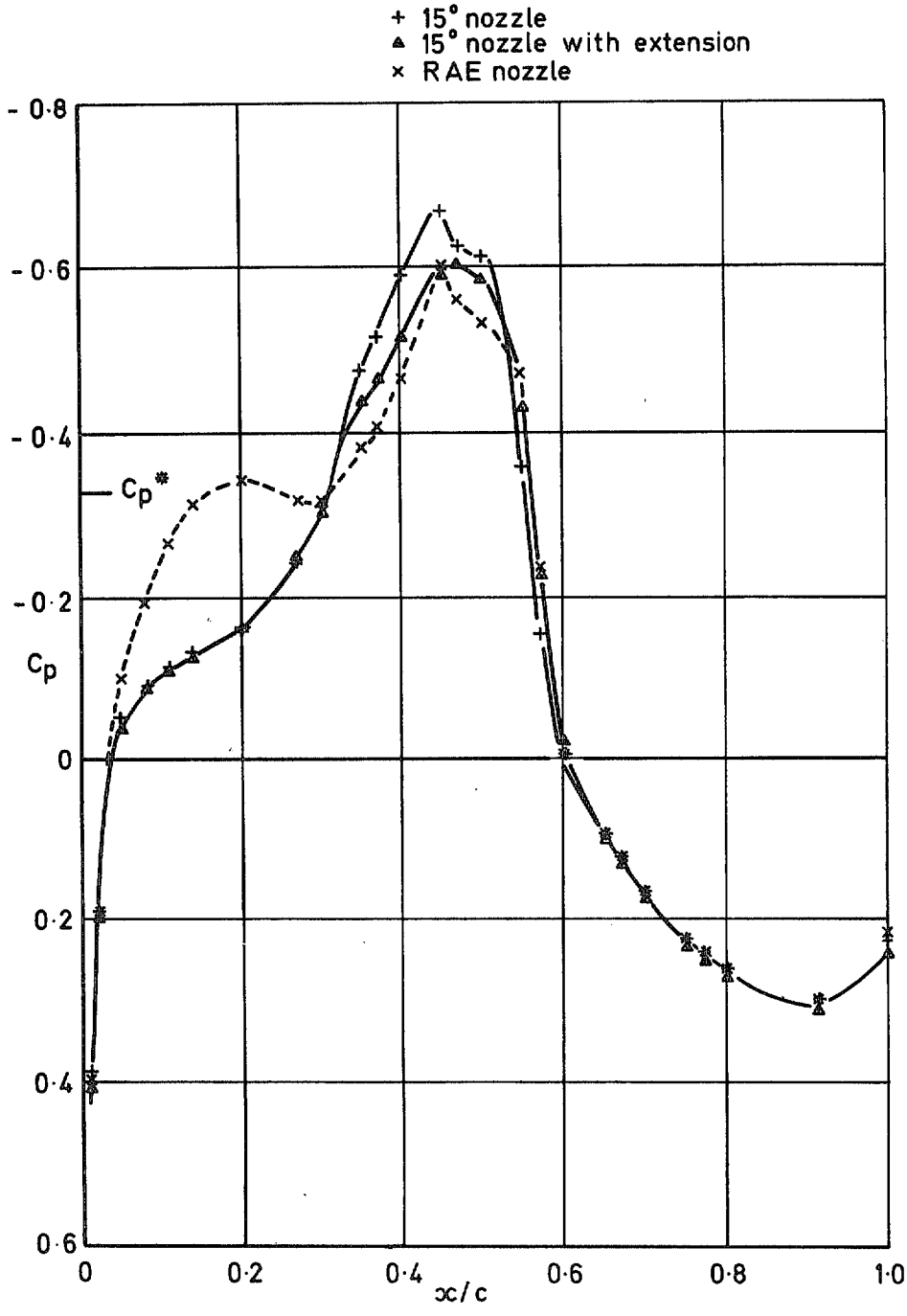

Fig 16 Pressures on wing lower surface for $z_n/D_e \doteq 0.6$, $M_\infty = 0.84$ and $H_j/p_\infty \doteq 2.1$

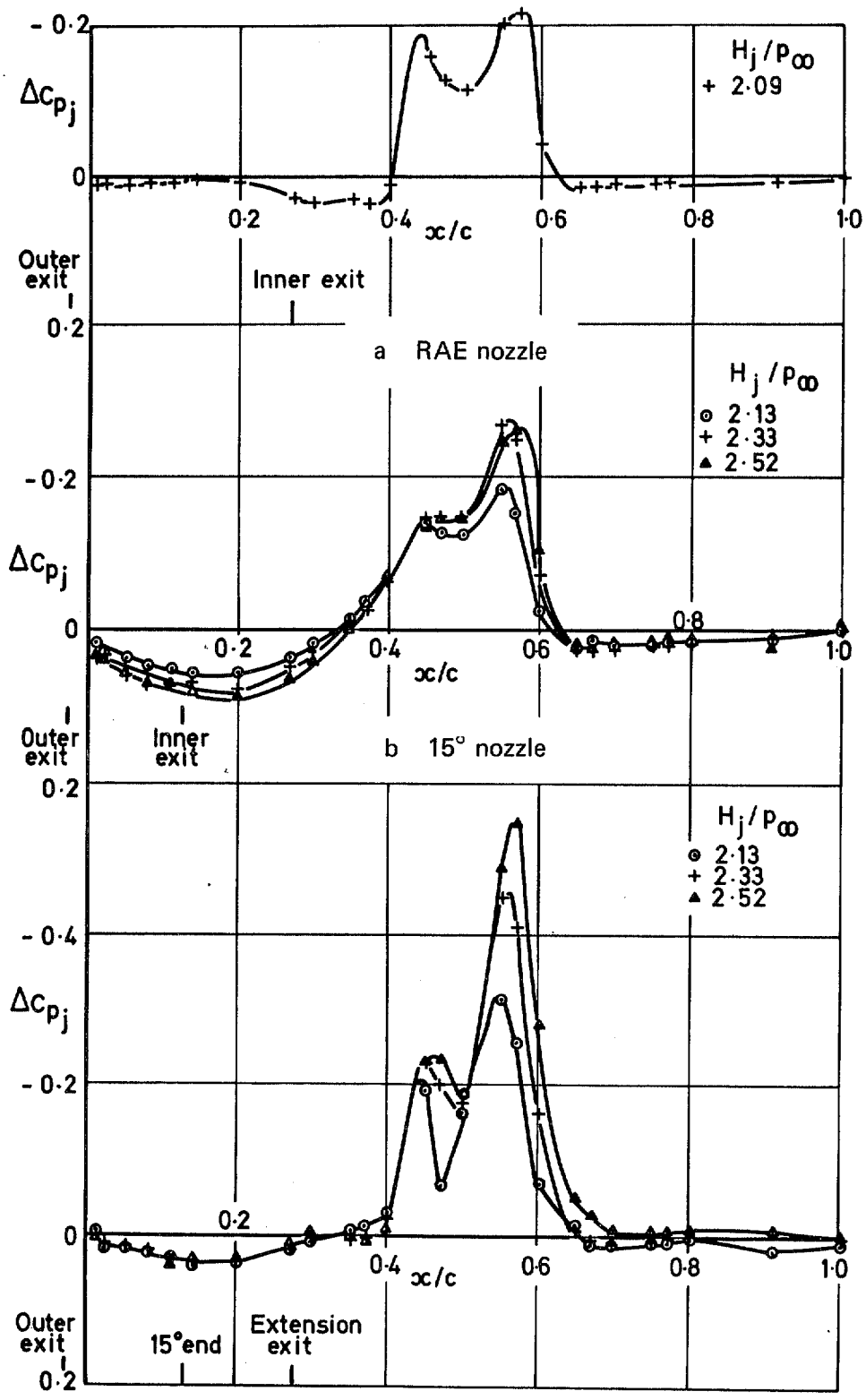

c 15° nozzle with extension

Fig 17 Interference on wing lower surface, $z_n/D_e \simeq 0.6$ and $M_\infty = 0.84$

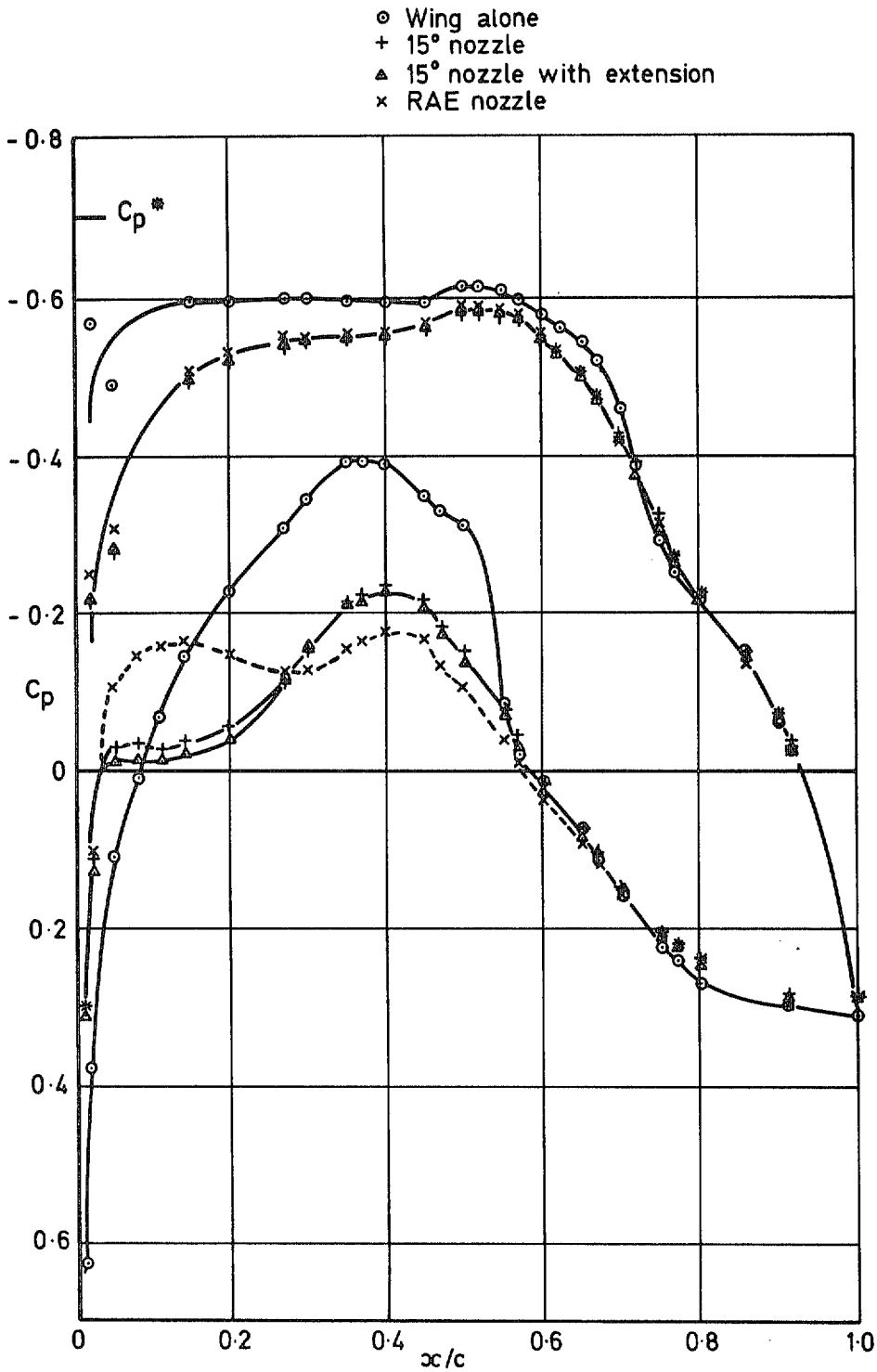

Fig 18 Wing pressure distributions for $z_n/D_e \triangleq 0.3$, $M_\infty = 0.72$ and $H_j \triangleq H_\infty$

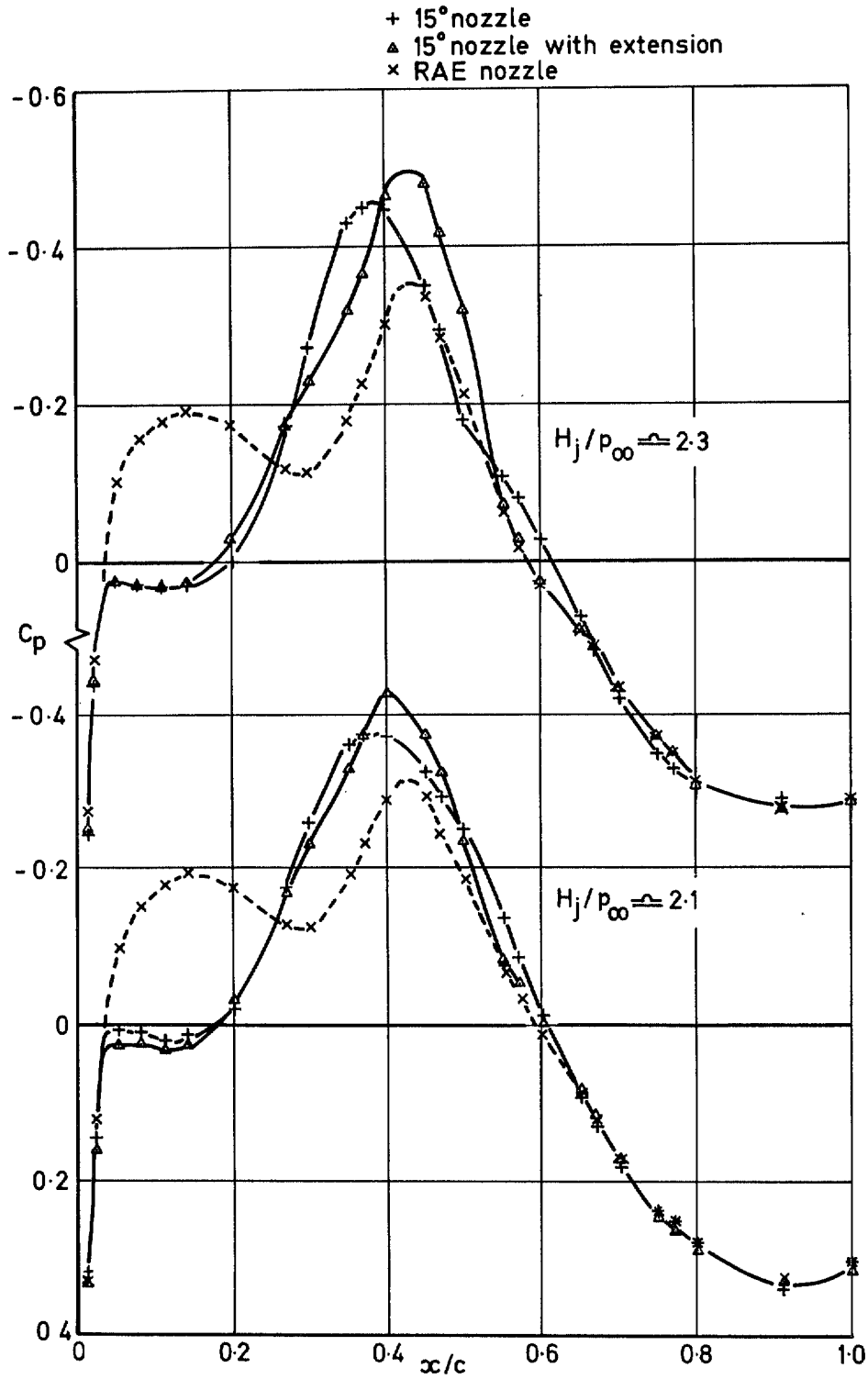

Fig 19 Pressures on wing lower surface for $z_n/D_e \simeq 0.3$ and $M_\infty = 0.72$

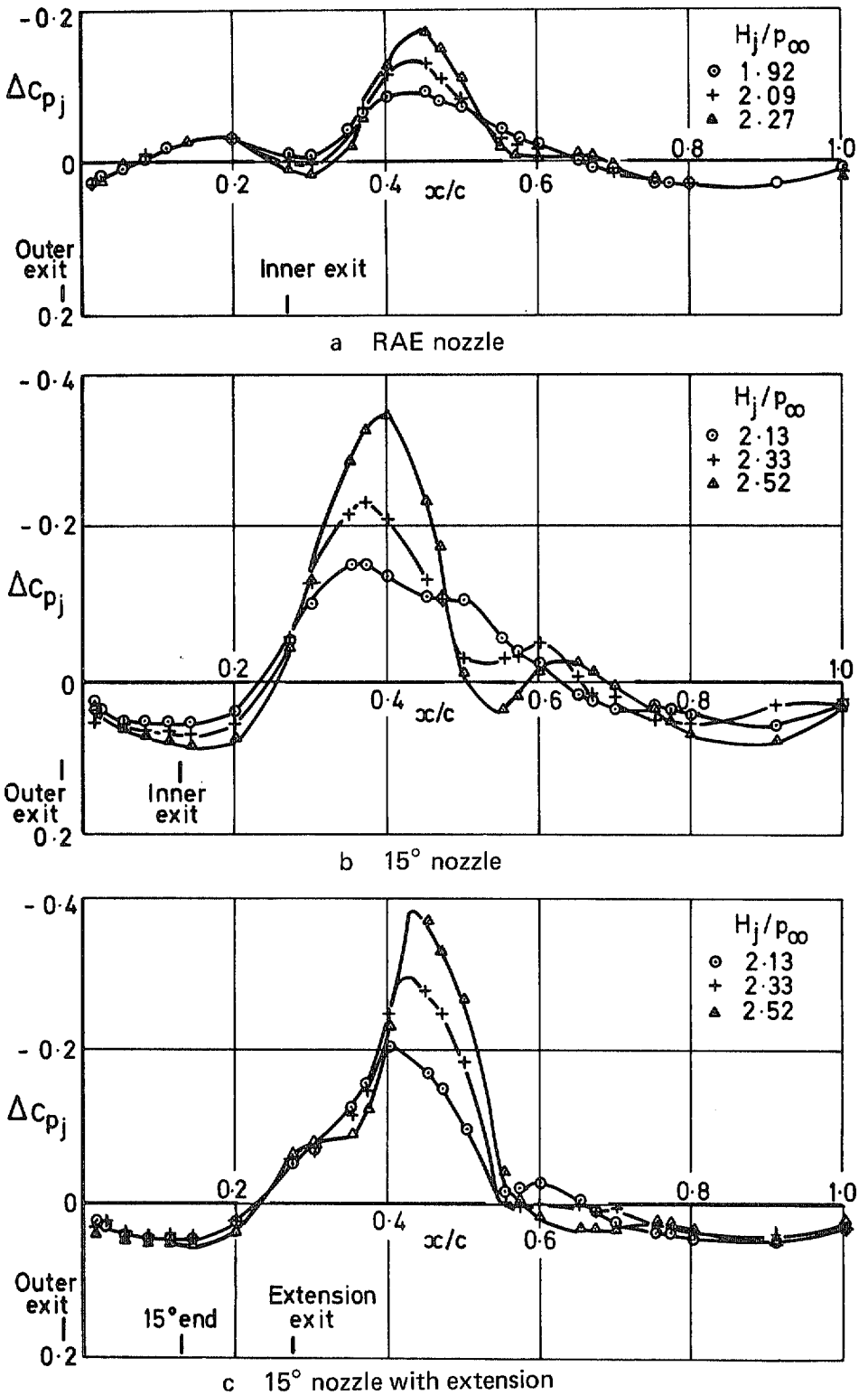

Fig 20 Interference on wing lower surface, $z_n/D_e \doteq 0.3$ and $M_\infty = 0.72$

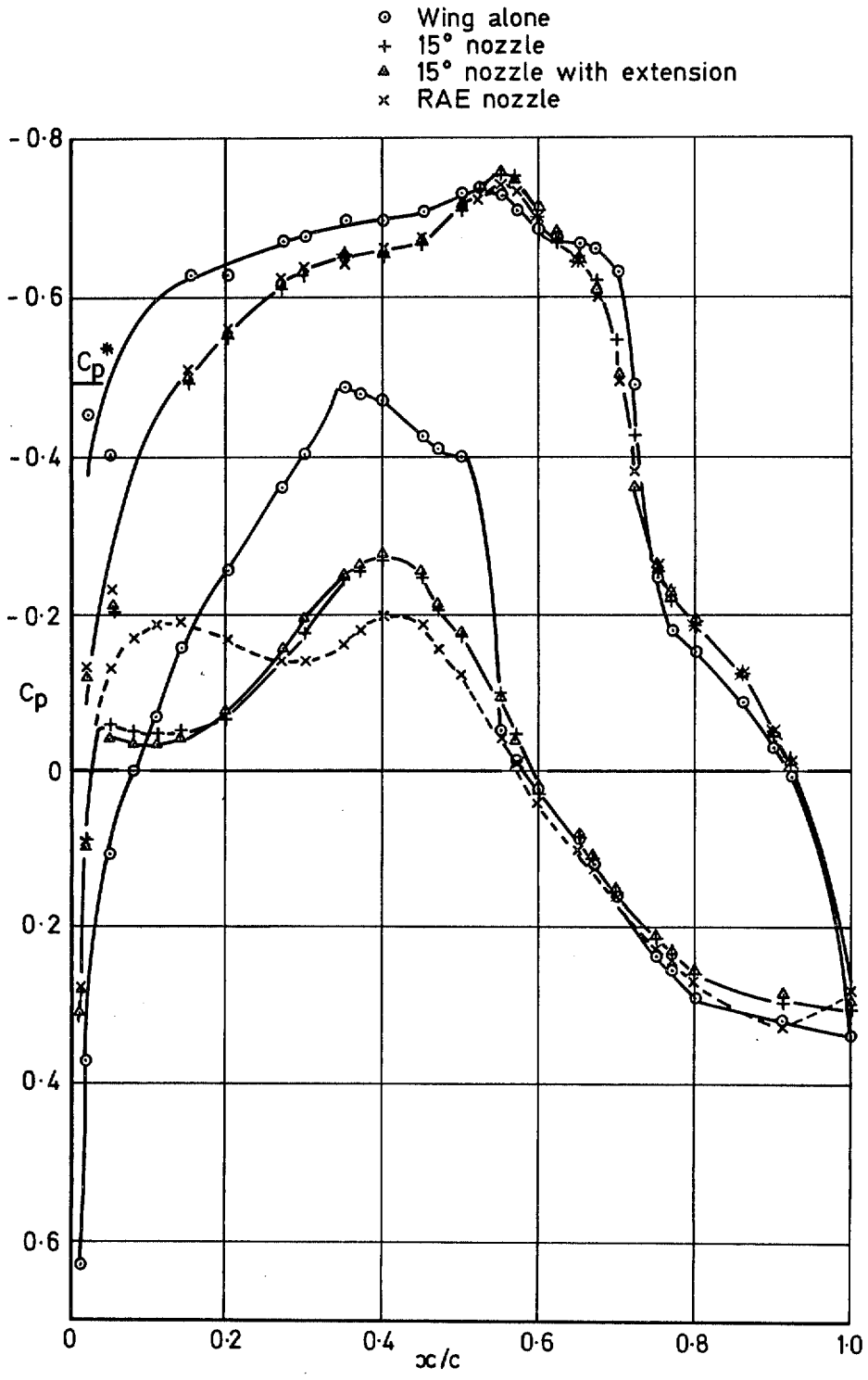

Fig 21 Wing pressure distributions for $z_n/D_e \doteq 0.3$, $M_\infty = 0.78$ and $H_j \doteq H_\infty$

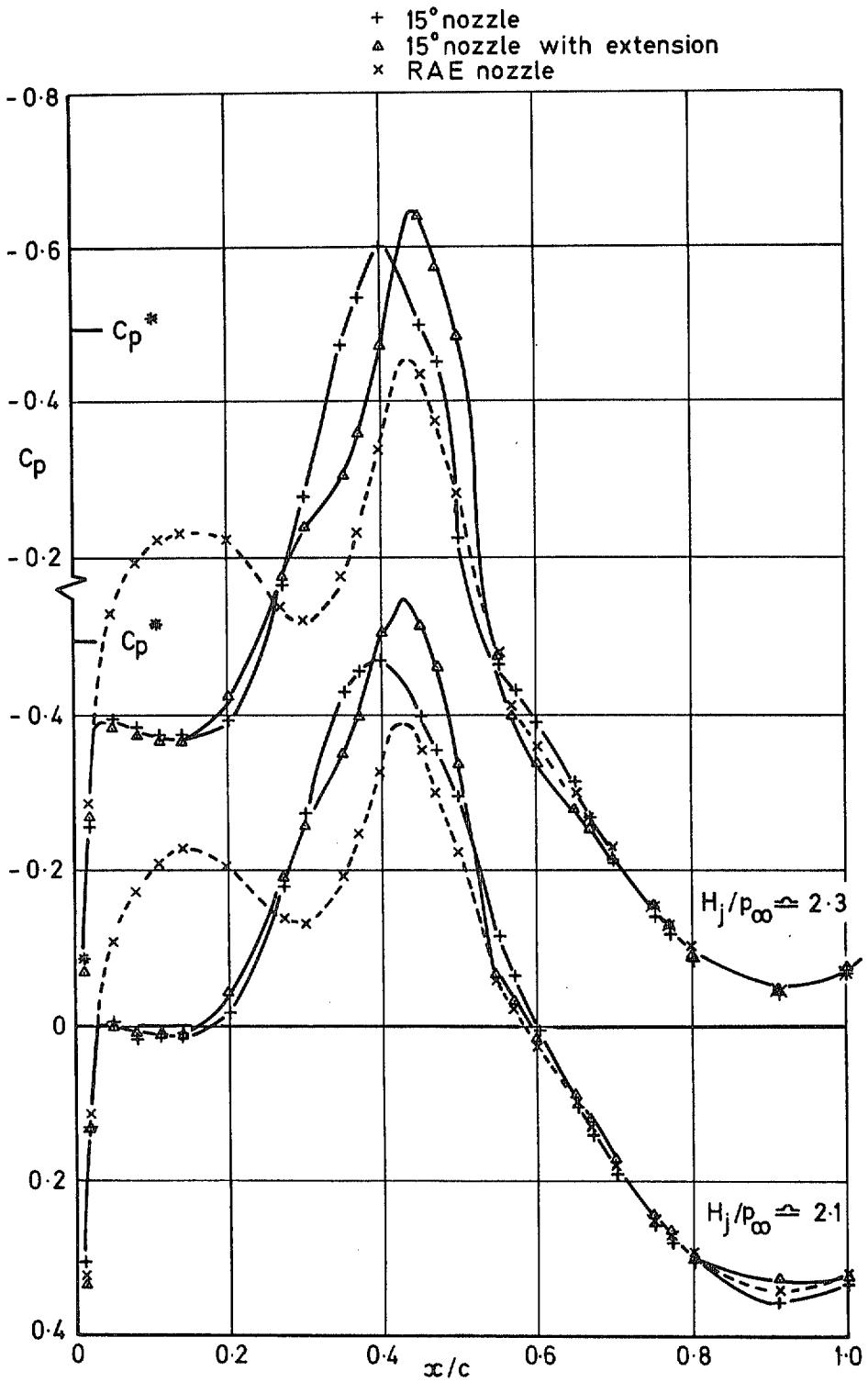

Fig 22 Pressures on wing lower surface for $z_n/D_e \simeq 0.3$ and $M_\infty = 0.78$

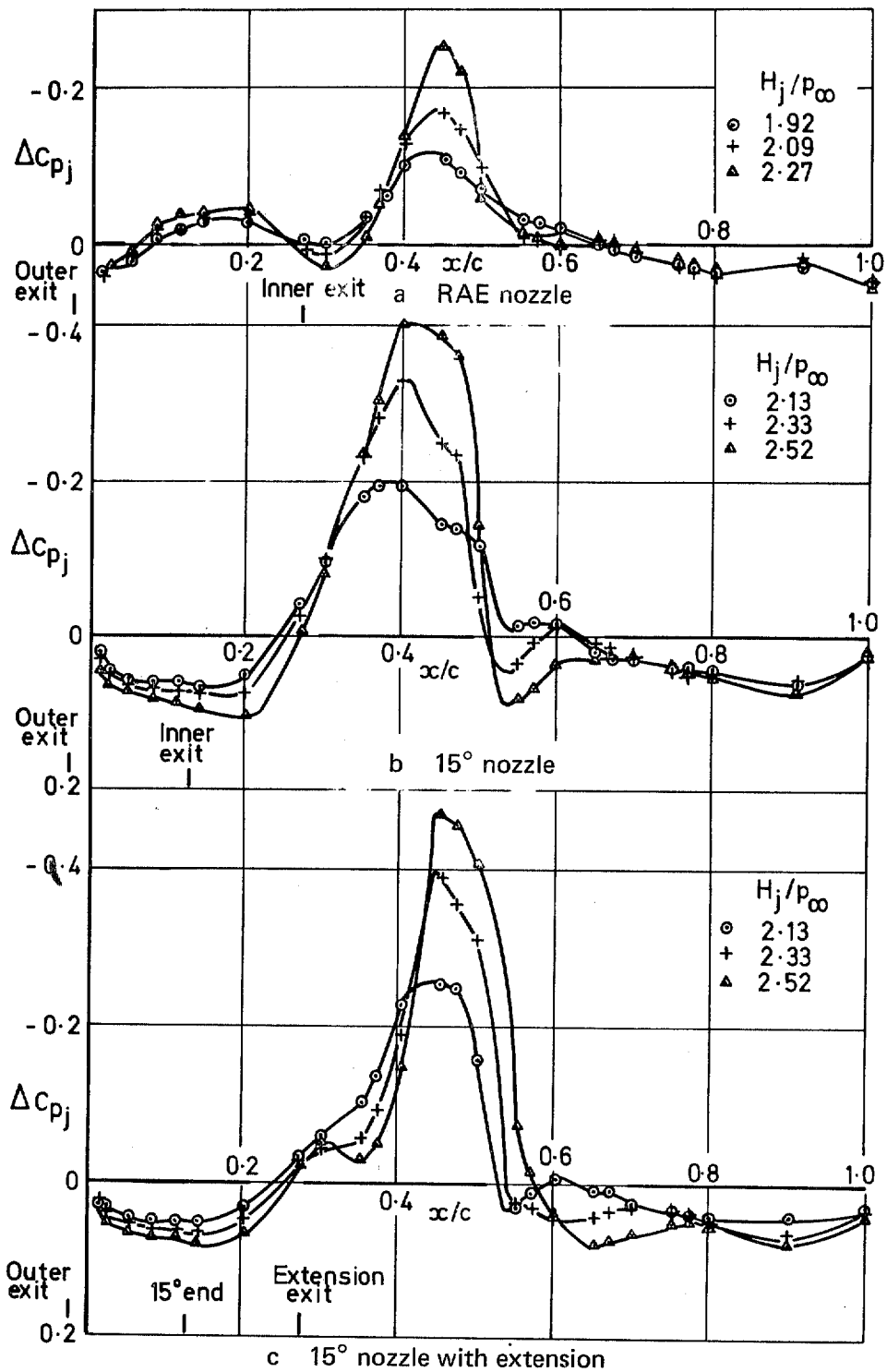

Fig 23 Interference on wing lower surface, $z_n/D_e \triangleq 0.3$ and $M_\infty = 0.78$

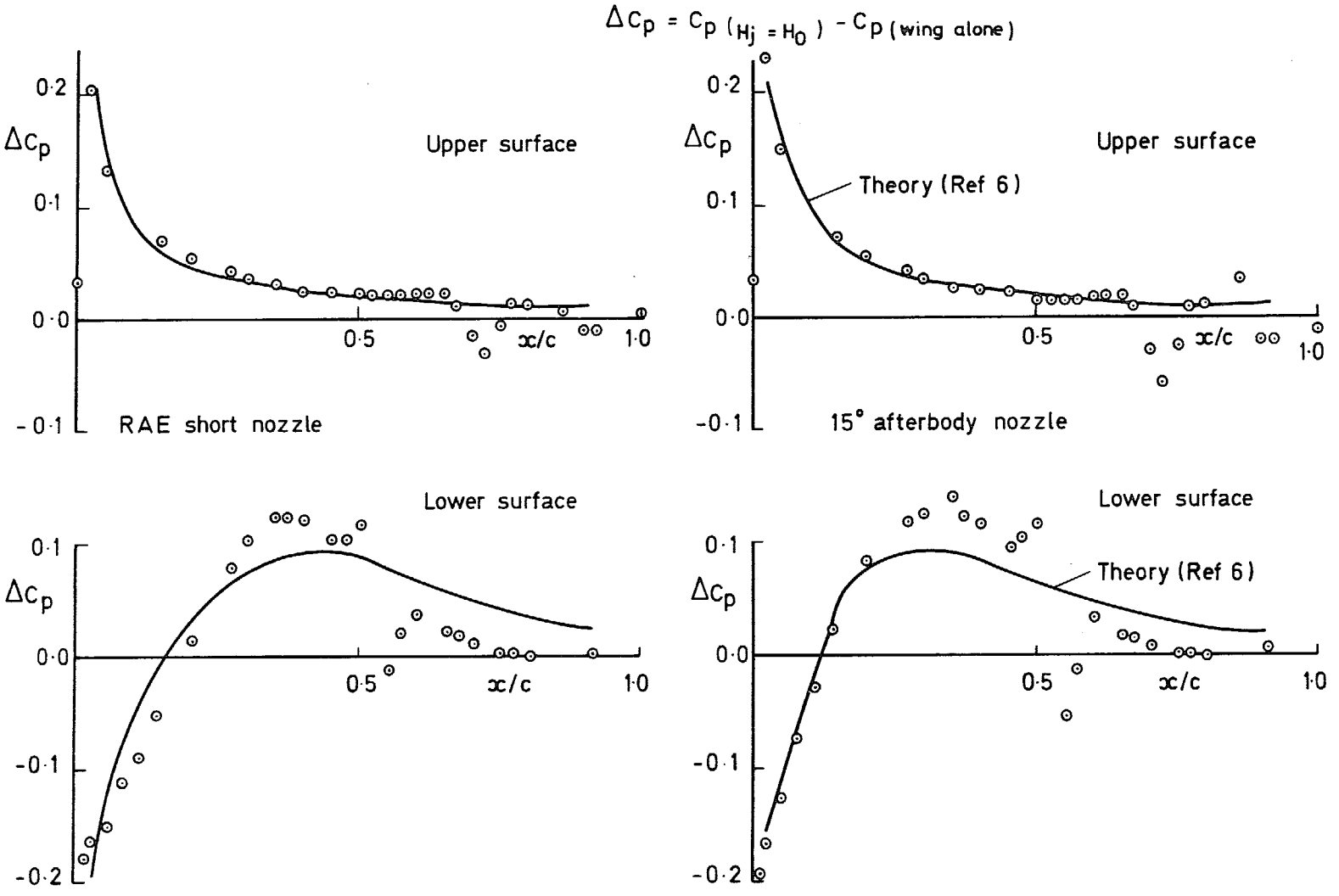

Fig 24 Interference effect of the nozzles on the wing pressure distribution, $M_\infty = 0.72$, $z_n/D_e = 0.64$ and $H_j = H_0$

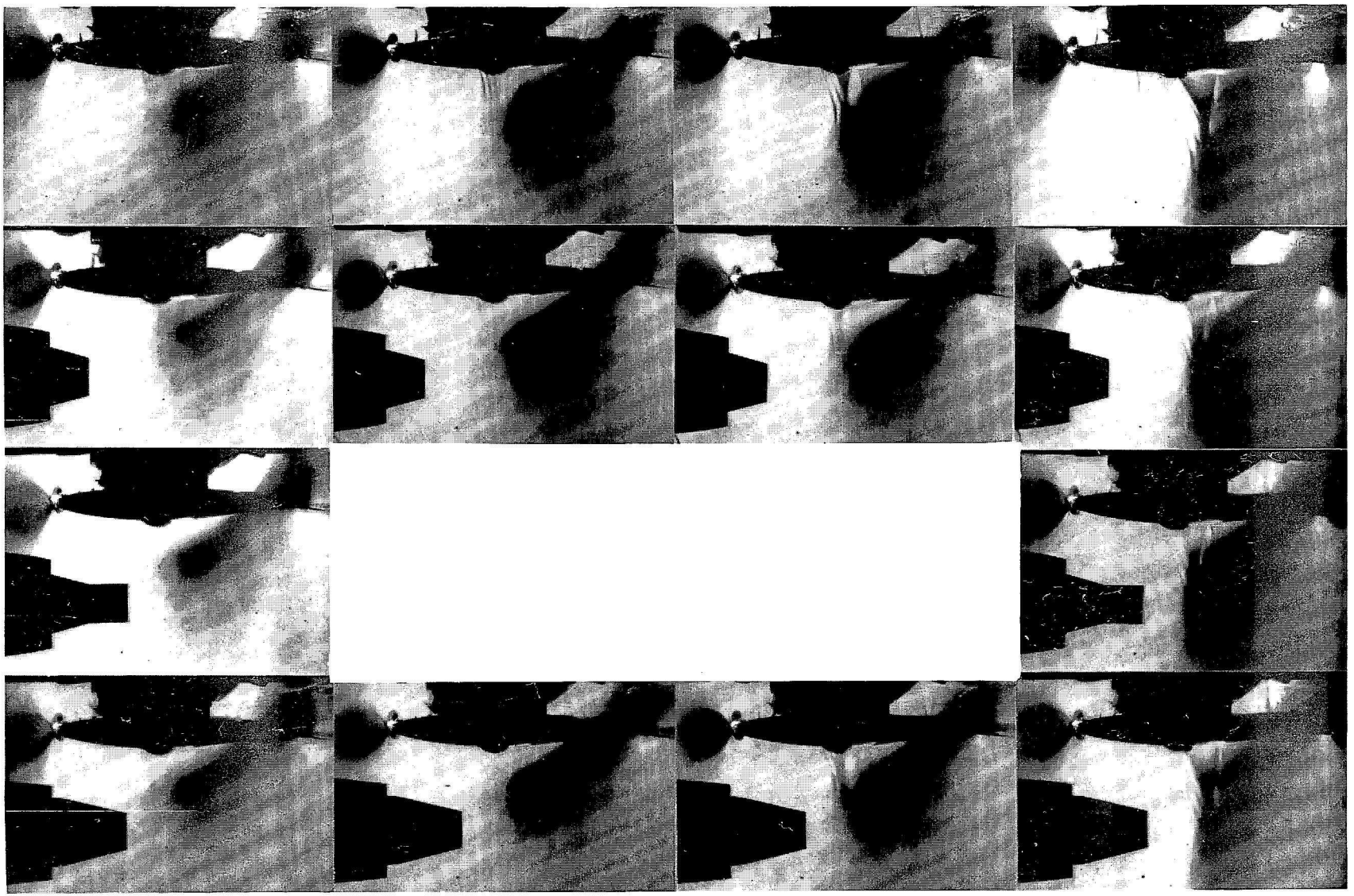

Fig 25 Wing shock development. $z_n/D_e \triangleq 0.6$. $H_j \triangleq H_\infty$

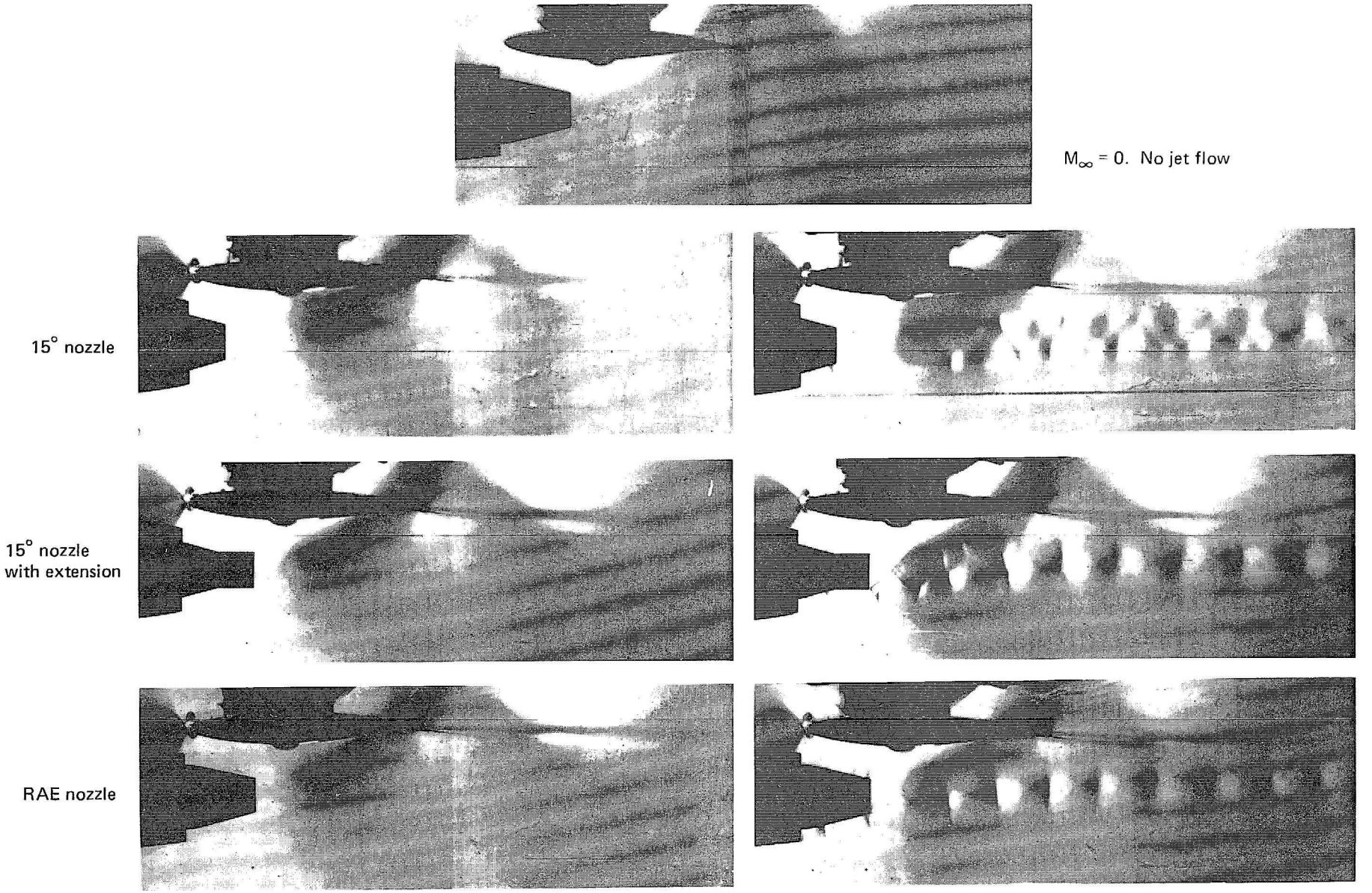

Fig 26 Jet flow at $M_\infty = 0.78$ and $z_n/D_e \simeq 0.3$

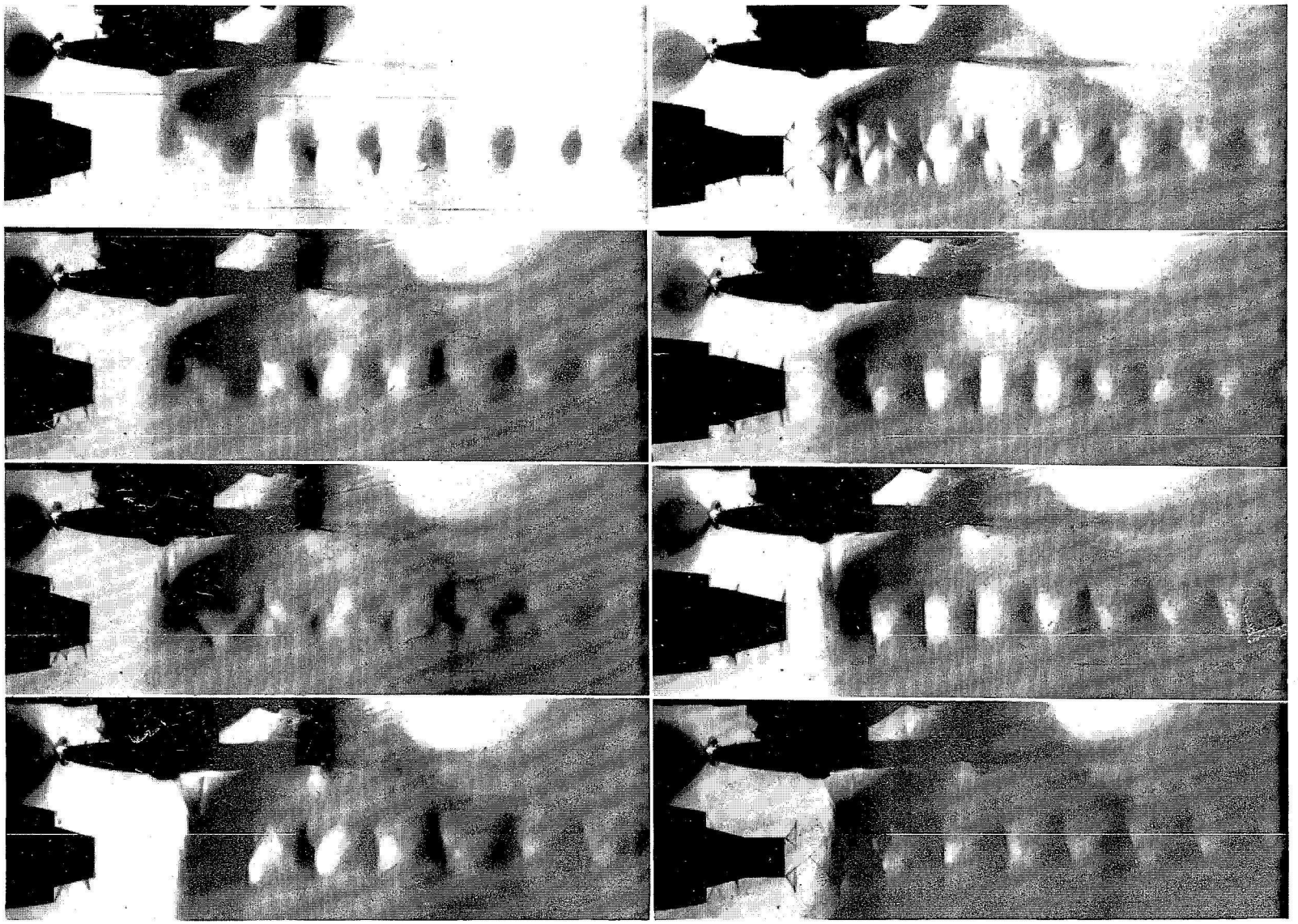

Fig 27 Jet shock variation with free stream Mach number and nozzle shape.
$z_n/D_e \doteq 0.6$. $H_j/p_\infty \doteq 2.3$

Part II

EXPERIMENTS ON A SWEPT WING

by

J. A. Bagley
A. G. Kurn

SUMMARY

Wind tunnel tests have been made to investigate the influence of the jets from several different nozzles on the pressure distribution on an adjacent swept wing panel with a supercritical profile. Tests were also made with pylons fitted to two of the nozzles.

The nozzle shapes and their location relative to the wing were chosen to represent a modern airbus configuration with fan engines. The results indicate that, in the cruise configuration, the influence of the jet is fairly small, and in most cases it simply reinforces certain features of the pressure distribution measured without jet blowing.

1 INTRODUCTION

The work reported here is a continuation of a programme of wind tunnel tests intended to investigate the influence of the jet flow from an under-wing engine nacelle on the pressure distribution around the wing. In Part 1 [1] of this series of Reports, an existing unswept wing was used as the subject of the tests; the results reported here were obtained with a 25 degree swept wing panel designed to simulate the wing of a typical modern 'airbus' type of aircraft at its design condition. The wing has a 'supercritical' section, with the characteristic features of

(a) an upper-surface velocity distribution with a uniform (supersonic) velocity over the front part and a steep reduction behind mid-chord,

(b) a lower-surface distribution with a peak velocity (just supersonic) near mid-chord, and a variation of velocity behind this corresponding to a considerable amount of rear loading.

Like the earlier tests in this series, the present programme was envisaged as an essentially exploratory investigation, intended to reveal any unexpected features of the flow or any gross differences between the characteristics of the four nacelles which were tested. The programme is therefore fairly limited in scope, mainly comprising pressure measurements at a single angle of incidence, along a single chord of the wing in line with the nozzle centre line for the isolated wing and in the presence of a jet blowing from each of the four nozzles.

Most of the tests were made with the wing and nacelle separately mounted, without the pylon which would join them on a practical aircraft installation. A limited number of tests were made with two different pylons fitted to two of the nacelles, and pressures were measured in the inboard and outboard wing-pylon junctions.

Details of the models and of the test programme are given in section 2. The results of the main series of tests, without pylon, are discussed in section 3, and those from the tests with pylon are presented in section 4.

2 EXPERIMENTAL DETAILS

2.1 Details of the models

The experimental rig was fully described in Ref 2. Briefly, it comprises a wing mounted between glass side-walls in the RAE 2ft × 1½ft transonic tunnel with a slotted roof and floor, and a long air-supply pipe cantilevered from the tunnel contraction, on the end of which opposite the wing is mounted a nozzle shaped to

represent the rear end of an engine nacelle. Part of the boundary layer developed along the pipe is removed by suction through slots near the end of the tube.

The wing used for this series of tests has 25 degrees of sweep, and the streamwise section is RAE 9550 ('wing C' of Ref 3) defined in Table 1. The streamwise chord is 152.4 mm, equal to that of the unswept wing panel used in earlier tests[1,2]. It was mounted on two spigots projecting spanwise through holes in the side-walls which were carried on two pillars outside the tunnel: these were adapted from the mounting used for the unswept wing.

Pressures were measured on the wing by two sets of 58 tubes, laid in the surface of the model and covered with clear araldite, and connected to self-balancing capsule manometers outside the tunnel. The two sets of tubes were placed at the same chordwise stations, and emerged from opposite ends of the model. By drilling into the tubes at appropriate spanwise locations, pressures could be measured on two streamwise sections simultaneously. For most of the tests, only a single distribution was measured, but in the later tests with pylons pressures were measured in the inboard and outboard wing-pylon junctions.

Four nozzles were used in the present test series:

(a) an existing RAE-designed nozzle used in the earlier tests[1,2];

(b) a nozzle designed to represent the '11 degree afterbody' used on the Rolls Royce RB 211 engine;

(c) a nozzle (also used in Ref 1*) designed to represent the '15 degree afterbody' of the RB 211 engine;

(d) a long nozzle intended to represent a possible 'silenced nacelle' for the RB 211 engine, based on preliminary Rolls Royce sketches.

Dimensions of the four nozzles are given in Table 2(a) to (d) and they are illustrated in Figs 1 to 4.

Nozzles (a) and (b) are very similar in general dimensions, but the RAE design, (a), has a curved afterbody with a slope of about 16 degrees at the exit, whereas the Rolls Royce design, (b), has a straight taper of 11 degrees. Nozzle (c) has a shorter afterbody, whilst (d) is much longer and, unlike the others, it has a common exit for the fan and core engine jet streams. All the nozzles were

* When this nozzle was used in Ref 1, it was found that the mass flow from the outer 'fan' nozzle was less than desired. For the present series of tests, a restrictive collar was inserted in the central duct, as shown in Fig 1, to increase the amount of flow passing through the fan nozzle. A similar collar was inserted in nozzle (b) after preliminary calibrations.

mounted at a distance below the wing chord which is typical of a modern 'airbus' installation, and at fore- and aft-positions which represent the same engine location for all four nozzles - also chosen to represent a typical 'airbus' installation. The positions of the various nozzles relative to the wing are shown in Figs 3 and 4.

The two pylons which were used in the latter part of the programme are also shown in Figs 3 and 4. Pylon A had its leading edge well behind the leading edge, initially at 9% chord, and after preliminary tests described in section 4.1 it was cut back to have its leading edge at 14% chord. Pylon B had its leading edge at the wing leading edge. Both pylons were hand-made from 3.2mm ($\frac{1}{8}$in) dural sheet, with the leading edge rounded to a roughly elliptical profile and the trailing edge chamfered. Thickness-chord ratios at the wing-pylon junction were 3.9% for Pylon A and 3.1% for Pylon B. The pylons were cambered by bending the plate so that the wing-pylon junction was roughly aligned with the local flow directions deduced from the pressures measured on the wing with nozzle (c) at $M_\infty = 0.84$ and $H_j = H_\infty$. The front part of the pylons, attached to the nozzle, was thus parallel to the free stream direction, but from the wing leading edge back to 40% chord the pylon was bent inwards by about 3 degrees and behind this the pylon was again parallel to the free stream direction. The method of fixing the pylons to the wing and nozzle was somewhat imprecise, and (as discussed in section 4.22) Pylon A became misaligned when fitted to nozzle (d). The pylons were nominally vertical (ie normal to the wing), but could have been inadvertently tilted by about 2 degrees during the tests. It was not possible to check this with any precision.

2.2 Test programme

Pressures on the wing were measured at 58 points along a single chord in line with the axis of the nozzle, as shown in Fig 3*. The tests were all made at a single value of wing incidence (α = 1.75 degrees) which gives an appropriate pressure distribution (in the presence of the nozzles) at $M_\infty = 0.84$. Tests were made at M_∞ = 0.82, 0.84, 0.86 and (for nozzles (c) and (d) only) 0.88 and 0.90. The tunnel pressure was constant throughout, and the Reynolds number (based on wing chord) varied from $R = 1.42 \times 10^6$ at $M_\infty = 0.82$ to $R = 1.48 \times 10^6$ at $M = 0.90$.

---

* The trailing edge hole was displaced 25 mm to one side. The trailing edge pressure is therefore not quoted in the results with the nozzles present, since there may be an unknown spanwise variation in the pressure in these cases.

In the first part of the test programme, where M_∞ did not exceed 0.86, no attempt was made to fix transition; earlier experience with the unswept wing[1,2] had suggested that this was not necessary. However, at the higher Mach numbers it appeared that shock-induced laminar separations might be responsible for misleading results, and it was decided that artificial transition-fixing was desirable. This was done by sticking a roughness band of ballotini* on both upper and lower surfaces of the wing between 5% and 7½% chord. A spanwise gap was left, extending 3mm either side of the line of pressure holes, to reduce the interference of the roughness band on the local pressures. A comparison of the pressure distribution at $M_\infty = 0.86$ on the isolated wing with and without transition fixing is given in Fig 5, and corresponding results in the presence of the 15 degree nozzle (c) are in Fig 6. On the isolated wing, the transition fixing has produced a forward movement of the shock on both upper and lower surfaces, as expected, but on the lower surface there is evidence of an excessive thickening of the boundary layer aft of 75% chord, causing a loss of pressure recovery. The results in Fig 6 with jet blowing from nozzle (c) show a similar forward movement of the shock on the upper surface, but much less influence of transition fixing on the lower surface. It is tentatively assumed that acoustic or other disturbances from the jet induced transition of the wing boundary layer earlier than on the isolated wing.

Tests were made using the four nozzles with the jet total-pressure equal to that of the free stream, simulating the zero-thrust condition (or the conditions which would obtain behind a free flow nacelle), and with the jet blown at pressure ratios H_j/p_∞ equal to 2.2, 2.4 and 2.6, covering the likely range of values appropriate to the fan jet of an engine like the RB 211.

Pitot traverses across the exits of the nozzles are plotted in Figs 7 and 8. The profiles are quite similar across the fan exits of the three nozzles (a) to (c), though substantially different in the centre jets. The quoted jet pressure ratios (2.2, 2.4 and 2.6) are the mean value of the fan jet exit pressure ratio. For nozzle (d) (Fig 8), the quoted value is the mean value across the single exit.

Tests were also made in the last part of the programme with the two pylons A and B in conjunction with nozzles (c) and (d). The full test programme is summarised in the following table.

---

* The roughness band consisted of 200 grade ballotini (0.076 mm to 0.102 mm) passed through a 170 grade sieve (0.089mm mesh).

M_∞	Isolated wing	Nozzle				Pylon		
		(a)	(b)	(c)	(d)	A with nozzle (c)	B with nozzle (c)	C with nozzle (d)
0.82	o T	o	o	o T	T	o T	T	T
0.84	o T	o	o	o T	T	o T	T	T
0.86	o T	o	o	o T	T	o T	T	T
0.88	T			T	T	T	T	T
0.90	T			T	T	T	T	T

o transition free
T transition fixed.

Note: All nozzles tested at $H_j = H_\infty$, $2{,}2p_\infty$, $2.4p_\infty$ and $2.6p_\infty$.

3 EXPERIMENTAL RESULTS WITHOUT PYLONS

As in the previous tests in this series, the experimental results have not been subjected to any form of wind tunnel correction. There is no simple way of correcting measurements on supercritical wings in slotted wall tunnels and since the experiment is intended only to be exploratory the uncorrected measurements are considered to be adequate.

Only a selection of the experimental results are presented, showing the salient features of the flow patterns. In all cases, the development of the flow with increasing jet pressure ratio or increasing Mach number was quite regular, and can be inferred from the results shown here. As in earlier tests, it was found that jet blowing had little or no effect on the pressures on the upper surface of the wing so most of the illustrations show only the measurements on the lower surface.

3.1 Measurements on the isolated wing

Pressure distributions measured at a streamwise section at mid-span of the isolated wing, with fixed transition, are shown in Fig 9. The development of the shock on the upper surface with increasing Mach number is characteristic of this type of section, and the appearance of a shock of similar strength on the lower surface is also noteworthy. At $M_\infty = 0.9$, the boundary layer on the lower surface is evidently separated, causing substantial loss of pressure recovery over the rear part of the section, though the trailing edge pressure is not altered. (This spearation may be scale-sensitive, and might well be reduced or even eliminated at higher Reynolds numbers.) Values of the critical pressure coefficients C_p^* corresponding to 0 degree and 25 degrees sweep of the isobars are shown on the figure, and it seems clear that the lower surface shock appears when

the suction exceeds the value appropriate to 25 degrees sweep, thus suggesting that the isobar sweep is maintained at this section of the wing.

3.2 Comparison of nozzles (a) and (b)

The pressure distributions on the wing in the presence of nozzles (a) and (b) at $M_\infty = 0.82$, 0.84 and 0.86 are shown in Figs 10 to 12. As in previous experiments it was found that the upper-surface pressures were virtually unaffected by increasing jet pressure ratio, so these are shown only for $H_j = H_\infty$. On the lower surface, the influence of increasing jet pressure ratio at $M_\infty = 0.82$ is shown in Fig 10; a similar consistent variation was found at $M_\infty = 0.84$ and 0.86, but the intermediate values have been omitted from Figs 11 and 12 in the interest of clarity.

It is immediately apparent that the two nozzles, with similar overall dimensions, have a very similar influence on the wing pressures. The exit of the RAE nozzle (a) is slightly nearer the leading edge than that of nozzle (b), and this is probably the main reason why the first compression (a shock at $M_\infty = 0.86$) occurs further forward for this case. Downstream of the nozzle there is a small expansion, which seems to be greater for nozzle (a); this may be related to the higher pressure ratio of the core jet shown in Fig 7. There is little evidence to suggest that the difference in afterbody shape between the straight taper of nozzle (b) and the curved profile of nozzle (a) has any significant influence on the wing pressures.

3.3 Comparison between nozzles (b) and (c)

The measured pressure distributions on the isolated wing and in the presence of nozzles (b) and (c) at zero thrust conditions ($H_j = H_\infty$) at $M = 0.82$, 0.84 and 0.86 are shown in Figs 13 to 15. The change in upper-surface pressures is very similar for the two nozzles, and corresponds to a local downwash over the forward part of the wing, associated with the converging flow round the afterbody. In Part 1 of this series[1] the same effect was shown on the unswept wing, and it was demonstrated that a simple inviscid theory could be used to calculate the effect.

On the lower surface, the difference between the influence of the two nozzles is very similar at all Mach numbers; in each case the initial suction peak ahead of the exit is higher for the longer nozzle. It is plausible to associate this with the constriction of the flow in the 'channel' between the wing lower surface and the nozzle afterbody, but this concept is essentially a two-dimensional one and certainly is not adequate to provide a full explanation

of the interference. It is significant that the shape of the curves is very similar, whether the local velocities are subsonic (at $M_\infty = 0.82$) or supersonic (at $M_\infty = 0.86$).

Both nozzles have an essentially favourable influence on the lower-surface pressures: they reduce the velocities over most of the forward part and eliminate the shock which develops around $x/c = 0.5$ at $M_\infty = 0.86$. The shorter nozzle (c) probably has the more favourable influence, since it increases the local lift, which would normally be advantageous on a complete aircraft. At higher Mach numbers, nozzle (c) may have an even more favourable influence on the wing flow, as indicated by the results at $M_\infty = 0.9$ shown in Fig 16. (These were measured with transition fixed; the effect of fixing transition at $M_\infty = 0.86$ has already been discussed in section 2.2 (Fig 6).) The most significant feature is that the flow separation on the lower surface of the isolated wing has been eliminated or at least postponed to a slightly higher Mach number, although as noted above this separation could be less severe at full-scale Reynolds numbers.

The influence of the jet at $M_\infty = 0.90$, 0.82, 0.84 and 0.86 respectively is shown in Figs 16 to 19, for a jet pressure ratio $H_j/p_\infty = 2.4$. The effect of varying jet pressure ratio is small, as illustrated in Figs 20 to 22, where values of ΔC_{p_j} are plotted, for the lower surface only. As in previous reports in this series, ΔC_{p_j} is defined as the difference between the pressure coefficient at a point on the wing measured at a specified jet pressure ratio and that measured with the total pressure in the jet equal to the free stream value (equivalent to the conditions behind a free-flow nacelle, or to zero thrust).

As usual, the change in pressures on the upper surface of the wing associated with jet blowing is negligible. On the lower surface, the influence of the jet appears to be to magnify the suction peaks which were present at zero thrust. With the short nozzle, the peak at about 40% chord (well behind the central nozzle) is increased, whereas for the longer nozzle it is the peak at about 15% chord which grows, and this is well ahead of the central nozzle.

It is interesting to compare these results with those obtained previously with nozzles (a) and (c) in conjunction with an unswept wing. (As pointed out above, nozzles (a) and (b) appear to produce very similar interferences on the wing.) Comparing for example, Fig 14 of Ref 1 with Fig 20 of this Report, it appears that the shape of the interference pressure coefficient ΔC_{p_j} on the two wings is very similar for the short nozzle, and quite different for the longer nozzle. But reference to the basic pressure distributions on the lower surface

shows that in each case the influence of the jet can be regarded as a magnification of the suction peak which already existed at the zero thrust condition $H_j = H_\infty$.

It is also noteworthy that, for both nozzles and at all values of jet pressure ratio, the 'interference' on the lower surface is essentially confined to the region ahead of 50% chord. There is little sign that the boundary layer is significantly thickened by its passage through the various peaks and troughs in the pressure distribution*.

It is also worth noting that the values of ΔC_{p_j} are quite small; only at the highest Mach number and jet pressure ratio do they exceed a value of 0.2. This seems to support earlier arguments[1] that the influence of jet blowing on the wing flow field would be quite small (for 'conventional' under-wing engine locations) so that wind tunnel tests with free-flow nacelles should not be seriously misleading†. However, tests with blown jets are doubtless required to obtain accurate drag values for a complete aircraft, since small localised changes in pressure distribution may still represent significant drag changes.

3.4 Comparison of nozzles (c) and (d)

The results for nozzle (c) have been presented in Figs 13 to 19. Measurements of the wing pressures with nozzle (d) are presented in Figs 23 to 25, and there are several noteworthy differences. The upper surface pressure distribution is much closer to that of the isolated wing, since the downwash induced by the longer nozzle is much smaller. There is a substantially larger influence on the lower surface from nozzle (d), with a strong shock at about 30% chord, which provokes boundary layer separation at the higher Mach numbers with a marked loss of pressure recovery over the rear part of the profile. Unlike the separation discussed in section 3.1, this appears to be clearly shock-induced, and so will tend not to be modified significantly at higher Reynolds numbers.

The influence of jet blowing from nozzle (d) is almost negligible, as shown by the values of ΔC_{p_j} in Fig 26. There is a small shift in the shock position at the higher Mach numbers which is represented by the peak in ΔC_{p_j} at 32% chord.

---

* The small differences in pressure coefficient at the end of the adverse gradient (behind 80% chord) which are noted in Figs 20 to 22 are essentially random. The pressure tubes in this region had a very small diameter and it is now judged that in these initial tests, inadequate time was allowed for a change in pressure to be recorded accurately at the capsule manometer outside the tunnel.

† It should be pointed out, however, that the effect of jet blowing on the wing is given only for the pressure distribution immediately above the jet. It is possible that the three-dimensional effect of the jet produces a more adverse condition at some other spanwise region.

It seems clear that the adverse interference of nozzle (d) would be unacceptable on an actual aircraft installation; but the evidence presented in section 4 suggests that substantial improvements are possible when a pylon is added.

4 THE INFLUENCE OF PYLONS

A rather limited investigation was made of the effect on the wing pressure distributions of adding a pylon to the 15 degree nozzle (c) and the extended nozzle (d). The main purpose of the tests was to establish whether any unexpected features appeared when the pylon was added to a supercritical wing.

At low speeds, it is well known that the main effect of a pylon on the wing pressures is to act as a partial reflection plate; the isobars become less swept in the inboard junction, and this leads to premature appearance of shock waves as Mach number increases. These effects can be minimised by shaping the pylon so that (at a design condition) it conforms to the streamlines of the basic wing flow field. As explained in section 2.1 above, in the present tests the pylons were rather crudely shaped to match the streamlines of the flow field of the wing in the presence of nacelle (c). Because these pylons were thinner than a realistic pylon would be, it was not necessary to allow for the difference between inboard and outboard junction shapes; in a realistic design it would be preferable to shape the inboard junction.

4.1 Preliminary development of pylon shapes

As originally constructed, Pylon A had its leading edge at 9% chord behind the wing leading edge. Pressures in the inboard junction were measured with this pylon attached to nozzle (c), and the results at $M_\infty = 0.82$ and $H_j = H_\infty$ are shown in Fig 27, compared with the pressures measured without a pylon.

As expected, the pylon had no influence on the upper surface pressure distribution. On the lower surface, it was clear that there was an excessive suction peak at about 13% chord, which was thought to be associated with high velocities on the 'shoulder' of the pylon leading edge. The leading edge was therefore reshaped, in two stages, to increase its sweep and to reduce the surface slopes; the pressures measured on the wing of the second stage of modification are also shown in Fig 27. The suction peak had been reduced significantly, and the junction pressure distribution was smoother; it was decided that this pylon shape should be used for the remaining tests. (It was found later that at higher Mach numbers, this suction peak was not much lower for the reshaped pylon than for the original, so it is not clear in retrospect whether the reshaping was necessary.)

When Pylon A was fitted to the long nozzle (d), problems arose due to twisting of the pylon. The results shown in Fig 28 are for a configuration where the pylon had twisted to the extent that the inward slope of the fore-part was about ½ degree instead of the intended 3 degrees. The results quoted in section 4.2.2 below are also for this geometry.

Pylon B was first tested with no camber, in conjunction with nozzle (c), and the results obtained (only for the inboard junction) are shown in Fig 29. It was then bent to conform approximately with the streamlines of the flow field without pylon, and the results were very satisfactory. As shown in Fig 29, the pressures measured in the inboard and outboard junctions were almost symmetrically disposed about the 'no-pylon' measurement, and the shape of the pressure distributions seemed to be free of unwanted suction peaks or steep gradients.

4.2 Experimental results for pylon-nozzle configurations

Measurements were made of the wing pressures at Mach numbers of 0.82, 0.84, 0.86, 0.88 and 0.90, at jet pressure ratios H_j/p_∞ = 2.2, 2.4 and 2.6, and with $H_j = H_\infty$. Analysis of the results revealed, somewhat unexpectedly, that the effect of the pylon could be separated almost completely from the influence of jet blowing; an interference pressure coefficient ΔC_{p_p} , defined as the difference between pressures measured (at the same value of H_j/p_∞) on the wing with and without pylon, is plotted in Figs 30 to 34.

4.2.1 Pylon A with nozzle (c)

The results for Pylon A with the short nozzle (c) are illustrated in Fig 30 at M = 0.82, 0.86 and 0.90. The pattern is essentially the same at all test conditions. Ahead of the pylon leading edge at 14% chord the interference pressure is generally positive, representing the flow approaching an attachment line on the pylon*. A sharp negative peak in the interference pressures a little further aft corresponds to the expansion in the local-flow where the rounded nose of the pylon blends into the flat side, and this is then followed by a fairly uniform transition to a positive peak between 40% and 50% chord, which represents the elimination of a suction peak in the distribution present without the pylon. Only at the highest Mach number is there a small variation in ΔC_{p_p} with jet pressure ratio, which is probably directly associated with shock movements in the basic pressure distribution (Fig 16).

---

* The picture is slightly confused by the influence of the transition band on the wing between 5% and 7½% chord.

Behind the trailing edge of the pylon (at 68% chord), the pylon has virtually no further influence on the pressures. However, there is a slight reduction in the pressure recovery towards the trailing edge of the wing presumably due to a local increase in boundary layer thickness due to the presence of the pylon.

Pressures were not measured on the outboard side of this pylon-nozzle configuration.

4.2.2 Pylon A with nozzle (d)

The effect of adding Pylon A to the wing with nozzle (d) is shown in Fig 31 for the inboard junction and Fig 32 for the outboard junction. The values of the pressure interference coefficient, ΔC_{p_p}, are again virtually independent of jet pressure ratio, and there is again no substantial change in the shape of the curve with increasing Mach number. However, the shape is totally different from that in Fig 30 with nozzle (c) and is generally dominated by a steep rise at around 30% chord which corresponds to the elimination of the shock in the distribution present without the pylon. The peak associated with the pylon nose shape is still present, at 18% chord, but is much reduced in the inboard junction (Fig 31) because the pylon is skewed round by about $2\frac{1}{2}$ degrees. Thus the pylon is no longer aligned with the local flow direction and a corresponding, but much more marked, peak appears in the outboard junction (Fig 32). There are no measurements behind 38% chord in this junction, because the misaligned pylon covered the pressure holes, but the indication is that the shock wave in the original distribution has been eliminated by the pylon on this side also. This is potentially an important result, because there can be little doubt that the pressure distribution for the configuration without pylon (shown in Figs 23 to 25) would be unsatisfactory on any actual aircraft, so the pylon can be said to produce 'favourable interference'. However, it would probably be difficult to design an optimum pylon configuration by 'cut-and-try' development, and thus further investigation has been deferred until a more satisfactory method of design becomes available*.

---

* It is hoped that work now in progress at RAE to calculate the supercritical flow on a wing-pylon-nacelle configuration with specified geometry will provide an essential element in such a new design method.

4.2.3 Pylon B with nozzle (c)

The effect of adding Pylon B to the wing with the short nozzle (c) is shown in Fig 33 for the inboard junction and Fig 34 for the outboard junction. Once again, the values of ΔC_{p_p} are essentially independent of jet pressure ratio, but a variation in the shape of the curves with changes in Mach number is this time quite noticeable.

The addition of the pylon has a small influence on the upper surface pressure distribution, but this is confined to the first 5% of the chord. On the lower surface, the positive peak in ΔC_{p_p} at about 1% chord in the inboard junction and the corresponding negative peak in the outboard junction indicate that the pylon leading edge is not aligned to the local flow direction. Immediately behind this, the sign of ΔC_{p_p} changes in both junctions, implying that this part of the pylon is misaligned in the opposite sense. In practice, it would probably be difficult to shape the pylon camber-line so that ΔC_{p_p} was minimised everywhere - and in any case this could be done only at one combination of incidence and Mach number. It is felt that the pressure distributions on the present configuration, while not ideal, would probably be acceptable as a compromise in practice on an actual aircraft.

5 CONCLUSIONS

The experiments reported here were concerned mainly to compare the influence of three different nozzle shapes ((b), (c) and (d)) fitted to a hypothetical engine at a specific position relative to the wing. This position was based on an actual aircraft design, and it is reasonable to assume that the engine location had been 'optimised' (in some sense) during the preliminary design. Any conclusions from the present work are therefore qualified by the fact that only one engine location was considerd, although this was one of considerable practical interest. On the other hand, earlier tests in this series[1,2] using an unswept wing have explored a greater range of engine locations, and these results suggest that the general conclusions from the present results would be applicable for a wider range of engine positions.

5.1 The significance of jet representation

The main conclusion from these tests is clearly that jet effects on the wing pressure distribution are small for all the nozzles over the range of Mach numbers and jet pressures tested (Figs 20, 22, 26) providing there are no adverse spanwise effects. The obvious deduction is therefore that tests with free-flow nacelles should not be seriously misleading. This conclusion is somewhat at variance with the general concensus of current

belief, and needs to be qualified. What has been demonstrated here is that values of ΔC_{p_j}, the 'interference' pressure field of the jet, are small and that changes in the shape of the pressure distribution on the wing, including the location of shock waves, are also small. It cannot be assumed, however, that the consequent drag changes on a complete aircraft would be negligible. In particular, if a wing has been carefully designed to have a supercritical flow pattern, the addition of any nacelle in a conventional under-wing location (ahead of the leading edge) will certainly produce a local reduction in lift near the nacelle. At a fixed overall lift coefficient, this local loss of lift must be balanced by an increase elsewhere on the wing, and this increase in lift may be accompanied by a significant drag change if the carefully designed pressure distribution of the wing is significantly altered. The implication is that for wind tunnel tests of a complete aircraft model from which accurate measurements of drag are required (for estimating performance guarantees, for example) the geometry of the engine installation must be as accurate as possible and should include jet representation. For the earlier stages of aircraft design, for example when engine location is being optimised, it should be quite adequate to use free-flow nacelles unless it is intended to place the engines very close to the wing.

5.2 The magnitude of jet-induced effects on the wing

The second conclusion from the present tests is that jet interference acts mainly to magnify the suction peaks which already exist at zero thrust. It is not certain that this result can be generalised, but it is not contradicted by any of the previous measurements made on unswept wings in Refs 1 and 2. It does not seem to be possible to define a simple 'magnification factor' which might be applied to predict this effect, but it may be observed that the peak value of ΔC_{p_j} for a jet pressure ratio $H_j/p_\infty = 2.4$ (typical of a fan jet engine) is between -0.1 and -0.2 for all the configurations tested here, with the nozzle centre-line at $z_n/D_e = 0.6$. A similar result was obtained in Ref 1 for this value of wing-nacelle vertical spacing, which is typical of most current aircraft designs. Results in Refs 1 and 2 for configurations with z_n/D_e in the range 0.25 to 0.3 suggest that the peak values of ΔC_{p_j} may be roughly doubled.

5.3 Subsidiary results

The remaining conclusions from these tests are probably fairly specific to the configurations tested, though further work may show that some can be generalised.

(1) The comparison between nozzles (a) and (b) indicates that the interference on the wing is determined mainly by the overall proportions of the nozzle and is not much influenced by the detailed shaping.

(2) The comparison between nozzles (b) and (c) suggests that there is little to choose between them in terms of their interference effect on the wing, though the shorter nozzle (c) produces a slightly higher local lift at the adjacent wing section and may be slightly preferable on that account. At the highest Mach number tested, $M_\infty = 0.9$, the addition of nozzle (c) reduces the strength of a shock wave sufficiently to remove a boundary layer separation on the lower surface, and this would probably represent a 'favourable interference' on the local wing drag.

(3) The long nozzle (d), representing a possible configuration for a silenced nacelle, had a decidedly adverse influence on the wing pressure distribution when tested without a pylon, but was much improved by the addition of a pylon.

(4) The pylons tested here were thinner than would be required for a real aircraft installation, but the measured pressure distribution in the junction indicated that if pylons are designed to conform with local wing streamlines they can have small influence on the wing flow, at least at the design condition.

(5) The influence of the pylon on the wing flow field appears to depend mainly on the local geometry and is not influenced by the jet blowing.

Table 1

AEROFOIL ORDINATES FOR WING RAE 9550

x/c	z_u/c	z_L/c	x/c	z_u/c	z_L/c
0	0	0	0.36	0.0566	-0.0649
0.001	0.0063	-0.0066	0.38	0.0568	-0.0643
0.002	0.0086	-0.0092	0.40	0.0568	-0.0633
0.003	0.0103	-0.0112	0.42	0.0568	-0.0619
0.004	0.0116	-0.0129	0.44	0.0565	-0.0599
0.005	0.0128	-0.0143	0.46	0.0562	-0.0576
0.006	0.0138	-0.0155	0.48	0.0557	-0.0549
0.007	0.0147	-0.0166	0.50	0.0551	-0.0520
0.008	0.0155	-0.0176	0.52	0.0543	-0.0490
0.009	0.0163	-0.0186	0.54	0.0533	-0.0458
0.010	0.0170	-0.0194	0.56	0.0522	-0.0426
0.012	0.0183	-0.0211	0.58	0.0509	-0.0394
0.014	0.0195	-0.0225	0.60	0.0495	-0.0361
0.016	0.0205	-0.0239	0.62	0.0478	-0.0327
0.018	0.0215	-0.0251	0.64	0.0461	-0.0292
0.020	0.0224	-0.0263	0.66	0.0441	-0.0255
0.03	0.0261	-0.0313	0.68	0.0420	-0.0219
0.04	0.0289	-0.0353	0.70	0.0398	-0.0182
0.05	0.0313	-0.0387	0.72	0.0375	-0.0146
0.06	0.0335	-0.0416	0.74	0.0351	-0.0111
0.07	0.0354	-0.0442	0.76	0.0328	-0.0079
0.08	0.0371	-0.0465	0.78	0.0305	-0.0050
0.09	0.0386	-0.0486	0.80	0.0282	-0.0025
0.10	0.0401	-0.0504	0.82	0.0259	-0.0003
0.12	0.0427	-0.0536	0.84	0.0236	0.0015
0.14	0.0449	-0.0562	0.86	0.0212	0.0028
0.16	0.0469	-0.0584	0.88	0.0189	0.0036
0.18	0.0486	-0.0601	0.90	0.0166	0.0040
0.20	0.0501	-0.0616	0.92	0.0143	0.0040
0.22	0.0515	-0.0627	0.94	0.0120	0.0036
0.24	0.0527	-0.0636	0.96	0.0096	0.0028
0.26	0.0537	-0.0643	0.98	0.0073	0.0016
0.28	0.0545	-0.0648	1.00	0.0050	0
0.30	0.0553	-0.0651			
0.32	0.0558	-0.0652	c = 152.4 mm		
0.34	0.0563	-0.0652			

Table 2

(a) RAE nozzle ordinates
see also Fig 1

(Dimensions in millimetres.)

Outer cowl		
x_j	Inside diameter	Outside diameter
-139.70	41.66	63.30
-114.30	43.18	↓
-101.60	44.45	↓
-95.25	45.47	↓
-88.90	46.74	↓
-82.55	48.77	parallel
-76.20	50.80	↓
-69.85	52.83	↓
-62.99	54.10	↓
-57.91	54.36	63.30
-52.83	↓	63.25
-47.75	↓	62.97
-42.67	↓	62.59
-37.59	↓	62.10
-32.51	↓	61.49
-27.43	parallel	60.73
-22.35	↓	59.89
-17.27	↓	58.98
-12.19	↓	58.04
-7.11	↓	57.07
-2.03	↓	55.91
0	54.36	55.09

Inner cowl		
x_j	Inside diameter	Outside diameter
-85.09	24.13	24.13
-82.55	22.86	27.69
-76.20	↓	30.73
-69.85	↓	33.53
-63.50	↓	35.31
-60.33	↓	35.56
	↓	parallel
-25.40	↓	35.56
-15.88	↓	39.12
-6.35	↓	40.89
	parallel	parallel
0	↓	40.89
2.54	↓	40.62
5.08	↓	40.06
7.62	↓	39.24
10.16	↓	38.20
12.70	↓	37.01
15.24	↓	35.81
17.78	22.86	34.59
20.32	↓	33.78
22.86	↓	32.16
25.40	↓	30.94
27.94	↓	29.72
30.48	↓	28.50
33.02	st. taper	27.28
35.56	↓	26.09
38.10	↓	24.87
40.64	↓	23.65
43.18	↓	22.43
45.09	20.98	21.34

Table 2 (continued)

(b) 11 degree afterbody nozzle ordinates
see also Fig 1

(Dimensions in millimetres.)

Outer cowl		
x_j	Inside diameter	Outside diameter
-118.05 to -34.95	Same as 15 degree nozzle Table 2 (c)	
-32.41	parallel	61.85
-26.39	55.22	st. taper
-19.71	st. taper	59.79
-14.00	53.75	radius
-7.49	parallel	56.54
-6.71	53.75	st. taper
	radius	
0	52.67	53.69

Inner cowl		
x_j	Inside diameter	Outside diameter
-88.90	23.92	23.92
-87.90	21.92	
-87.43		27.19
-86.04		28.48
-83.18		30.20
-80.33		31.40
-77.47		32.30
-74.61		32.99
-71.75		33.52
-68.90		33.91
-66.04		34.18
-63.18		34.34
-60.32	parallel	34.39
		parallel
-10.72		34.39
		radius
-7.20		35.39
		radius
0.93		37.39
		radius
23.87		32.14
		st. taper
48.88	21.92	22.42

Table 2 (continued)

(c) 15 degree afterbody nozzle ordinates
see also Fig 1

(Dimensions in millimetres.)

Outer cowl		
x_j	Inside diameter	Outside diameter
	parallel	parallel
-118.05	41.66	63.50
	radius	↓
-105.10	43.99	↓
	st. taper	parallel
-79.89	52.88	↓
	radius	↓
-66.93	55.22	↓
-52.73	↓	63.50
-50.19	↓	63.48
-47.65	↓	63.39
-45.11	↓	63.27
-42.57	↓	63.08
-40.03	parallel	62.86
-37.49	↓	62.57
-34.95	↓	62.24
-32.41	↓	61.85
-29.87	↓	61.41
-27.33	↓	60.91
-26.39	55.22	
-24.79	↓	60.37
-22.25	↓	59.78
-19.71	st. taper	59.13
-17.17	↓	58.42
-14.63	↓	57.67
-14.00	53.75	
-13.18	st. taper	57.21
-9.30	54.05	st. taper
-4.72	53.54	54.56
-4.65	radius	radius
-2.49	52.63	53.59
-2.39	st. taper	st. taper
0	51.31	52.38

Inner cowl		
x_j	Inside diameter	Outside diameter
-88.90	23.83	23.83
-87.90	21.83	
-87.47	↓	27.93
-86.04	↓	29.56
-83.19	↓	31.71
-80.33	↓	33.21
-77.47	↓	34.84
-74.61	↓	35.20
-71.76	↓	35.87
-68.90	↓	36.36
-66.04	↓	36.70
-63.18	↓	36.90
-60.33	↓	36.96
	parallel	parallel
-26.39	↓	36.96
	↓	st. taper
-16.26	↓	34.39
-14.81	↓	34.24
-12.09	↓	34.85
-8.18	↓	36.47
-5.99	↓	37.08
-5.18	↓	37.22
-4.12	↓	37.03
-1.85	↓	36.17
	↓	st. taper
23.01	21.83	22.83

Table 2 (concluded)

(d) Extended nozzle ordinates
see also Fig 2

(Dimensions in millimetres.)

x_j	Inside diameter	Outside diameter
-80.04	41.66	63.51
	st. taper	parallel
-63.04	41.30	63.51
-58.04		63.50
-53.04		63.48
-48.04		63.43
-43.04		63.32
-38.04		63.15
-33.04		62.93
-28.04		62.66
-23.04		62.34
-18.04		61.96
-13.04		61.53
-8.04		61.04
-3.04		60.49
1.96		59.87
6.96	parallel	59.16
11.96		58.32
16.96		57.35
21.96		56.30
26.96		55.19
31.96		54.04
36.96		52.82
41.96		51.49
46.96		50.02
51.96		48.43
56.96		46.77
61.96		45.11
66.96		43.42
71.96	41.30	41.76

LIST OF SYMBOLS

A_j	nozzle area at the central insert and annular exit
A_p	area of the jet air supply pipe upstream of the nozzle
C_p	pressure coefficient on the wing surface
C^*_p	pressure coefficient equivalent to a Mach number of one
c	wing chord (see Fig 3)
D_e	outer cowl diameter at nozzle exit (see Fig 3)
H_j	mean pitot pressure at the annular exit of the nozzle
H_{j_L}	local pitot pressure at the nozzle exit
H_p	pitot pressure in the air supply pipe to the nozzle
H_∞	pitot pressure in the free stream
M_∞	Mach number in the free stream
p_∞	static pressure in the free stream
R	outer cowl radius at the nozzle exit
r	radial position of pitot at the nozzle exit
x	distance along wing chord from leading edge
x_j	distance along nozzle centre-line downstream from outer cowl exit (Fig 1)
x_n	distance along nozzle centre-line from outer cowl exit to wing leading edge (Fig 3)
z_n	distance from upper lip of outer cowl to wing leading edge (Fig 3)
ΔC_{p_p}	incremental change in wing pressure coefficient due to adding a pylon to the wing and nacelle, ie $\Delta C_{p_p} = C_p$ (with pylon) $- C_p$ (without pylon) at a given value of H_j/p_∞
ΔC_{p_j}	incremental change in wing pressure coefficient due to an increase in jet pressure from $H_j = H_\infty$: ie $\Delta C_{p_j} = C_p(H_j > H_\infty) - C_p(H_j = H_\infty)$.

REFERENCES

No.	Author	Title, etc
1	J.A. Bagley A.G. Kurn	Jet interference on supercritical wings. Part 1 Experiments on a two-dimensional wing. ARC R & M No.3845, Part I (1977)
2	A.G. Kurn	A further wind-tunnel investigation of under wing jet interference. ARC CP No.1156 (1969)
3	R.C. Lock J.L. Fulker	Design of supercritical aerofoils. Aero. Qu. 25, 245 (1974)

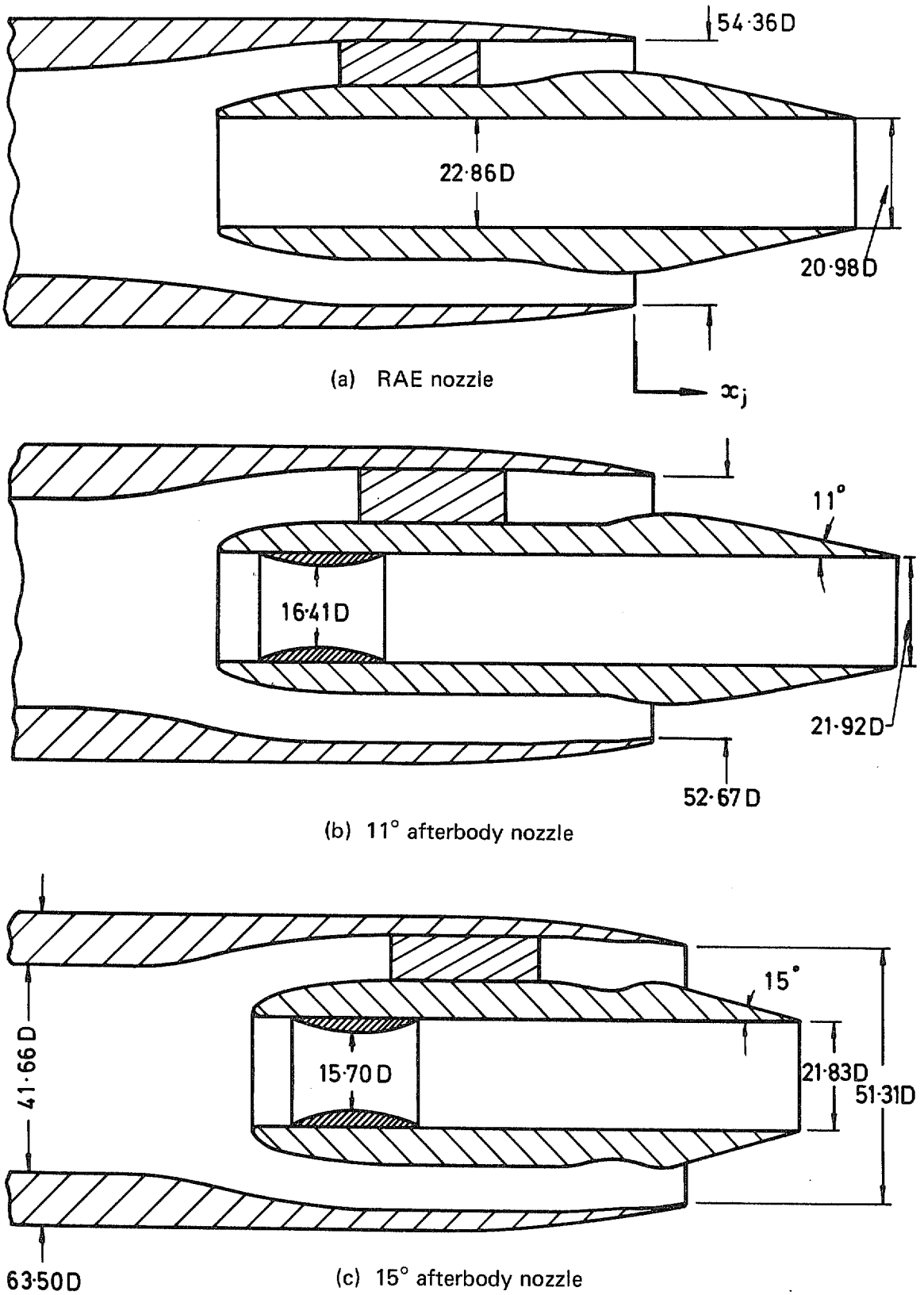

Fig 1 Details of coaxial nozzles

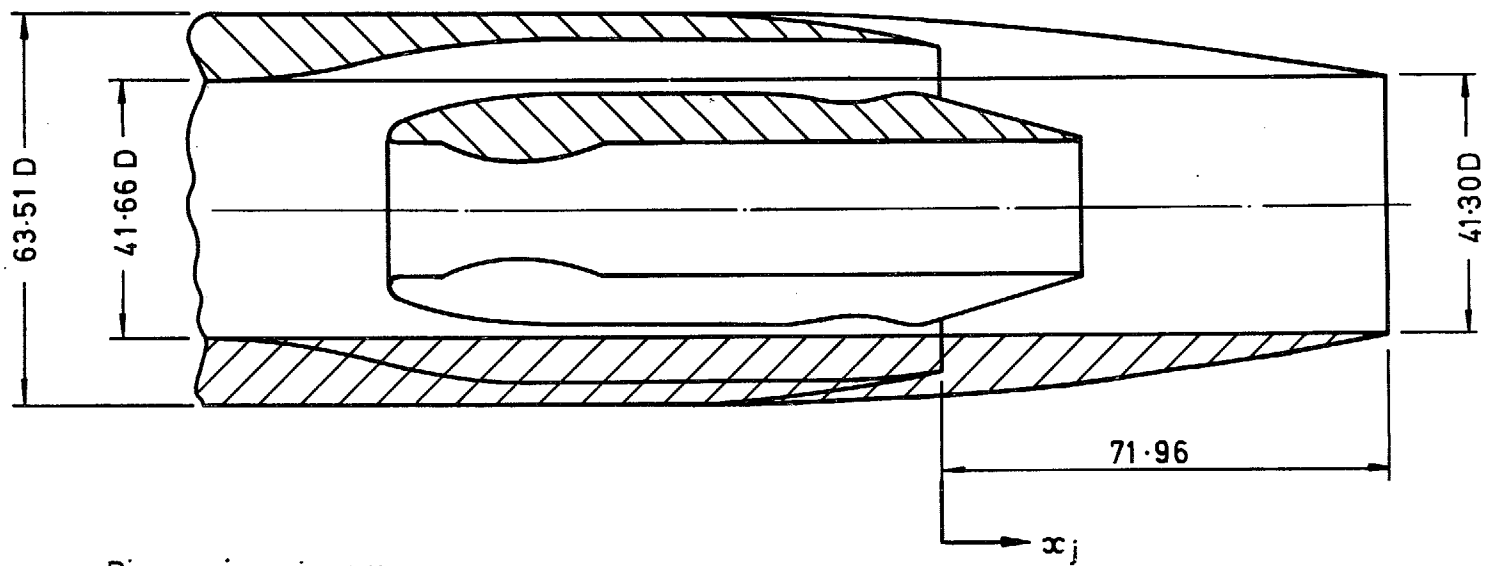

Fig 2 Comparison of 15° nozzle (c) with extended nozzle (d)

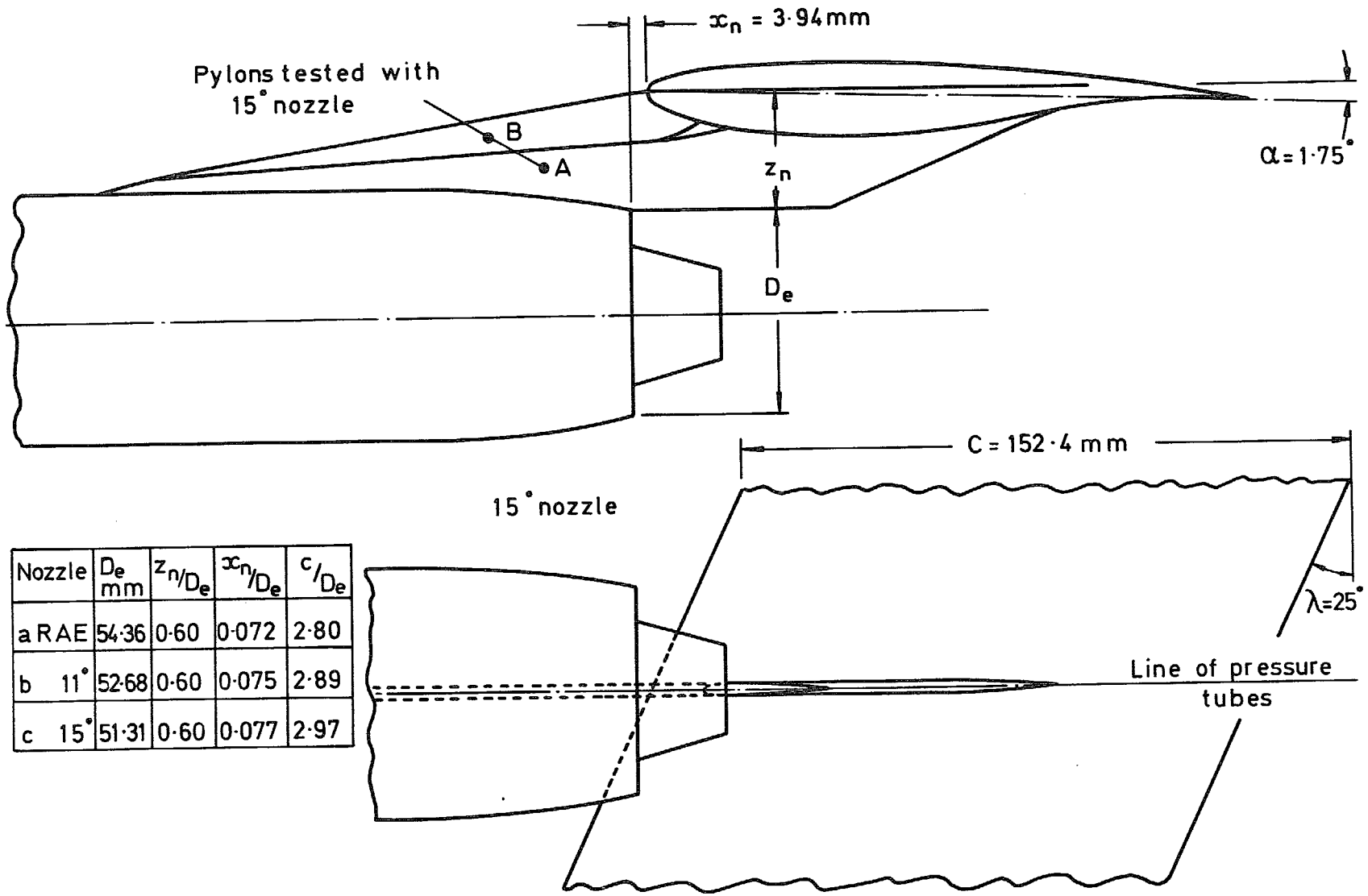

Nozzle	D_e mm	z_n/D_e	x_n/D_e	c/D_e
a RAE	54·36	0·60	0·072	2·80
b 11°	52·68	0·60	0·075	2·89
c 15°	51·31	0·60	0·077	2·97

Fig 3 Position of coaxial nozzles relative to wing

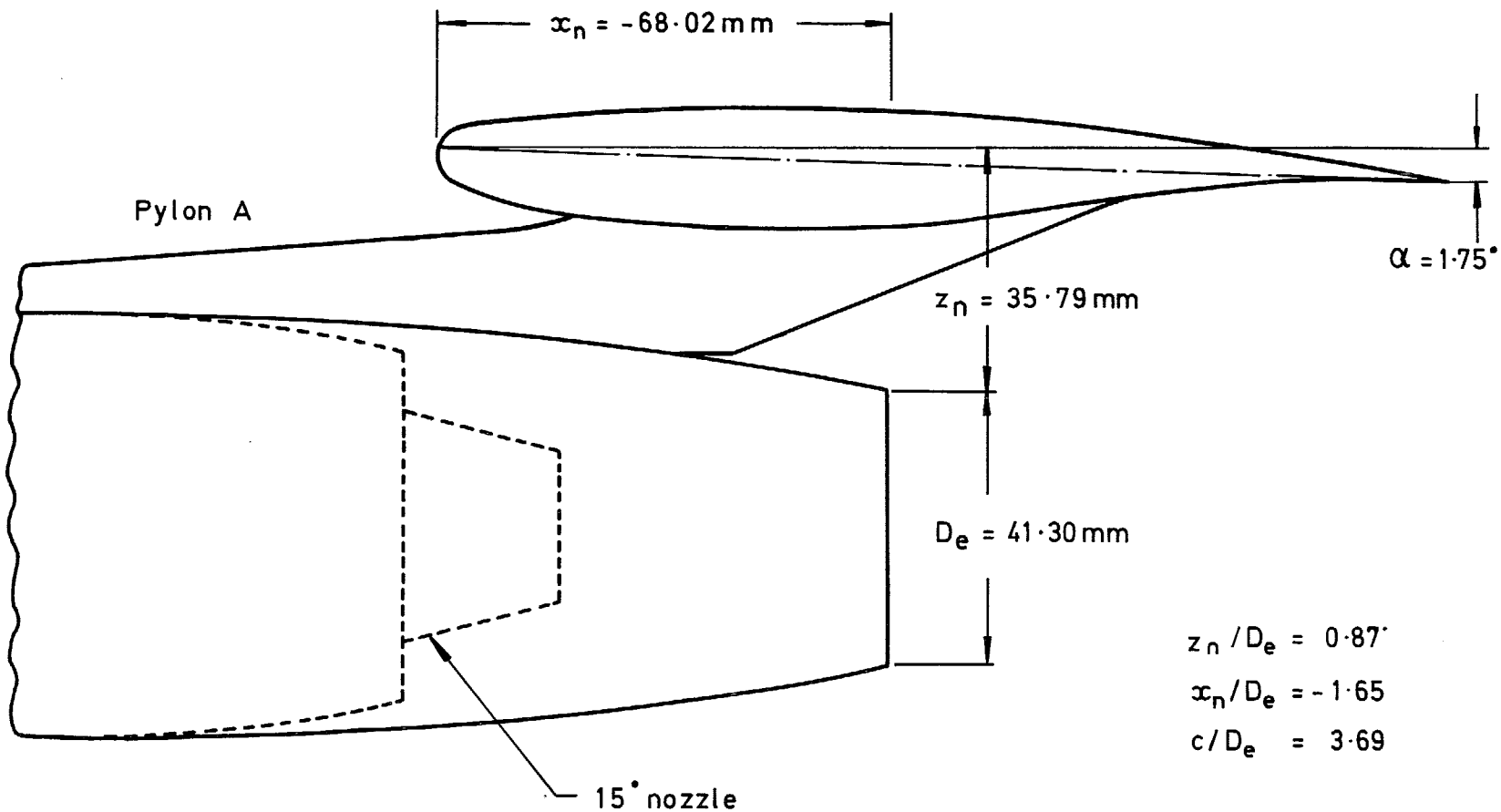

Fig 4 Position of extended nozzle (d)

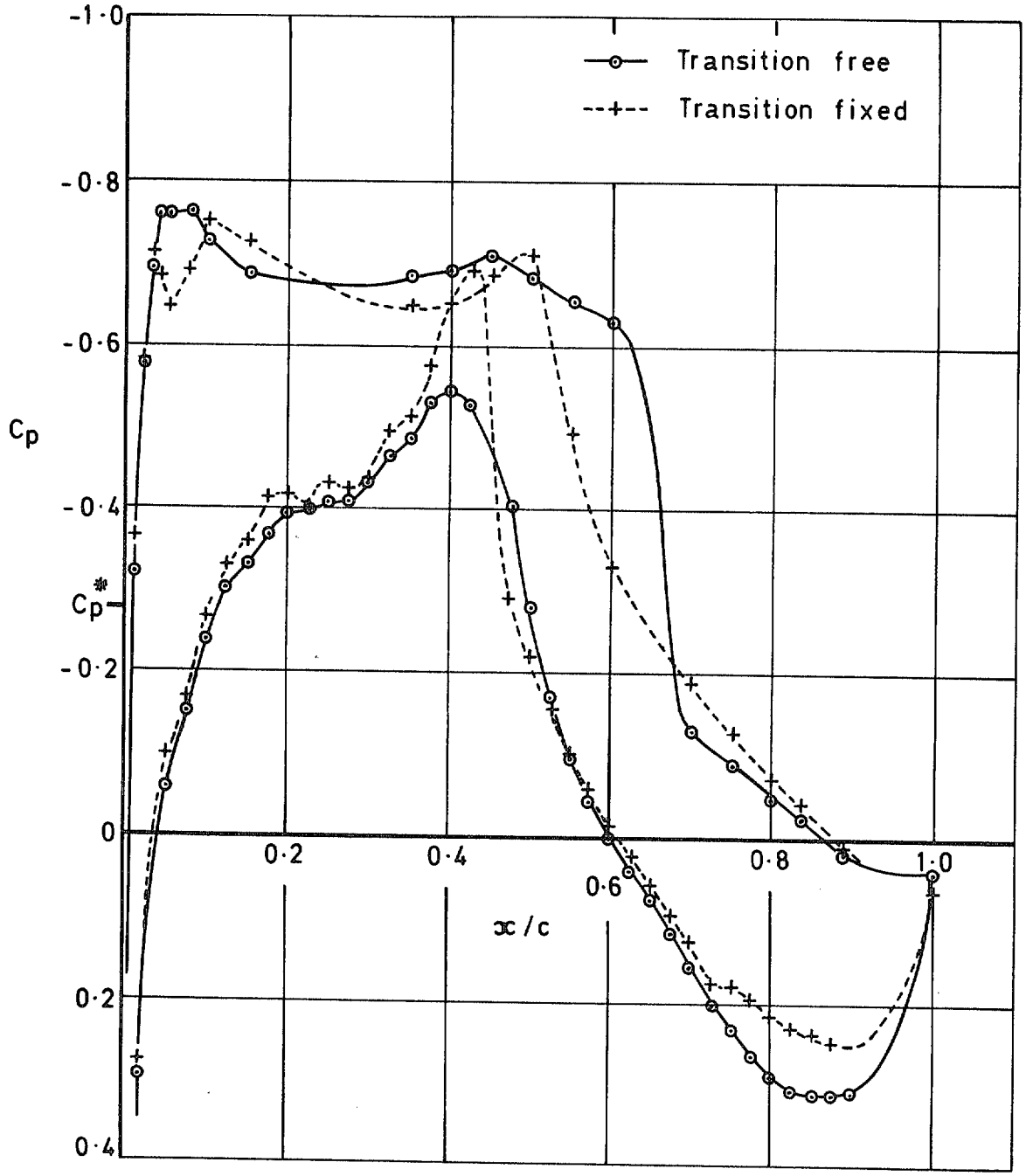

Fig 5 Pressure distributions on the wing alone showing the effect of transition fixing, $M_\infty = 0.86$

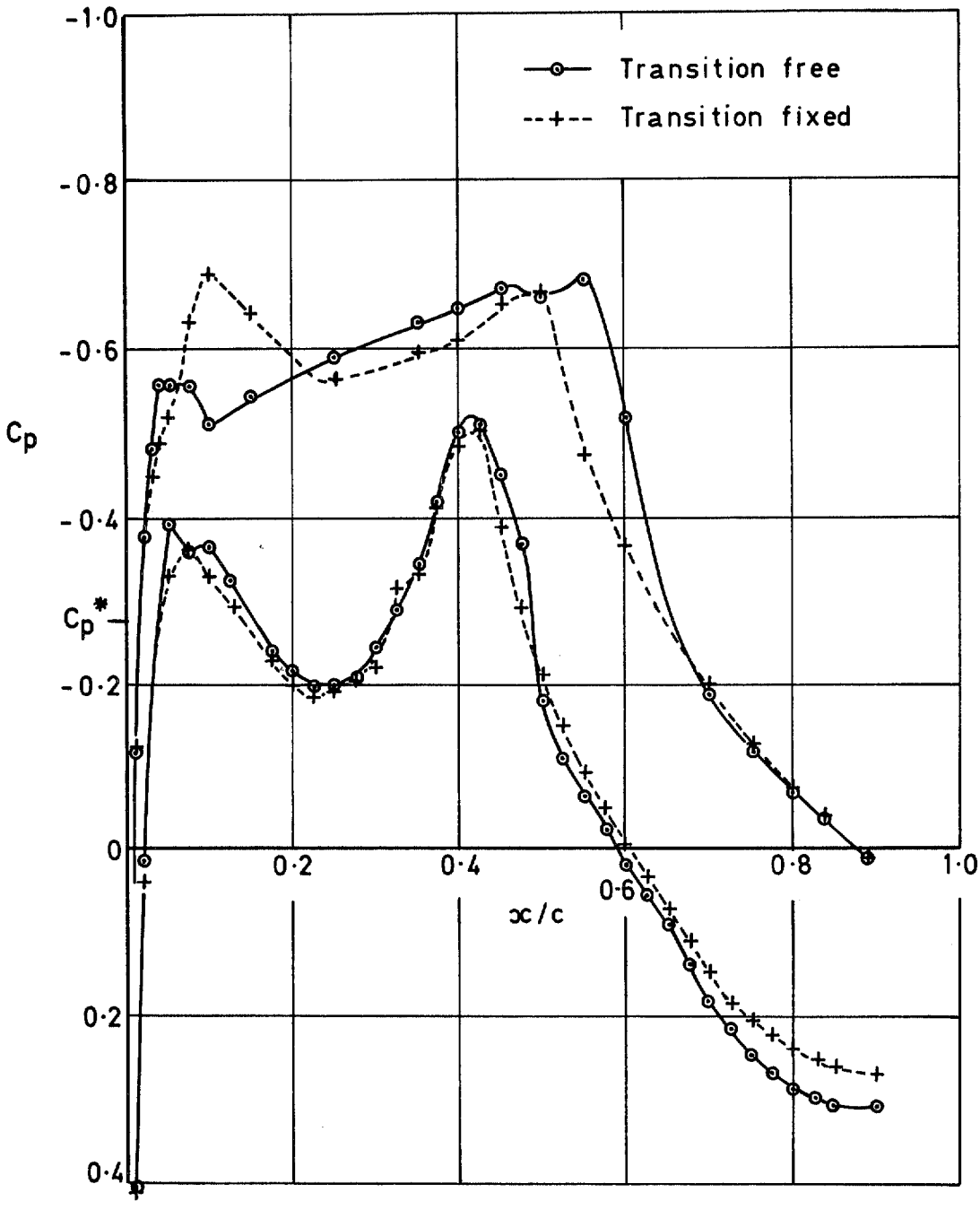

Fig 6 Pressure distributions on the wing with jet blowing at $H_j = 2.4p_\infty$ from 15° nozzle (c), $M_\infty = 0.86$

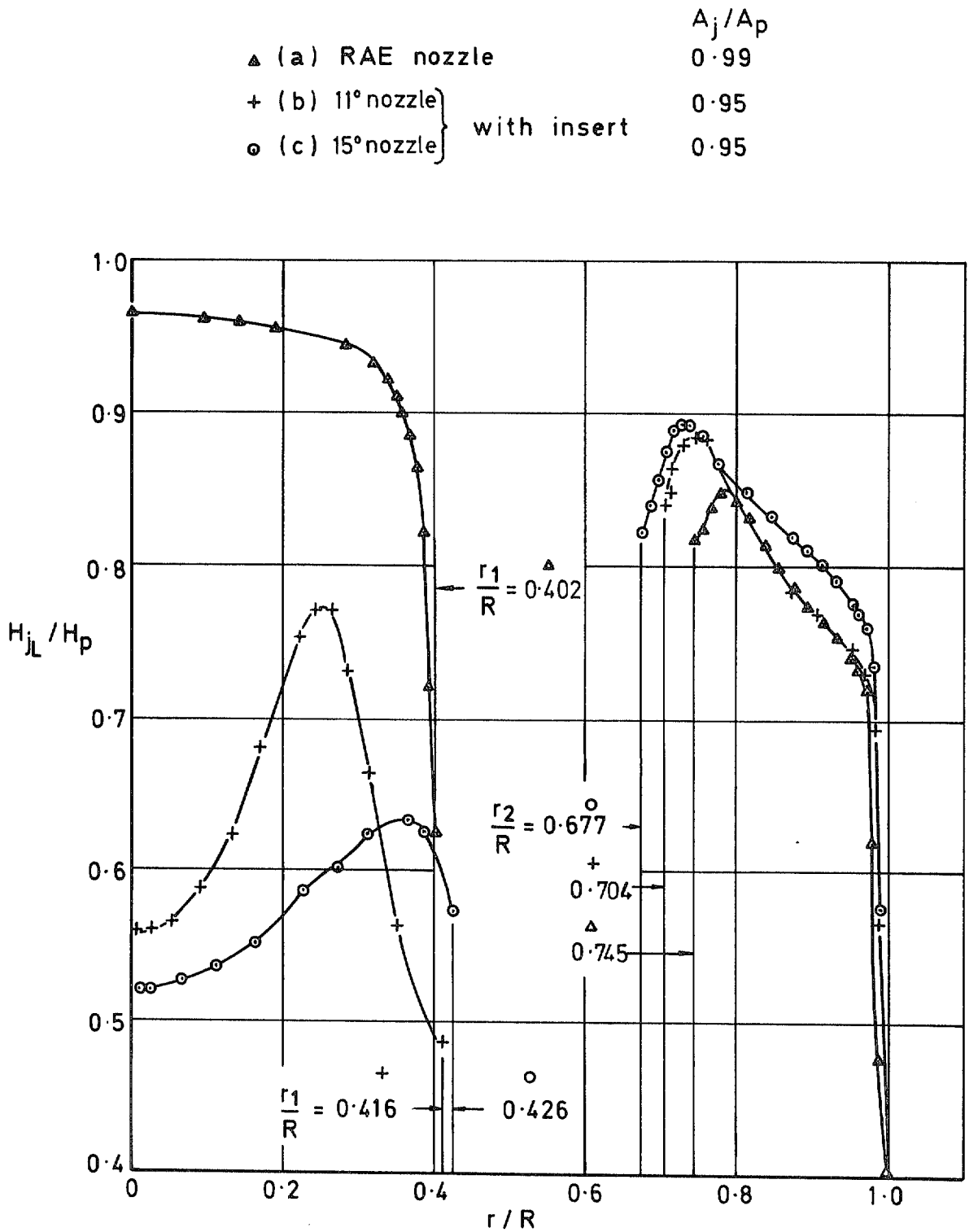

Fig 7 Pitot pressure distributions at the exits of the coaxial nozzles for $H_j/p_\infty > 2$

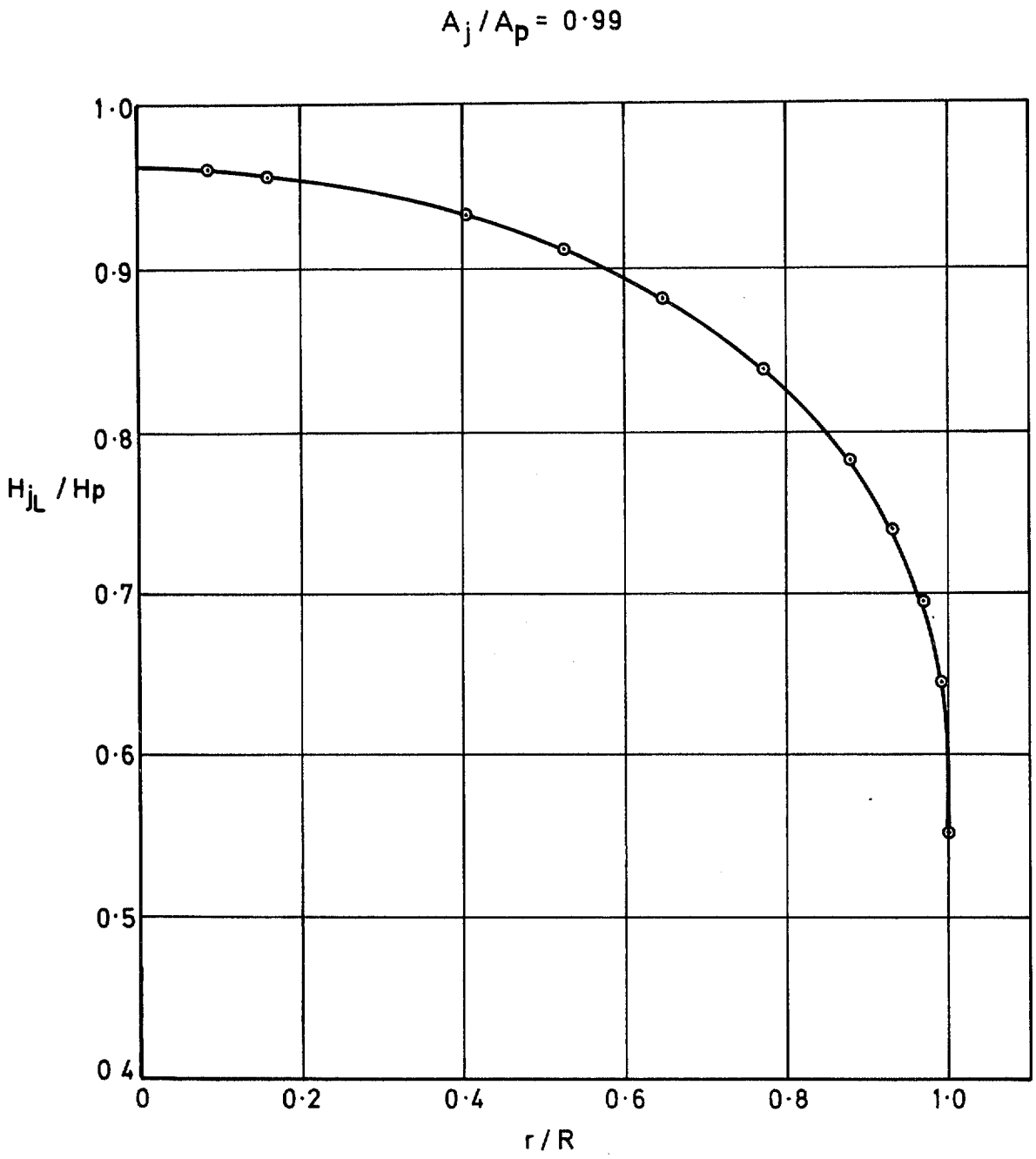

Fig 8 Pitot pressure distribution at the exit of the extended nozzle (d) for $H_j/p_\infty > 2$

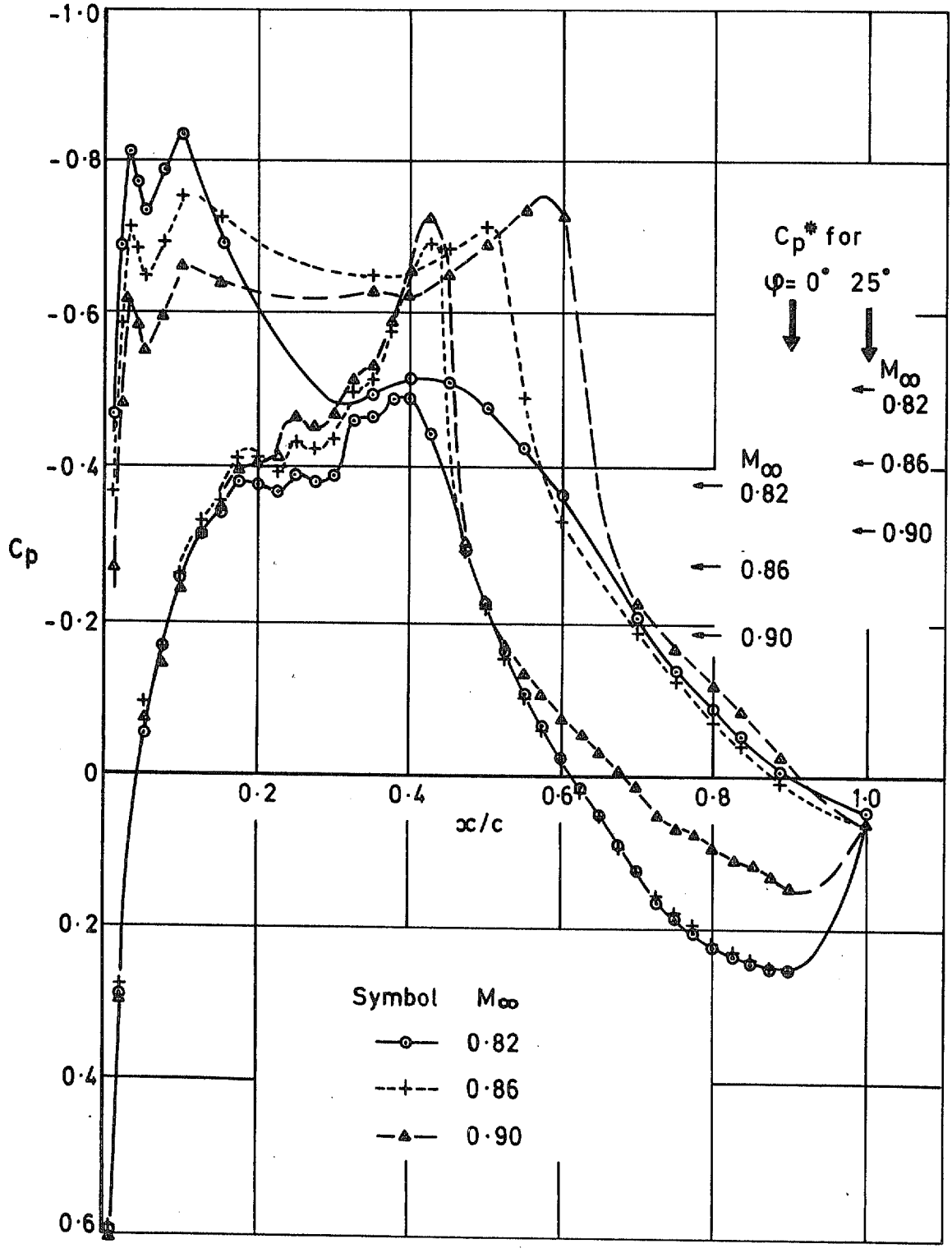

Fig 9 Pressure distribution on the wing alone with fixed transition

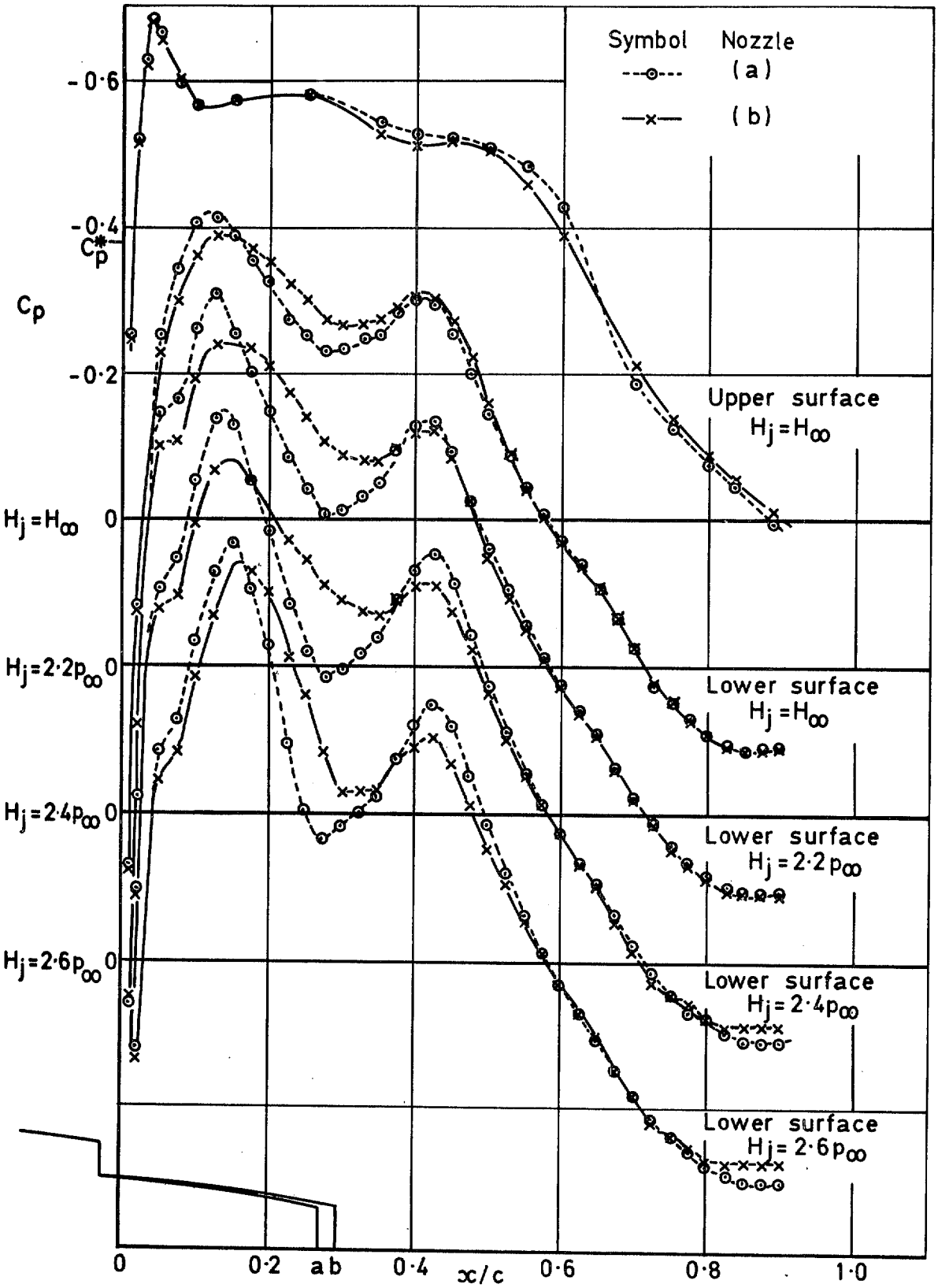

Fig 10 Comparison of wing pressure distributions with nozzles (a) and (b), $M_\infty = 0.82$

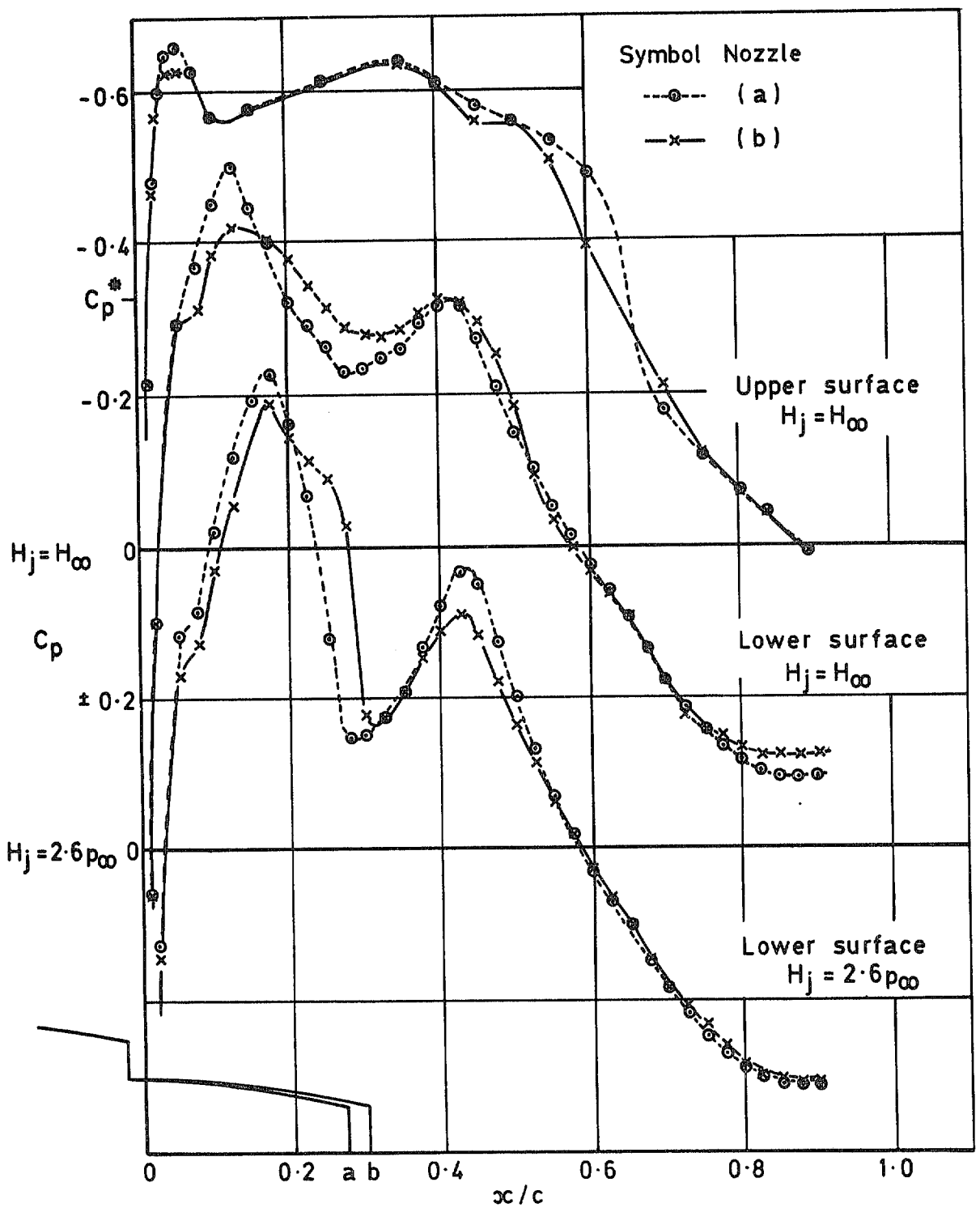

Fig 11 Comparison of wing pressure distributions with nozzles (a) and (b), $M_\infty = 0.84$

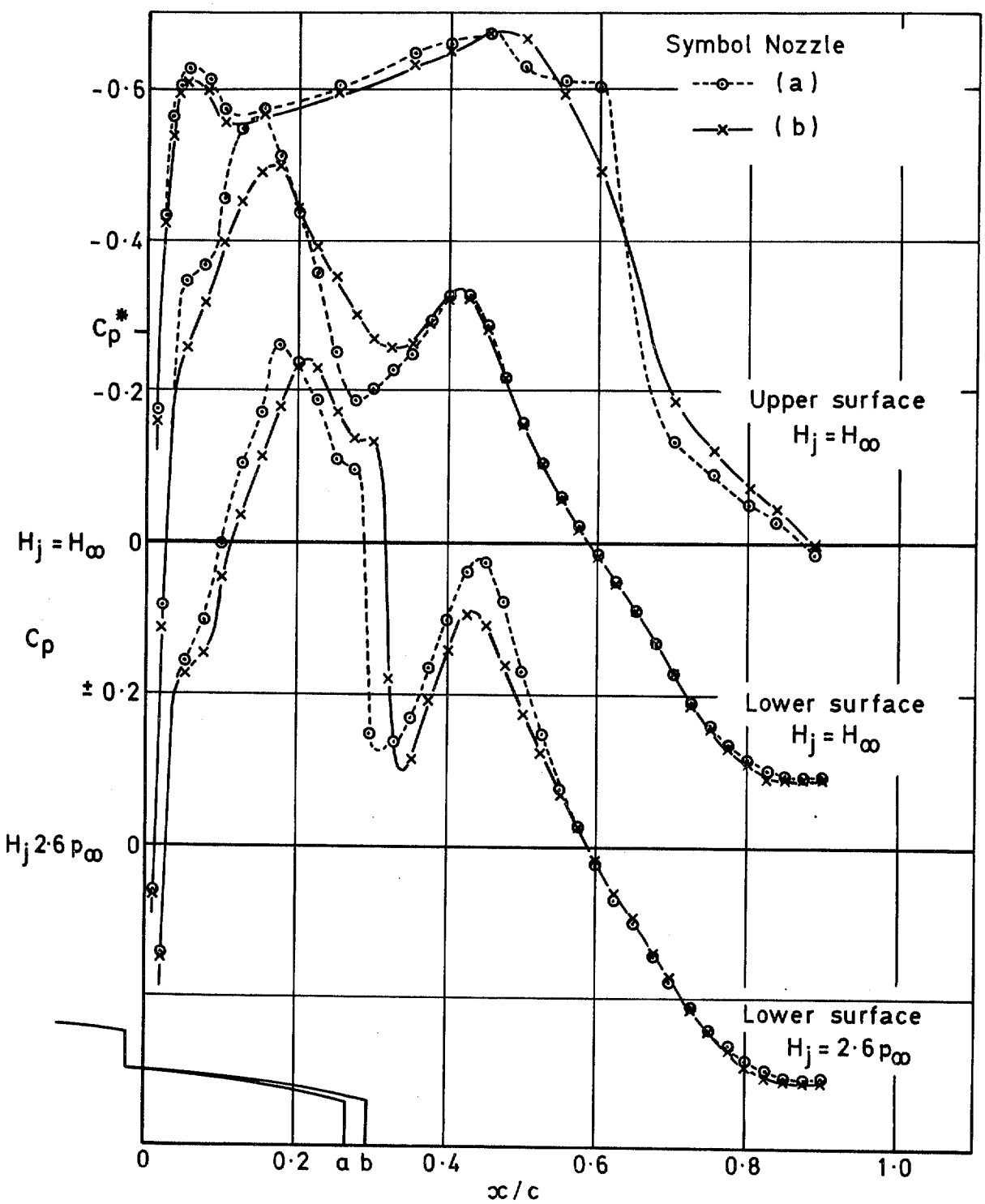

Fig 12 Comparison of wing pressure distributions with nozzles (a) and (b), $M_\infty = 0.86$

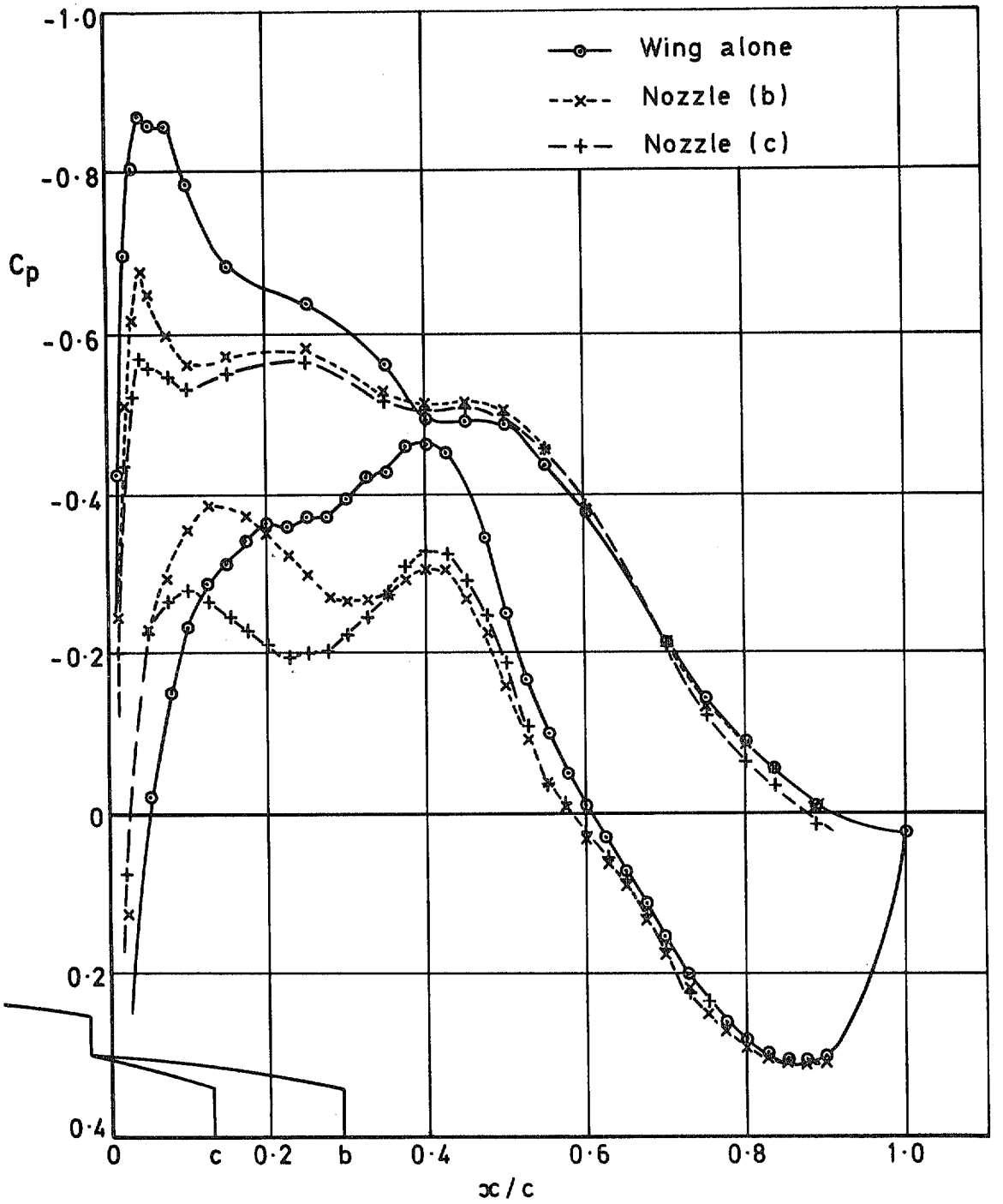

Fig 13 The effect on wing pressures when nozzles (b) and (c) are added to the wing, $H_j = H_\infty$, $M_\infty = 0.82$

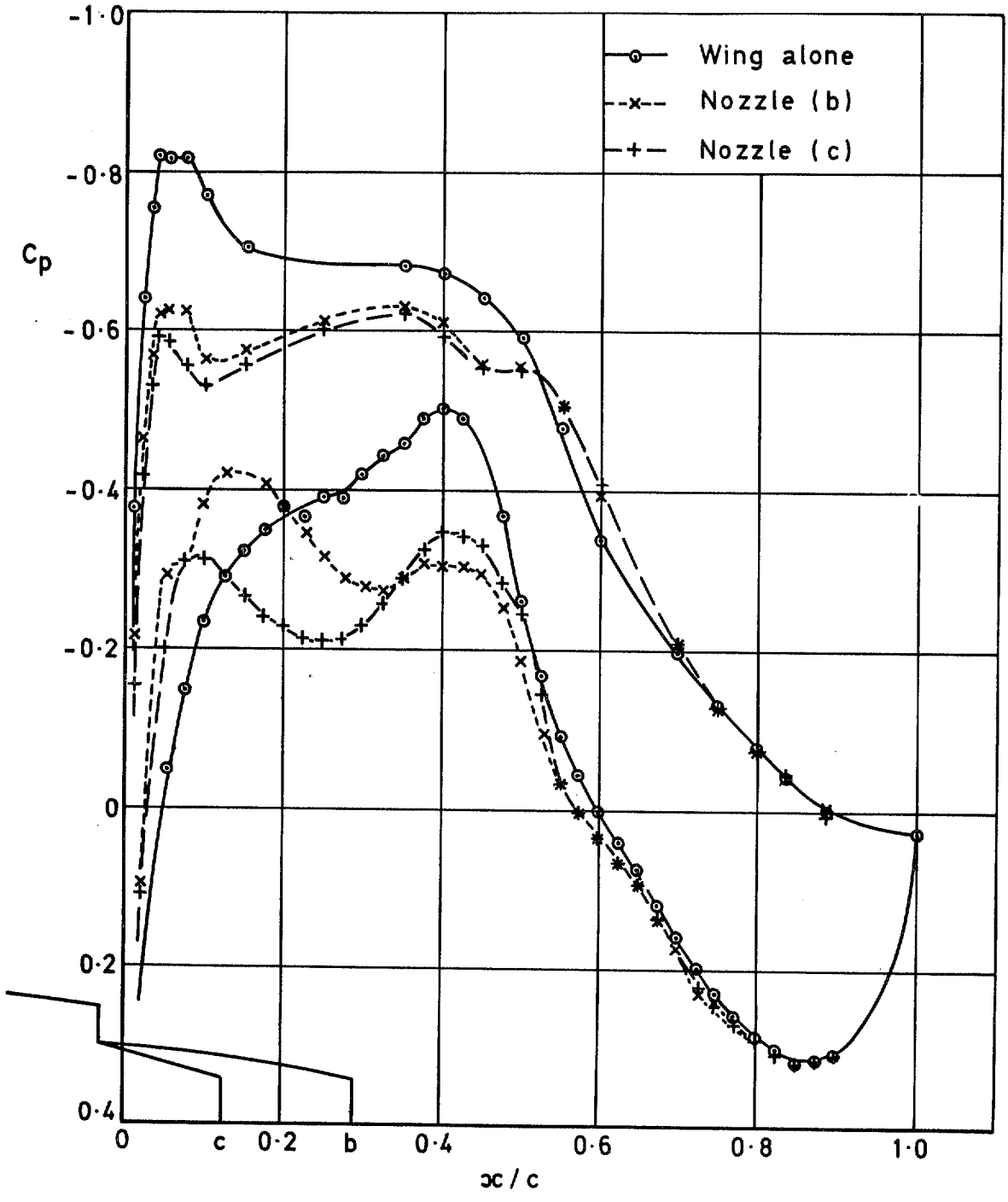

Fig 14 The effect on wing pressures when nozzles (b) and (c) are added to the wing, $H_j = H_\infty$, $M_\infty = 0.84$

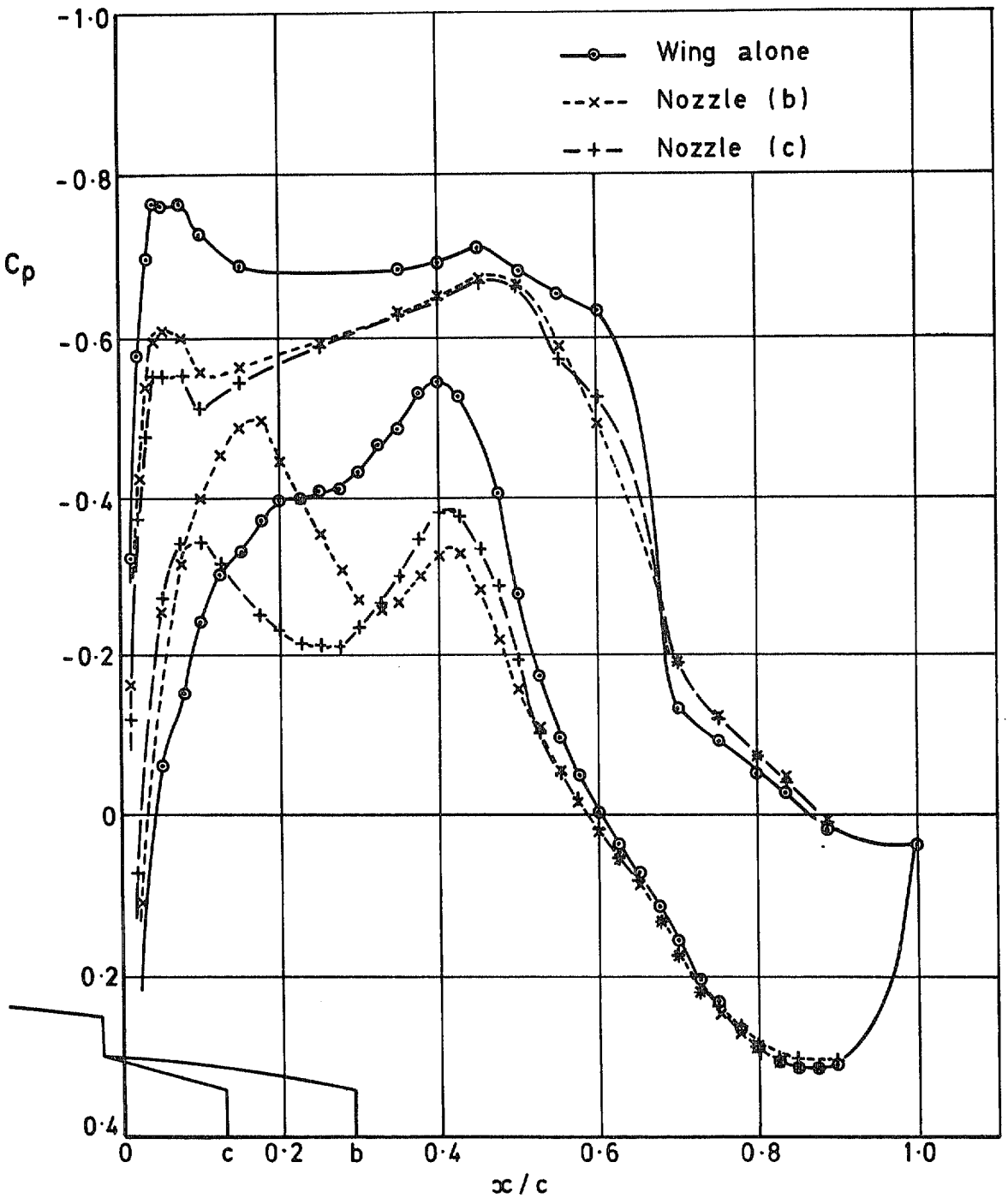

Fig 15 The effect on wing pressures when nozzles (b) and (c) are added to the wing, $H_j = H_\infty$, $M_\infty = 0.86$

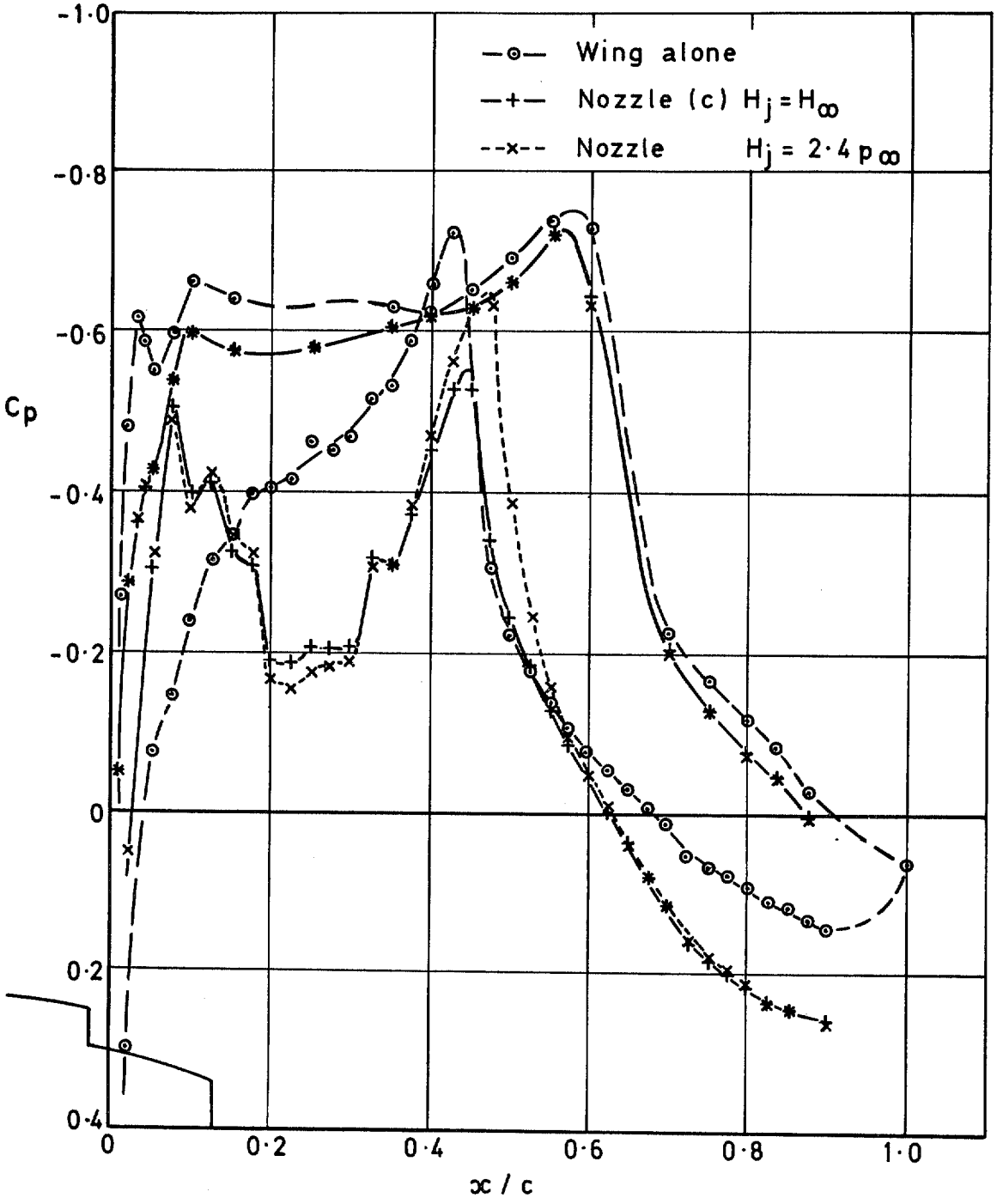

Fig 16 Wing pressure distributions showing the effect of adding nozzle (c) at $M_\infty = 0.90$

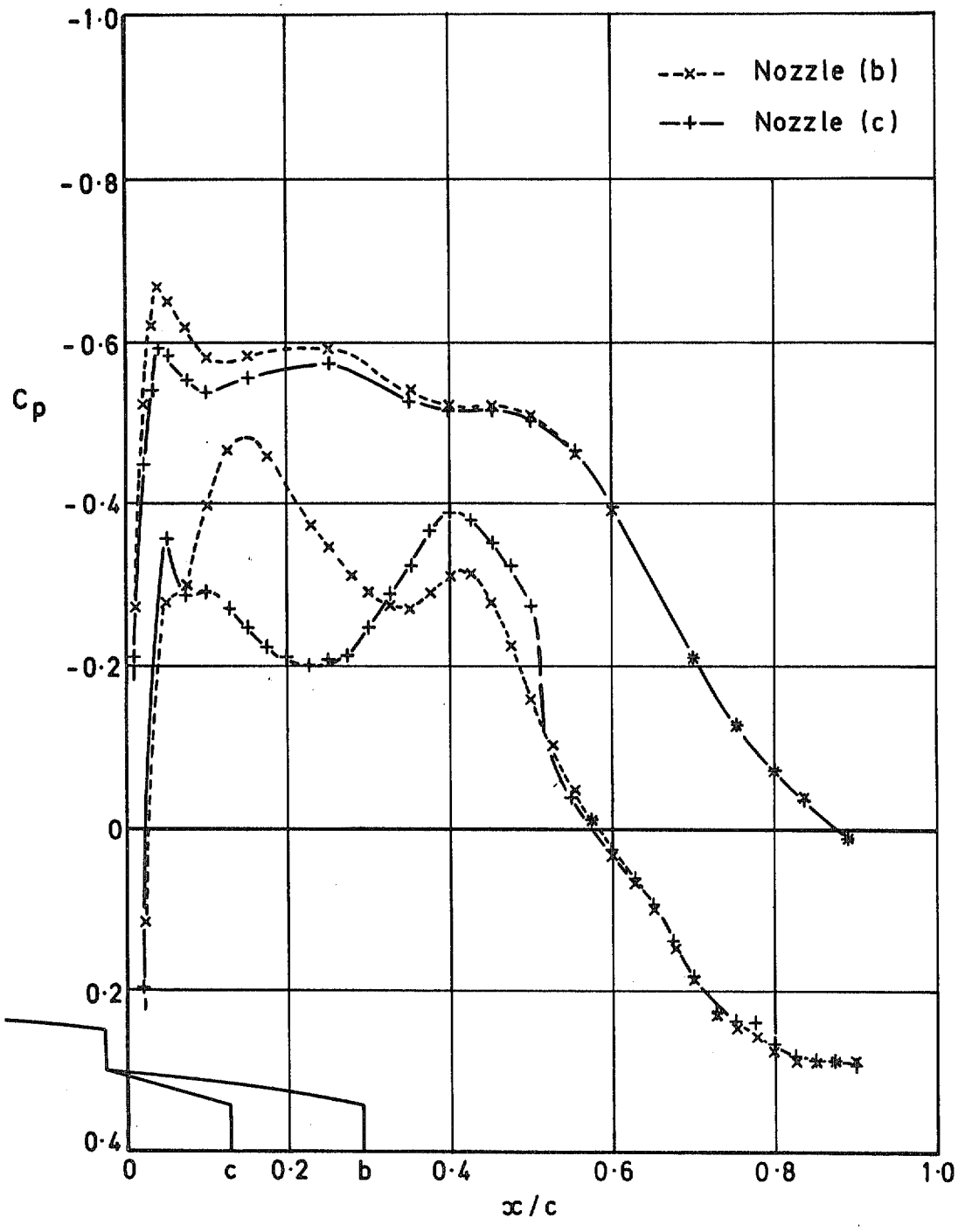

Fig 17 Wing pressures with nozzles (b) and (c) blowing at $H_j = 2.4p_\infty$, $M_\infty = 0.82$

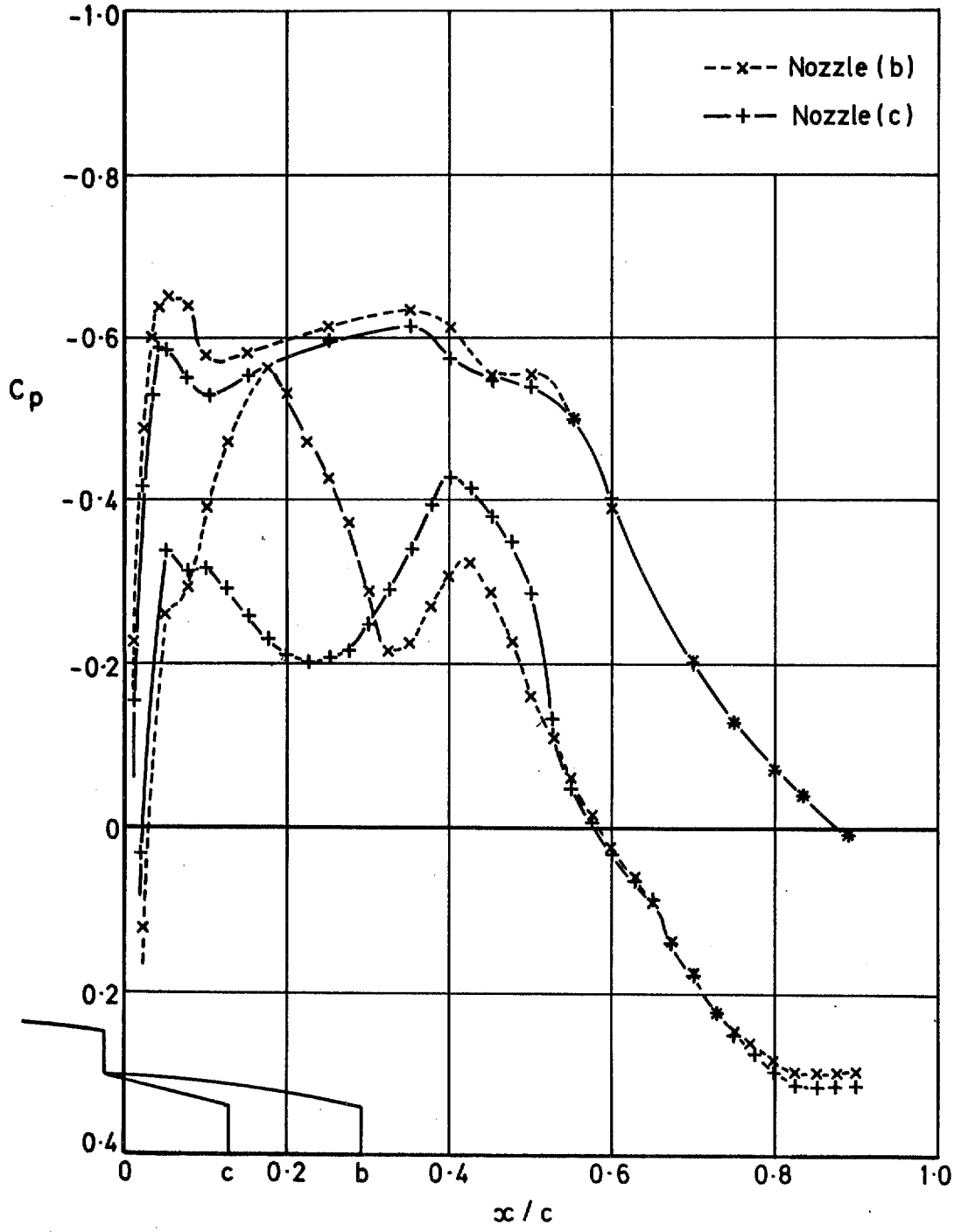

Fig 18 Wing pressures with nozzles (b) and (c) blowing at $H_j = 2.4p_\infty$, $M_\infty = 0.84$

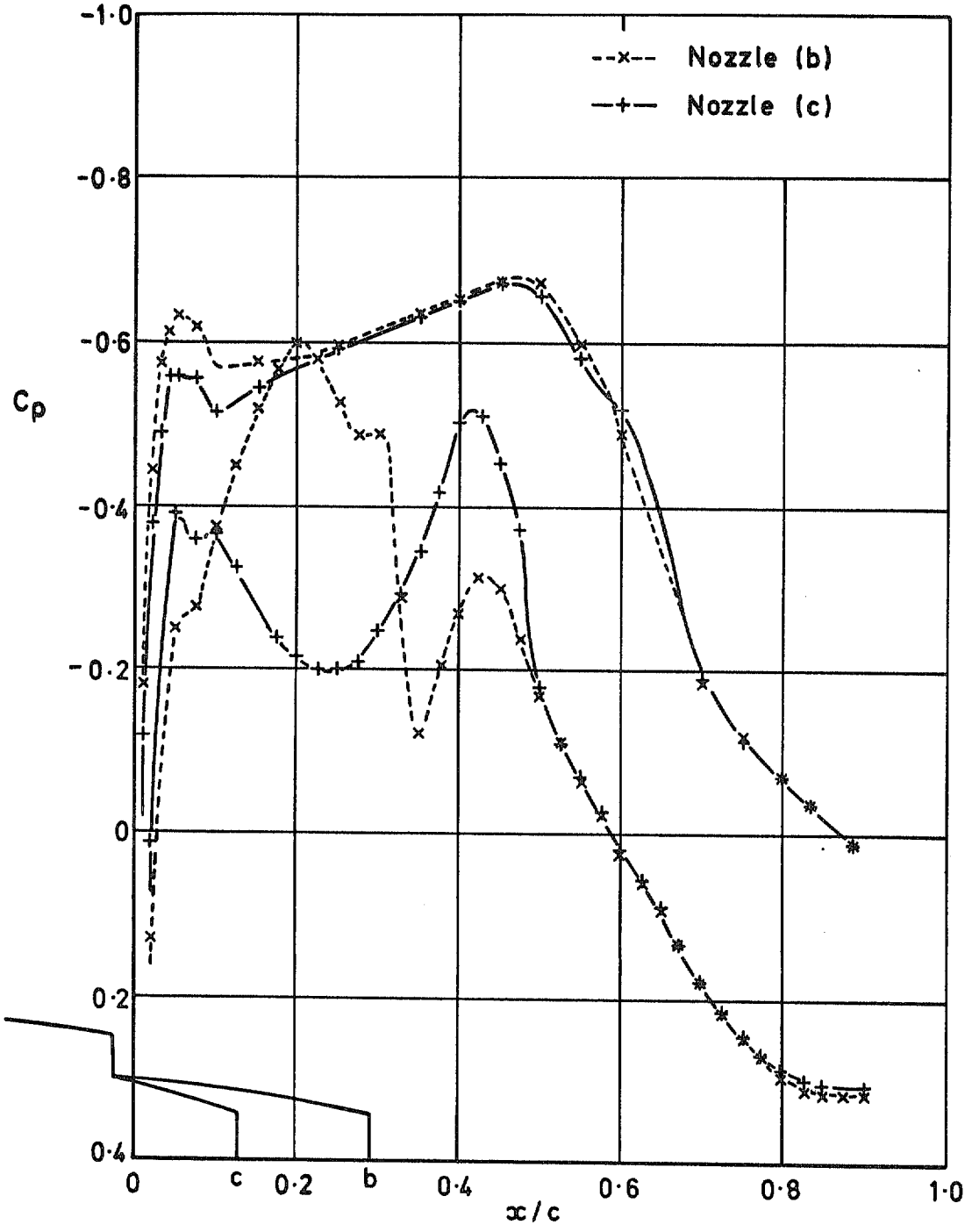

Fig 19 Wing pressures with nozzles (b) and (c) blowing at $H_j = 2.4p_\infty$, $M_\infty = 0.86$

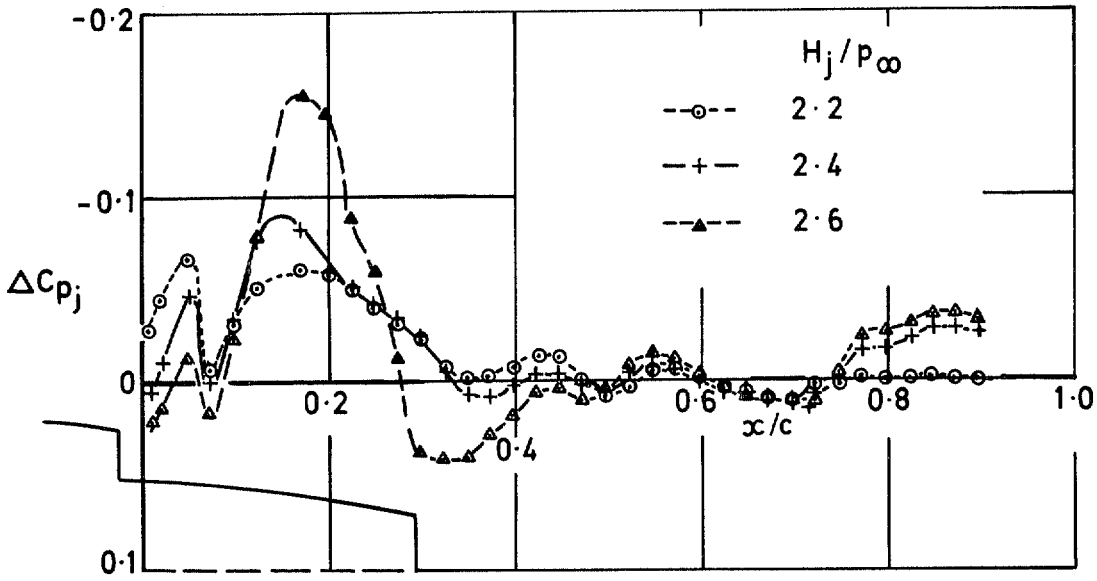

(b) 11° nozzle

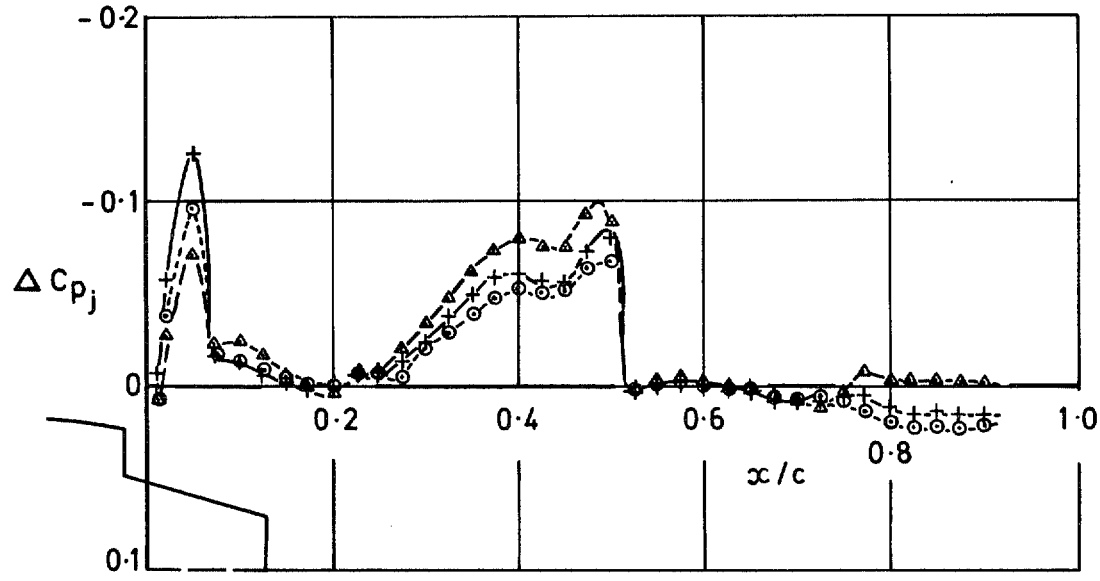

(c) 15° nozzle

Fig 20 Interference on the wing lower surface due to jet blowing from nozzles (b) and (c), $M_\infty = 0.82$

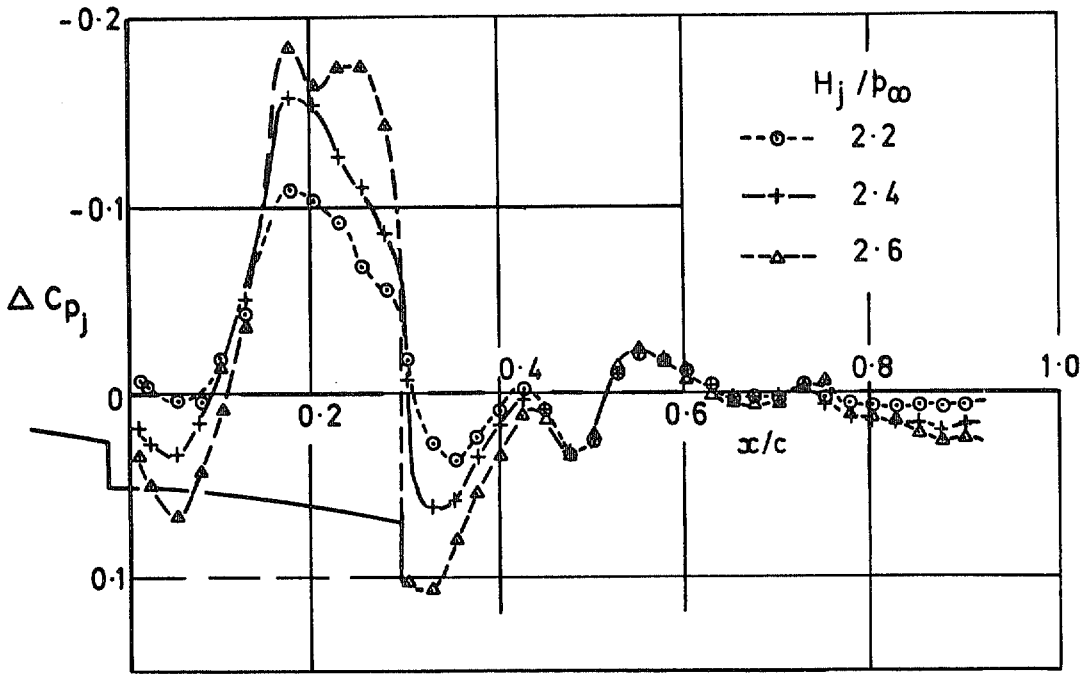

(b) 11° nozzle

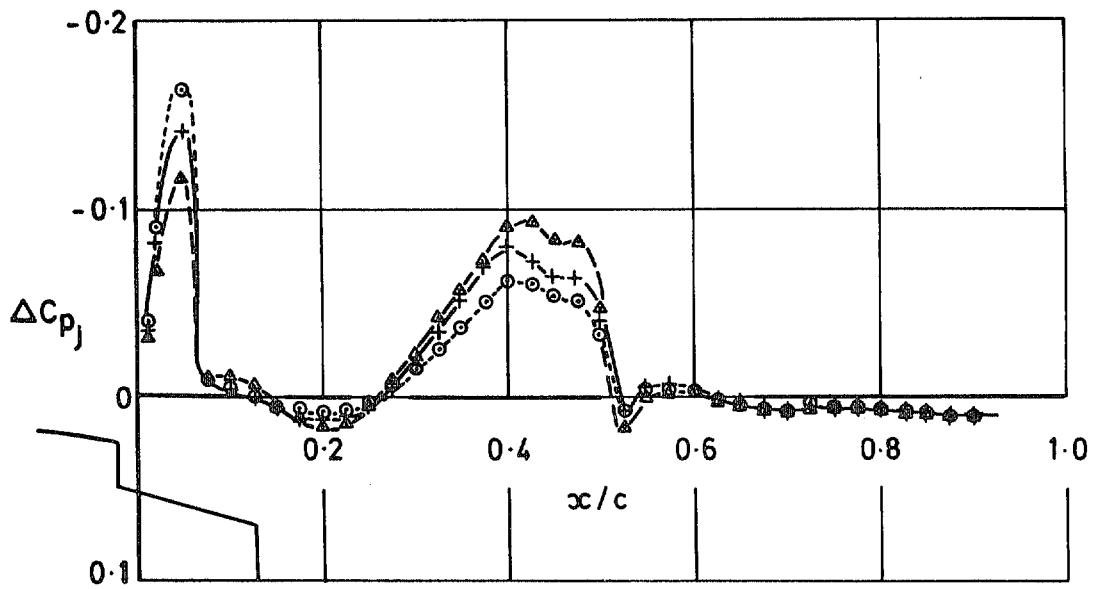

(c) 11° nozzle

Fig 21 Interference on the wing lower surface due to jet blowing from nozzles (b) and (c), $M_\infty = 0.84$

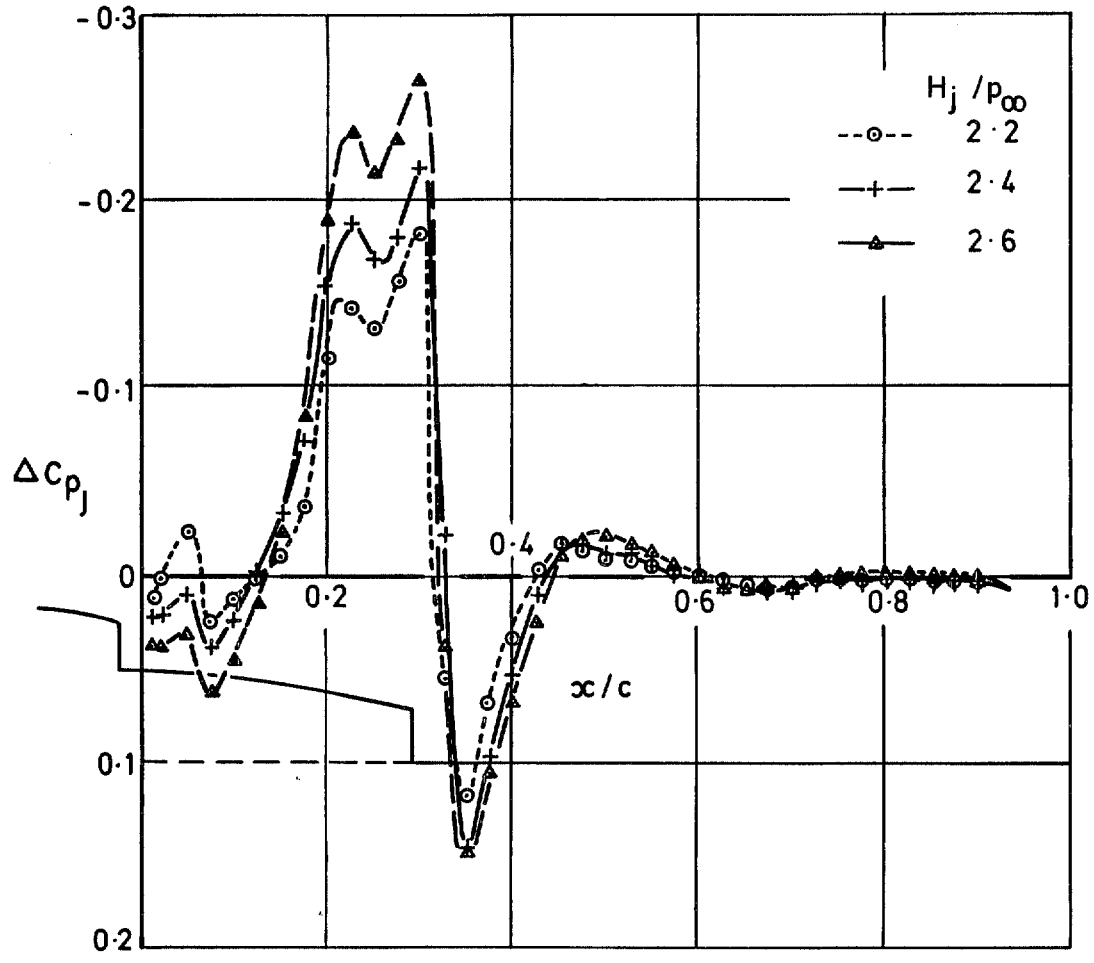

(b) 11° nozzle

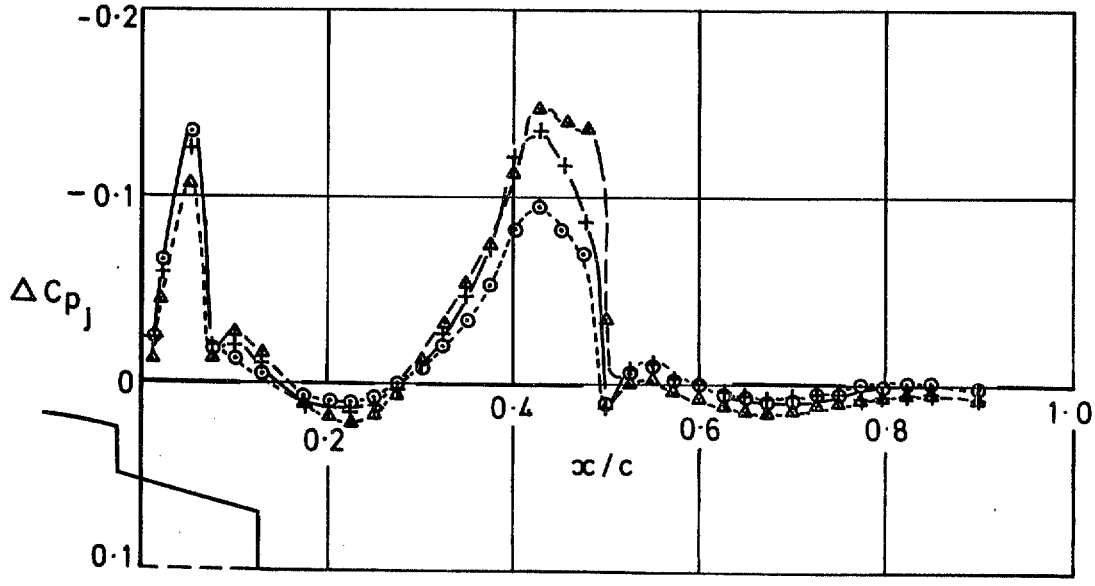

(c) 15° nozzle

Fig 22 Interference on the wing lower surface due to jet blowing from nozzles (b) and (c), $M_\infty = 0.86$

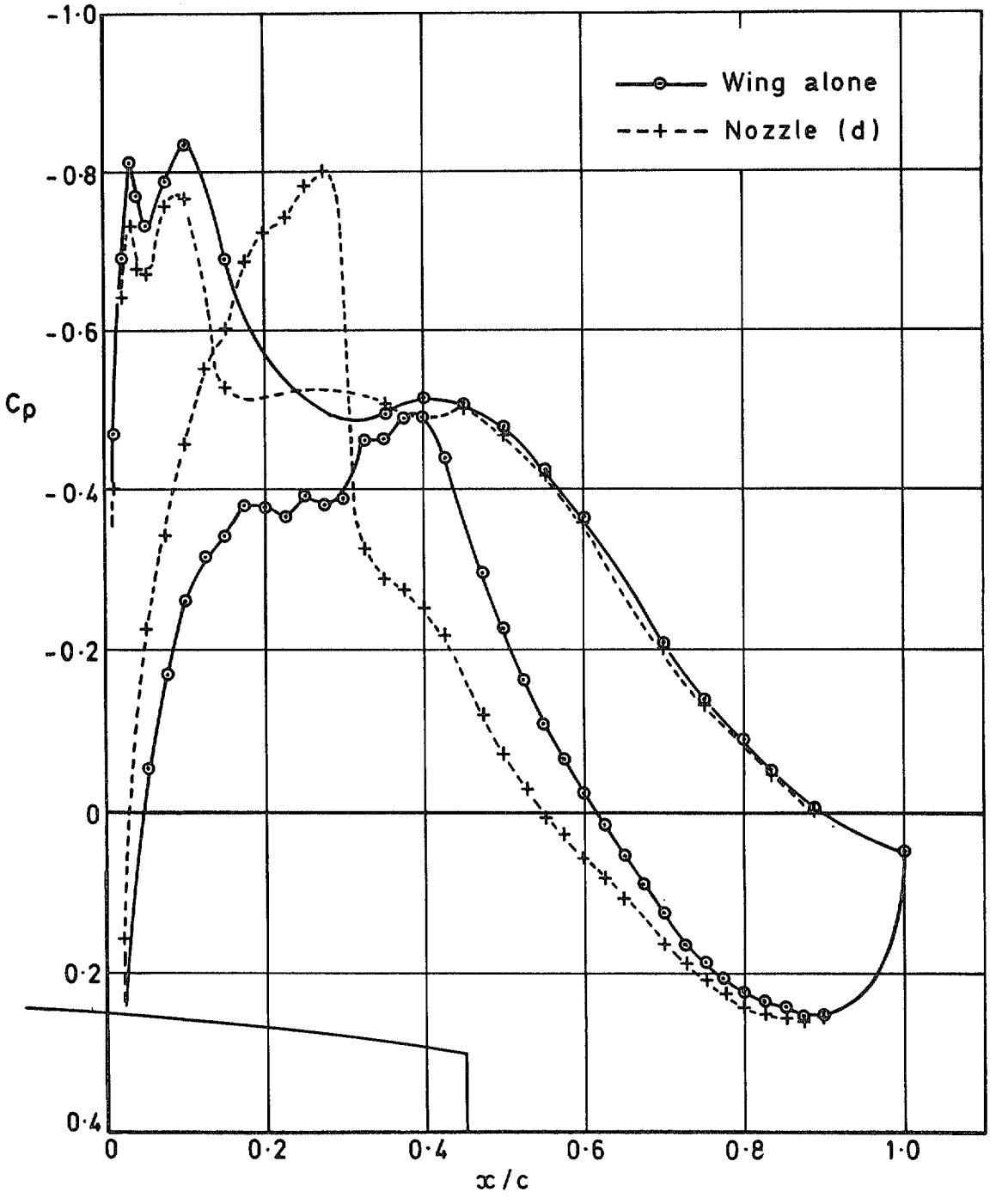

Fig 23 Effect on wing pressures when nozzle (d) is added to wing at $M_\infty = 0.82$, $H_j = H_\infty$

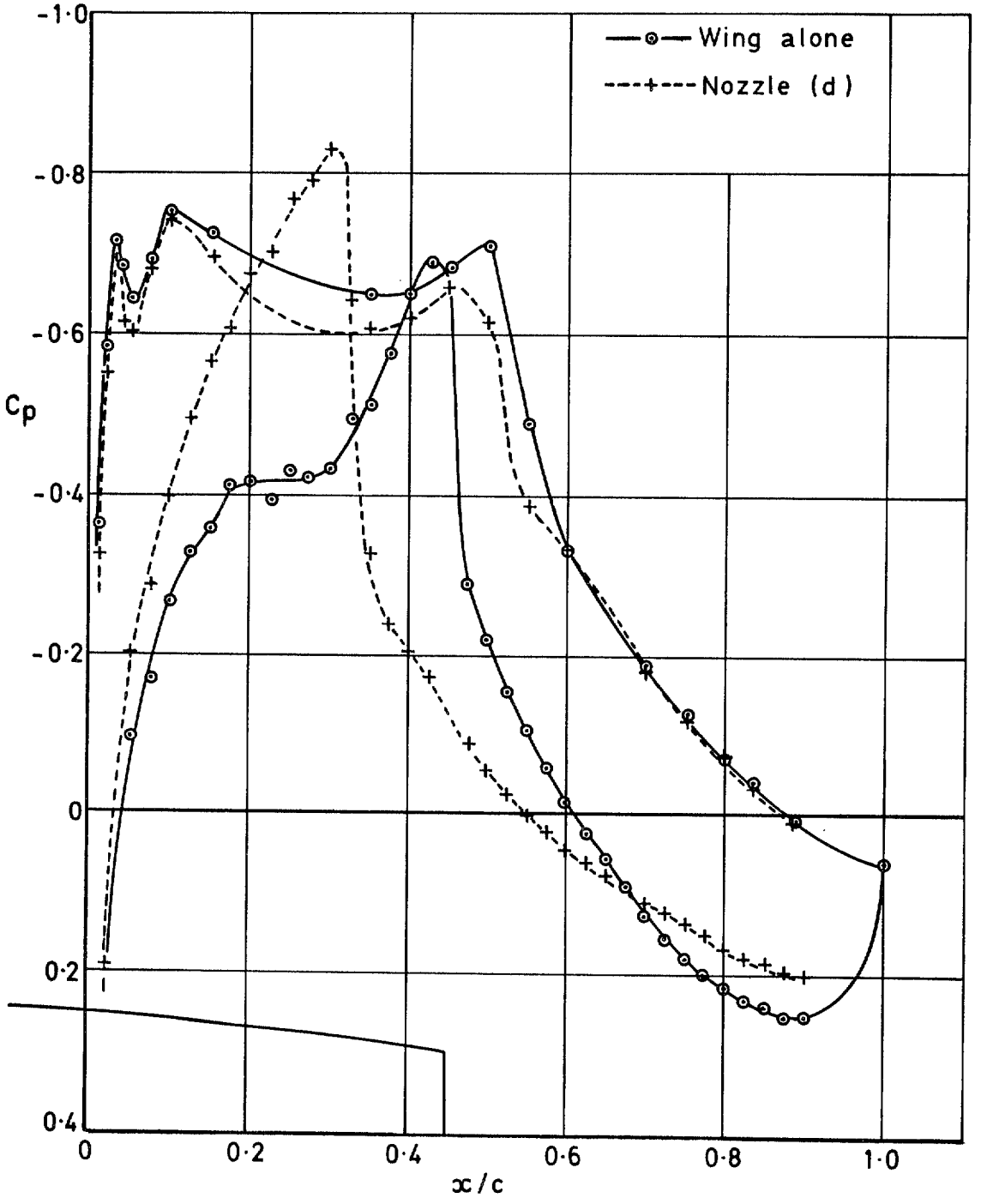

Fig 24 Effect on wing pressures when nozzle (d) is added to wing at $M_\infty = 0.86$, $H_j = H_\infty$

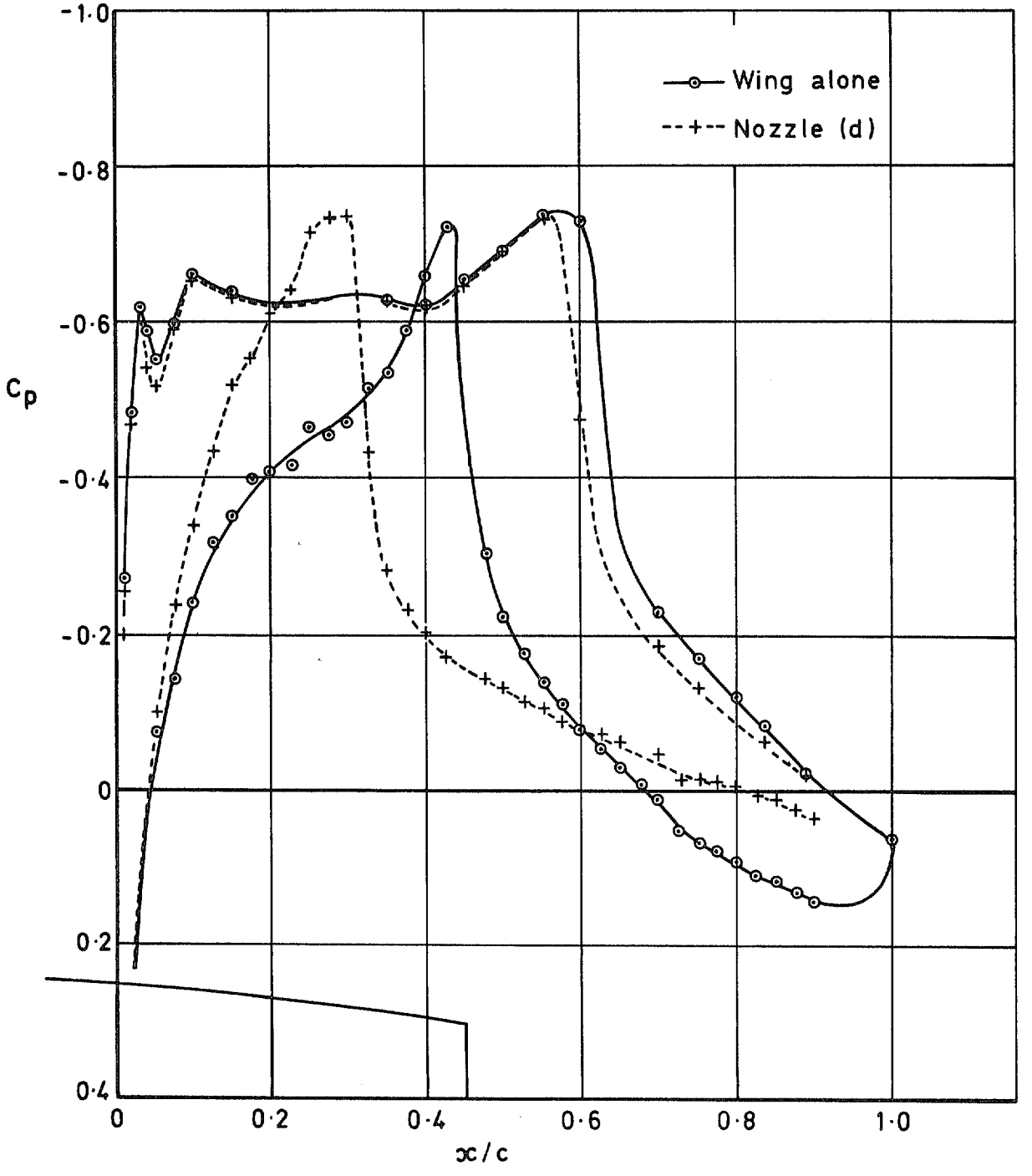

Fig 25 Effect on wing pressures when nozzle (d) is added to wing at $M_\infty = 0.90$, $H_j = H_\infty$

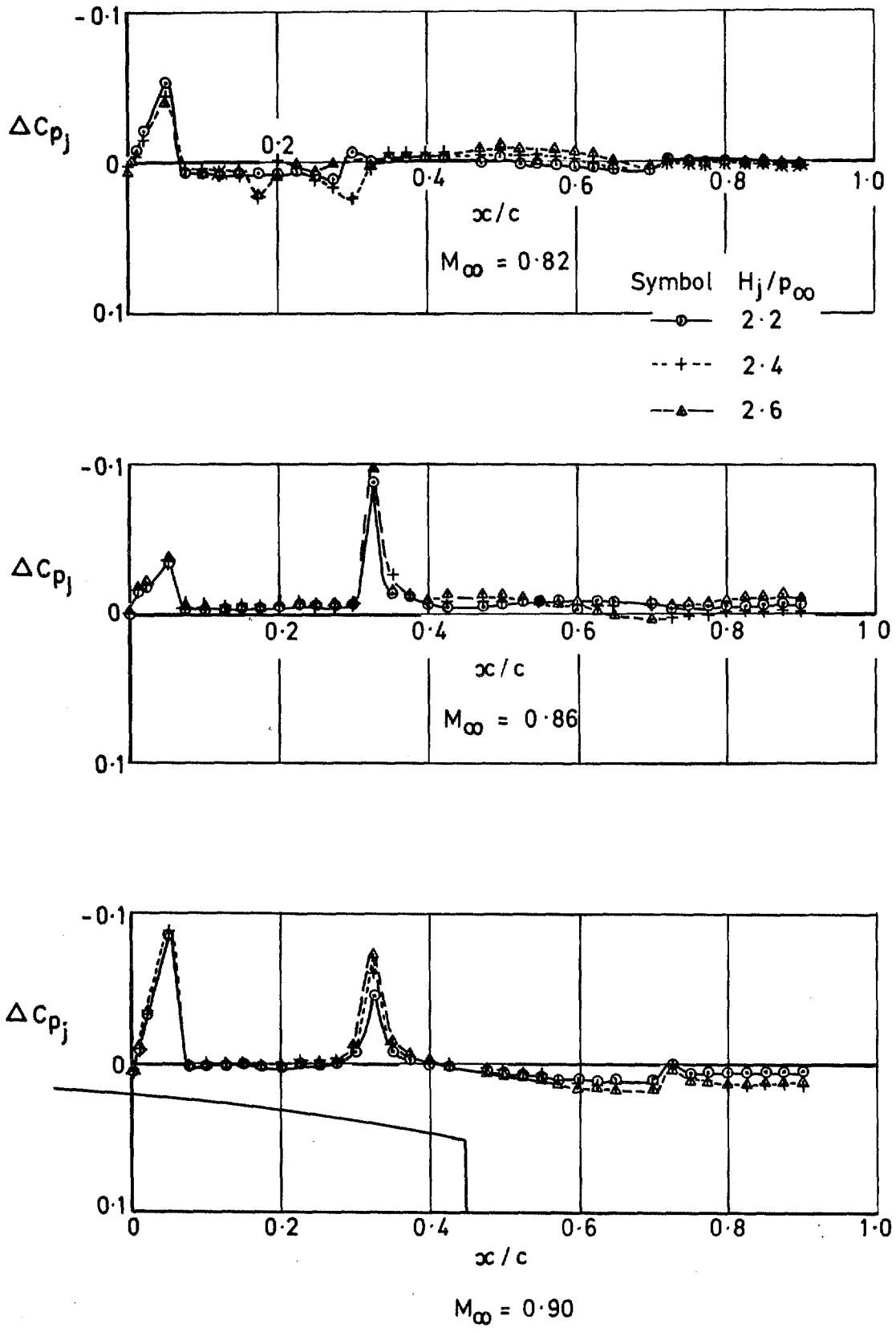

Fig 26 Effect on wing lower surface with nozzle (d) and jet blowing

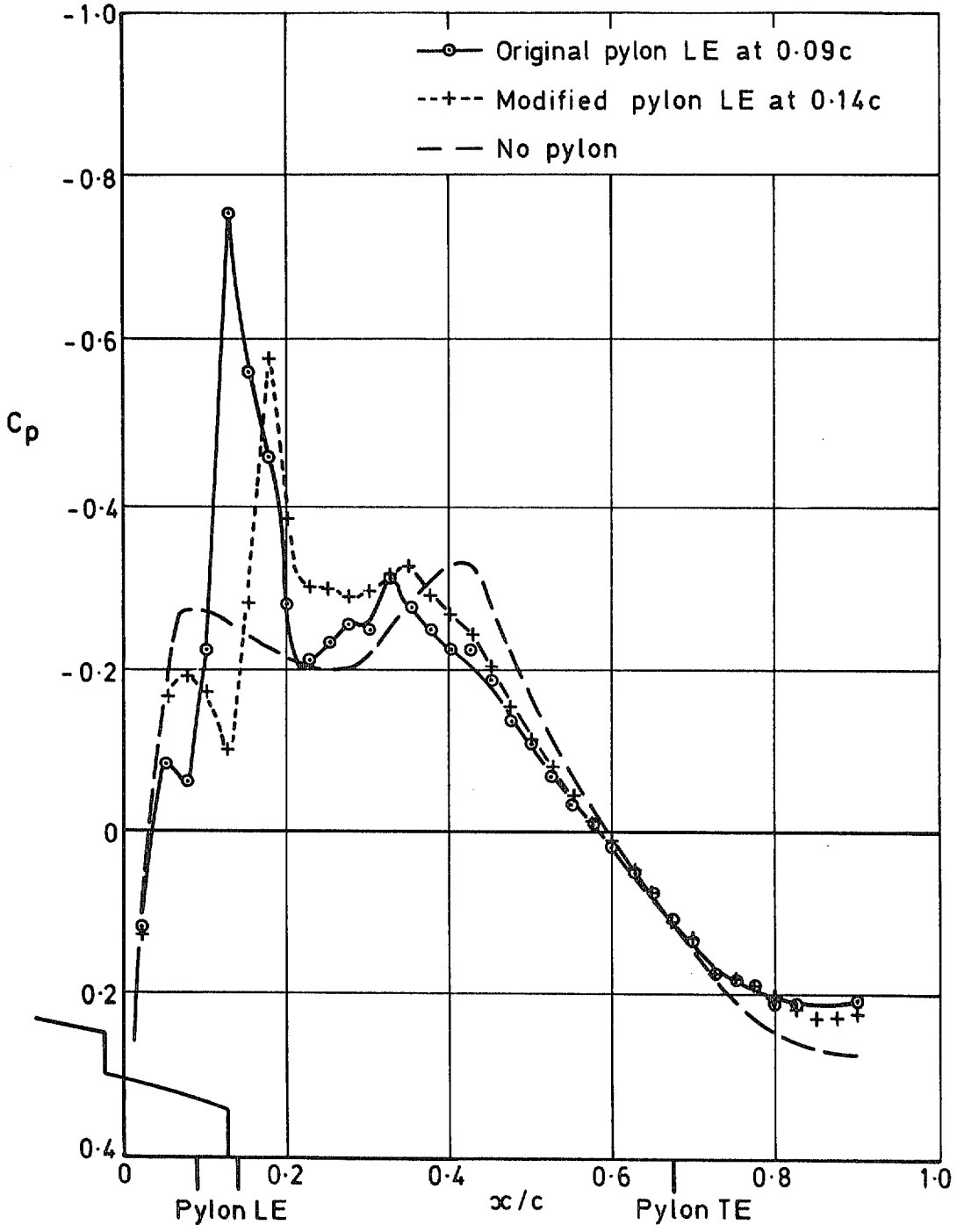

Fig 27 Pressure distributions at wing/pylon inboard junction for 15° nozzle (c) with Pylon A, $M_\infty = 0.82$, $H_j = H_\infty$

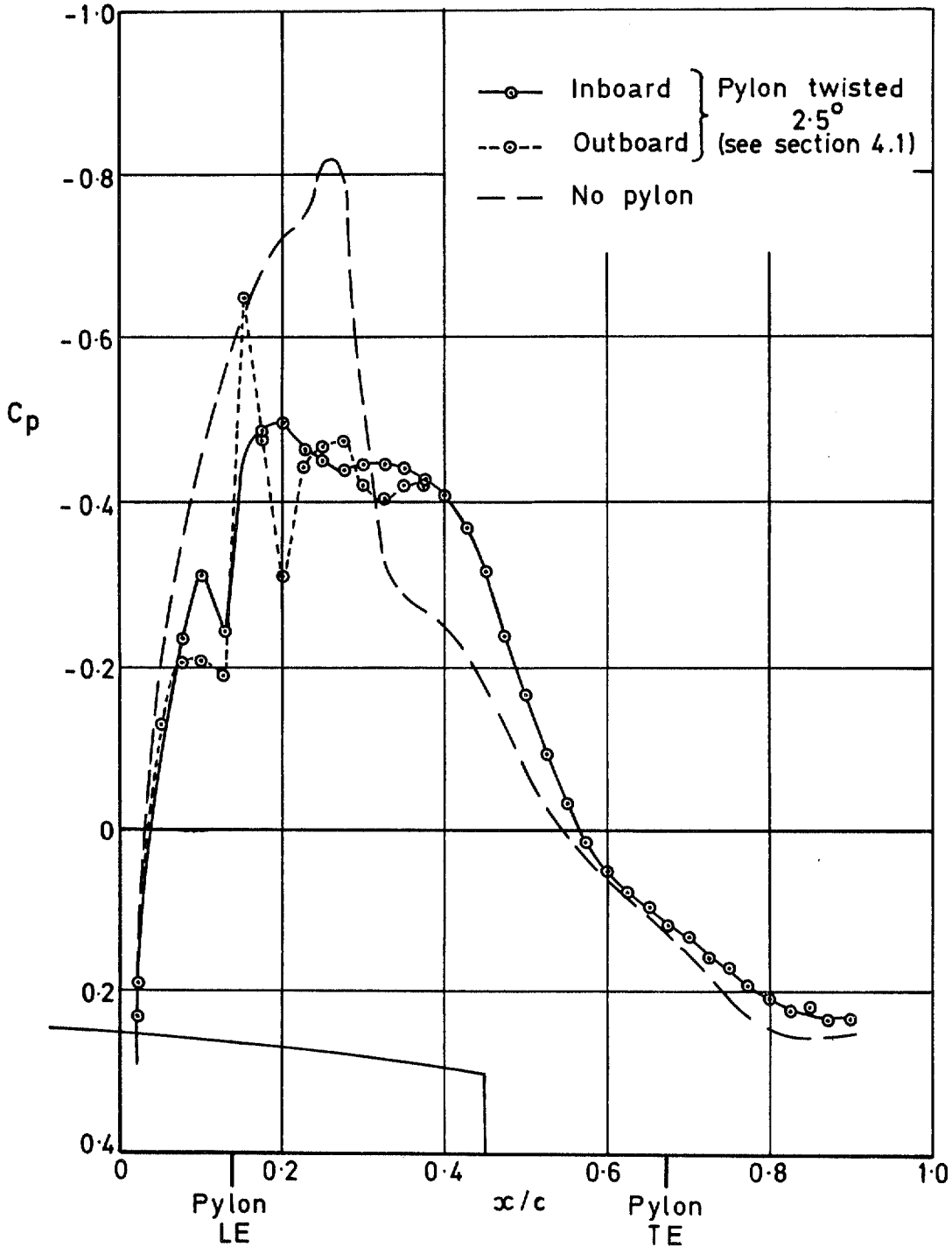

Fig 28 Pressure distributions at wing/pylon junction for extended nozzle (d) with Pylon A, $M_\infty = 0.82$, $H_j = H_\infty$

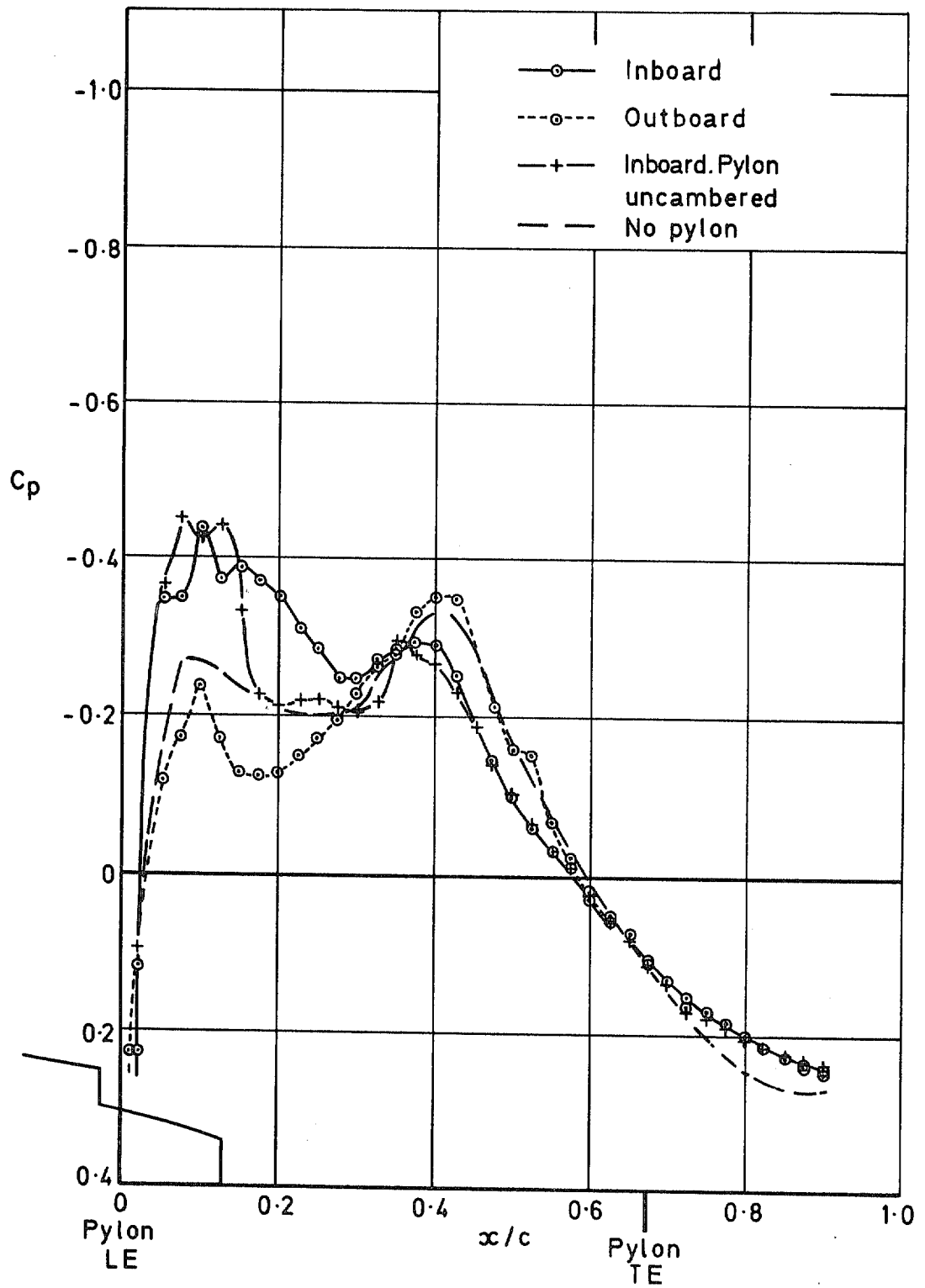

Fig 29 Pressure distributions at wing/pylon junction for 15° nozzle (c) with Pylon B, $M_\infty = 0.82$, $H_j = H_\infty$

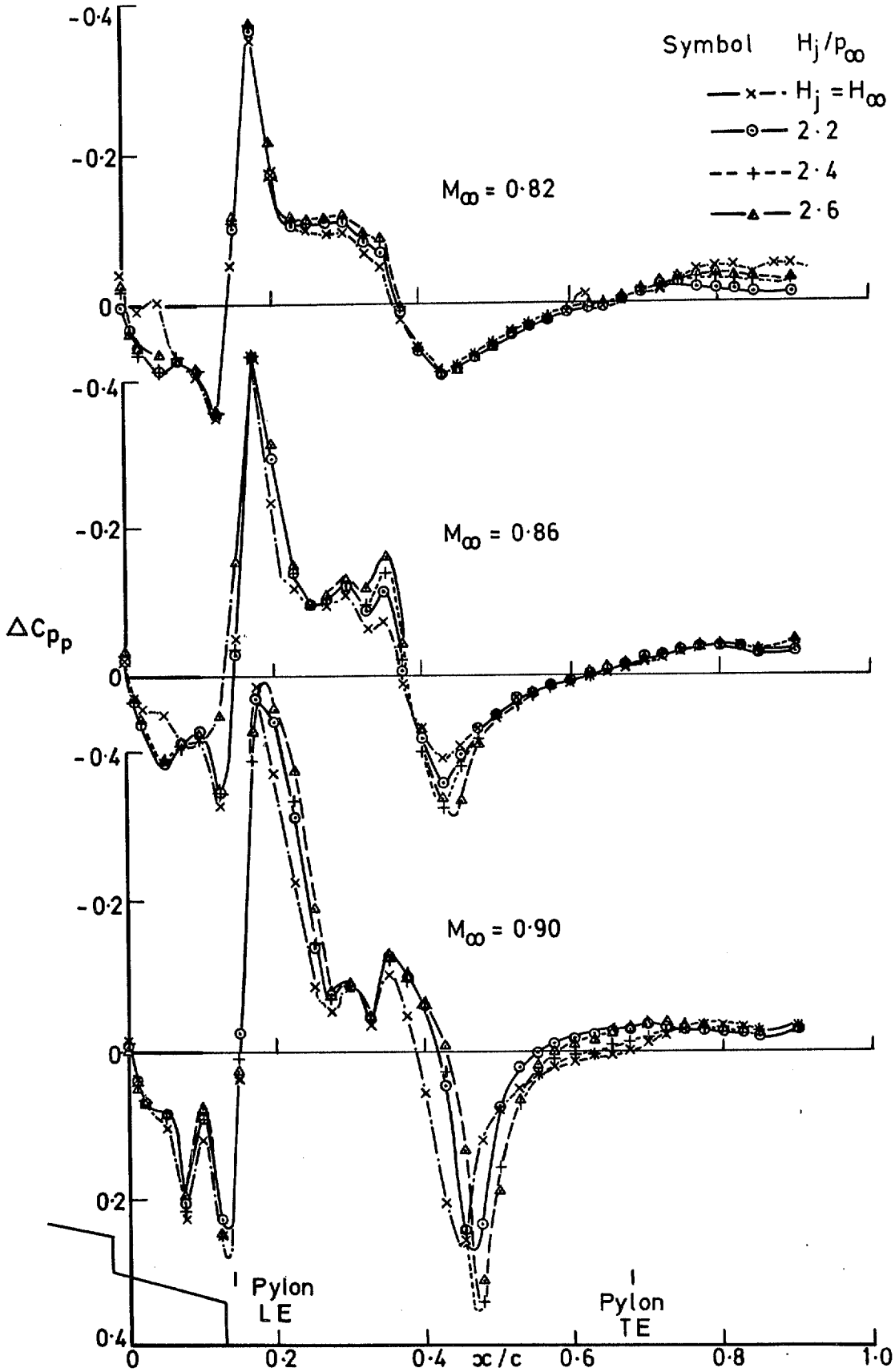

Fig 30 Interference at wing/pylon inboard junction when Pylon A is added to 15° nozzle (c) with jet blowing

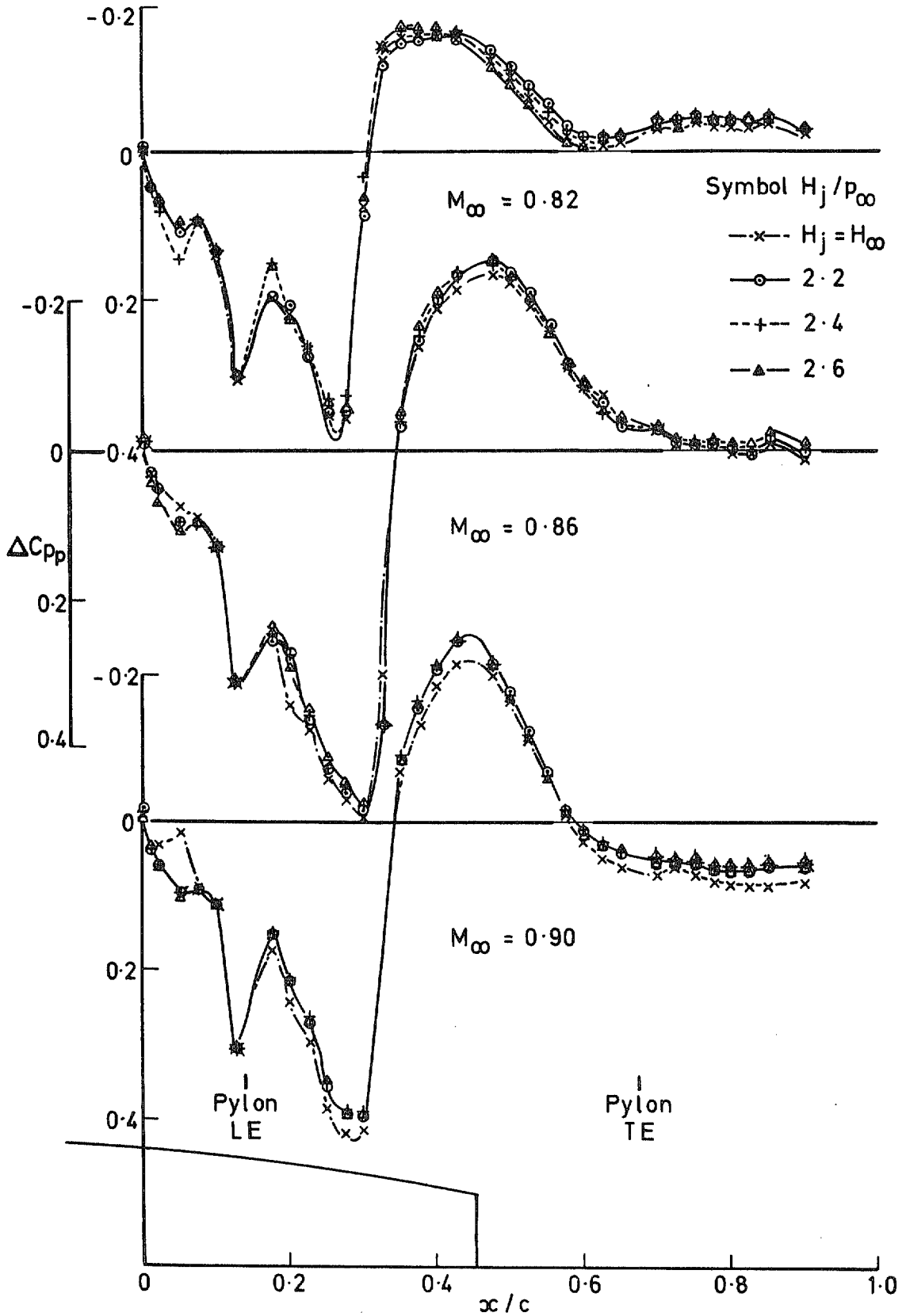

Fig 31 Interference at wing/pylon inboard junction when Pylon A is added to long nozzle (d) with jet blowing

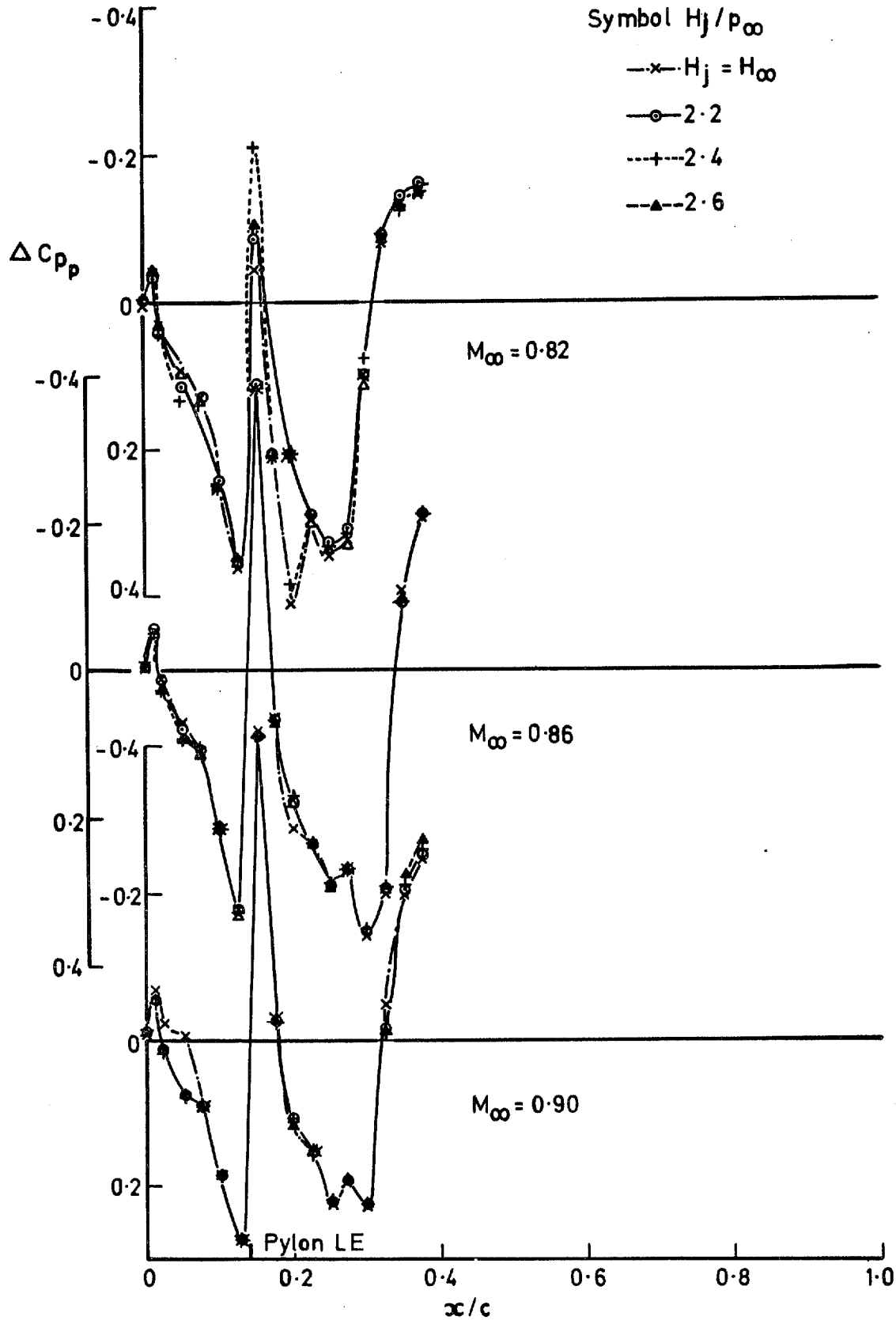

Fig 32 Interference at wing/pylon outboard junction when Pylon A is added to long nozzle (d) with jet blowing

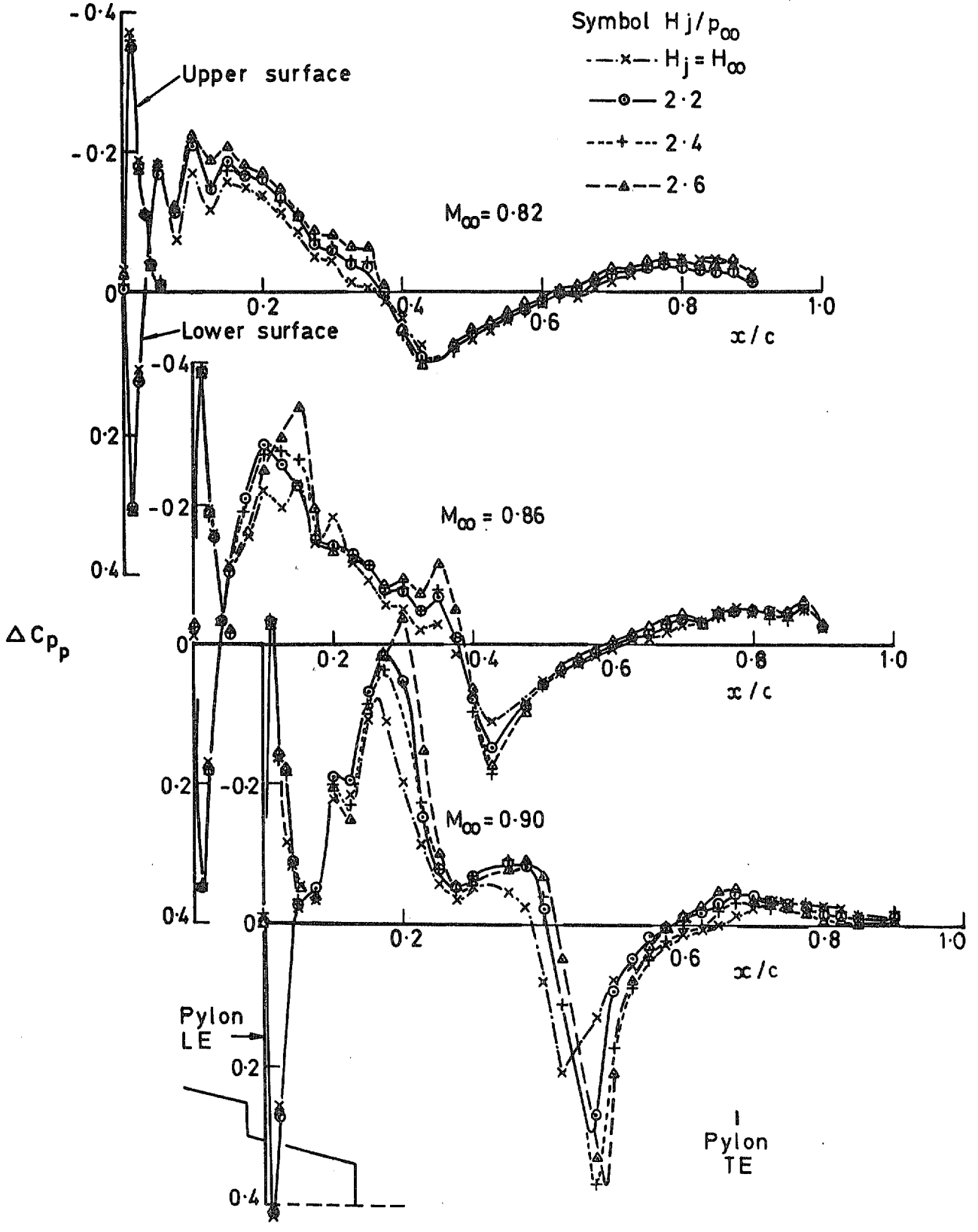

Fig 33 Interference at wing/pylon inboard junction when Pylon B is added to the 15° nozzle (c) with jet blowing

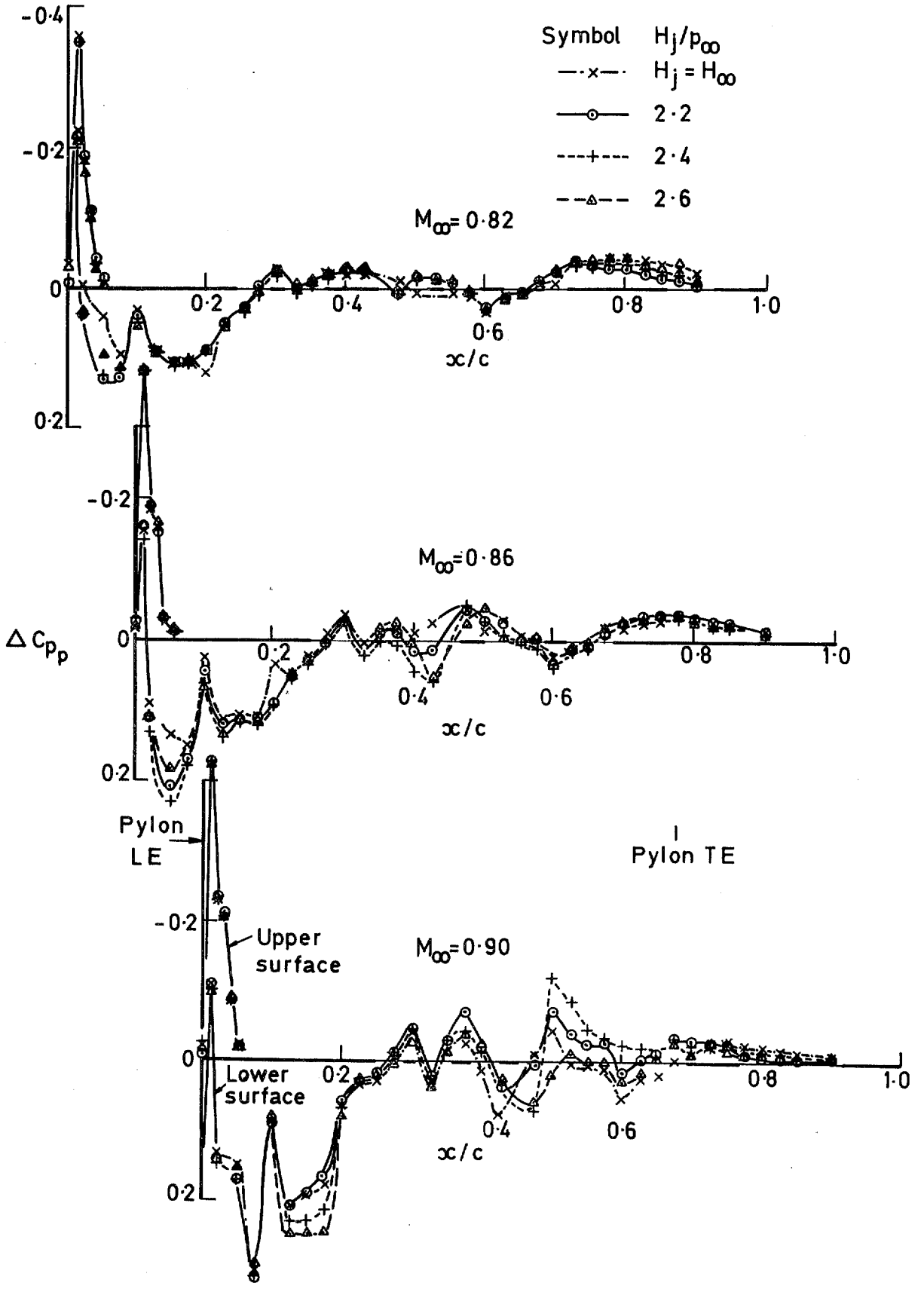

Fig 34 Interference at wing/pylon outboard junction when Pylon B is added to 15° nozzle (c) with jet blowing

Printed in England for Her Majesty's Stationery Office by the Royal Aircraft Establishment, Farnborough. Dd.596060 K4/2/80.

First published 1980

HER MAJESTY'S STATIONERY OFFICE

Government Bookshops
49 High Holborn, London WC1V 6HB
13a Castle Street, Edinburgh EH2 3AR
41 The Hayes, Cardiff CF1 1JW
Brazennose Street, Manchester M60 8AS
Southey House, Wine Street, Bristol BS1 2BQ
258 Broad Street, Birmingham B1 2HE
80 Chichester Street, Belfast BT1 4JY

Government Publications are also available through booksellers

R &M No. 3845
ISBN 0114711798